EUR 4434 e

COMMISSION OF THE EUROPEAN COMMUNITIES

EXPERIMENTAL AND THEORETICAL PHYSICS WORK ON PLUTONIUM ENRICHED LWR'S LATTICES

by

L. BINDLER (BN)
L. LEENDERS and H. VAN DEN BROECK (SCK/CEN)

1972

EURATOM/US Agreement for Cooperation

EURAEC Report No. 2145 prepared by
BelgoNucléaire, Brussels - Belgium and
Centre d'Etude de l'Energie nucléaire, Mol - Belgium

Contract Euratom/BelgoNucléaire/CEN No. 001-64-1 TRUB

LEGAL NOTICE

This report is on sale at the addresses listed on cover page 4

at the price of B.Fr. 250.—

When ordering, please quote the EUR number and the title, which are indicated on the cover of each report.

Printed by Guyot s.a., Brussels
Luxembourg, February 1972

EUR 4434 e

COMMISSION OF THE EUROPEAN COMMUNITIES

EXPERIMENTAL AND THEORETICAL PHYSICS WORK ON PLUTONIUM ENRICHED LWR'S LATTICES

by

L. BINDLER (BN)
L. LEENDERS and H. VAN DEN BROECK (SCK/CEN)

1972

EURATOM/US Agreement for Cooperation

EURAEC Report No. 2145 prepared by
BelgoNucléaire, Brussels - Belgium and
Centre d'Etude de l'Energie nucléaire, Mol - Belgium

Contract Euratom/BelgoNucléaire/CEN No. 001-64-1 TRUB

ABSTRACT

This report describes the first part of a programme of critical experiments in UO_2-PuO_2-H_2O lattices and their theoretical interpretation; this work was supported by EURATOM and realized in the frame of the joint plutonium recycle study programme of the SCK/CEN (Mol) and BelgoNucléaire (Brussels).

The emphasis lies on the description of the installations, the measurement techniques and the theoretical methods and codes, as well as on the discussion of the results obtained for configurations containing UO_2 and slightly plutonium enriched UO_2-PuO_2 fuel. The calculations, performed with the PANTHER code chain, appear to be in good agreement with the measurements, i.e. within 0.5 to 1 % on k_{eff}, $\pm$ 4 to 5 % on power distributions and $\pm$ 10 % on control rod reactivity worth.

Since 1969 the programme is continued with the support of the Belgian Government, the investigations being mainly directed towards higher plutonium content mixed oxide fuels.

KEYWORDS

CRITICAL ASSEMBLIES
URANIUM DIOXIDE
PLUTONIUM OXIDES
WATER COOLED REACTORS
REACTOR LATTICES
MEASURING METHODS
MEASURED VALUES
ENRICHED MATERIALS
PLUTONIUM
P-CODES
MULTIPLICATION FACTORS
POWER
DISTRIBUTION
CONTROL ROD WORTH
ERRORS
MIXTURES

TABLE OF CONTENTS [1]

*) Manuscript received on May 5, 1971

* *
*

LIST OF APPENDICES

* *
*

FIGURES

All the figures are classified at the end of the report per chapter, including for each chapter the figures relevant to its appendices.

REPORT WRITTEN BY

L. BINDLER	BN
L. LEENDERS	SCK/CEN
H. VAN DEN BROECK	SCK/CEN

WORK DONE BY

H. BAIRIOT	BN
J. BASSELIER	BN
L. BINDLER	BN
A. CHARLIER	BN
J. DEBRUE	SCK/CEN
M. DE COSTER	SCK/CEN
R. DELRUE	BN
P. DERAMAIX	BN
F. de WAEGH	BN
G. EVRARD	BN
J.P. FONTINOY	SCK/CEN
E. FOSSOUL	BN
F. GHEERAERT	SCK/CEN
R. HECQ	SCK/CEN
L. LEENDERS	SCK/CEN
W. MEWISSEN	SCK/CEN
F. MOTTE	SCK/CEN
J. RANSBOTYN	SCK/CEN
J. VAESEN	SCK/CEN
H. VAN DEN BROECK	SCK/CEN

CHAPTER I : INTRODUCTION

I.1. The Belgian Plutonium Recycle Programme was set up by Belgonucléaire and by SCK/CEN (Mol). Its aim is to look for the best conditions of recycling plutonium in thermal light water moderated reactors. In order to allow a concretization of the studies, the well defined case of an existing reactor had to be chosen. Quite naturally the choice fell on the first Belgian (actually Belgian-French) large nuclear power plant : the 266 MWe PWR SENA reactor.

The programme was carried out under Euratom contract (001-64-1 TRUB) until 1968. Since then it is supported financially by the Belgian Government.

In the frame of the programme a wide range of problems is investigated : mixed oxide fuel development and fabrication, fuel behaviour under irradiation, fuel management calculations, dynamical phenomena, etc., one of the main parts being a reactor physics programme, comprising experimental and theoretical work. The SCK/CEN has been charged with the experimental work, whereas Belgonucléaire is responsible for the theoretical interpretation of these experimental results and for codes development.

The present report relates on the reactor physics work done under Euratom contract, with the exception of the studies made on sub-critical lattices, treated in another final report. The other subjects studied in the frame of the Plutonium Recycle Programme are also discussed in separate topical reports.

I.2. Since several years the technological feasibility of recycling plutonium in thermal reactors has been widely established. However, opinions were and still are much less uniform with respect to the economical interest of such an operation. This interest depends in the first place on the general nuclear policy of each country, e.g. on the speed with which fast reactors will become operational. In these circumstances it is necessary to perform with much care trustworthy economical calculations when plutonium recycle operations are proposed. The basis for such calculations is given by core design reactor calculations. The necessity

of performing the latter as precisely as possible is thus clear. Therefore well developed and well calibrated large size computer codes are needed. For uranium fuelled thermal cores most of these codes were able to furnish results with a sufficient accuracy in the early sixties. The presence of plutonium fuel constitutes a serious complication, due to the intricate resonance structure of the cross-sections of the different plutonium isotopes and to the rather poor knowledge of the basic parameters of these isotopes at the time when most plutonium recycle programmes were started. In order to test the ability of the developed codes for treating plutonium containing cores, experimental data are needed, which can be used as references for corresponding calculational results.

I.3. The codes used by Belgonucléaire for the considered core calculations all belong to the PANTHER chain. The basic code (PANTHER) performs zero dimensional calculations.

For the treatment of the thermal range the analytical secondary model of Cadilhac is used ; the 2200 ms^{-1} cross-sections are carefully chosen recent values. A MUFT type library has been adopted to represent the cross-sections in the non-thermal range. The thermal cutoff was chosen at 1.855 eV, in order to include the two main low energy plutonium resonances (0.3 eV in Pu^{239} and 1.05 eV in Pu^{240}) in the thermal range.

Code calibration has been undertaken in two important steps. The first one did consist in studying a certain number of plutonium containing lattices already measured in U.S. critical facilities. At that time only the SAXTON and HANFORD critical experiment results were available, so that a choice out of them was made in view of testing the used theoretical tools. From this work several interesting conclusions resulted, leading to some improvements of the codes.

The second step in code calibration activities consists then in the use as reference data of Belgian experimental results, obtained in conditions much closer to the ones met in the reactor type to be studied, than those for which the U.S. results were found.

I.4. So an extensive programme of critical experiments was prepared. The VENUS facility in Mol, in which critical experiments had been made during about two years in the frame of studies on the Anglo-Belgian VULCAIN spectral shift reactor type, was transformed and adapted to the needs of the new VENUS-Pu programme. With this adaptation some quite substantial changes were involved, the most important one being the design of a fast dump system to control the reactor in emergency cases instead of using control rods. This dump system, which allows to drain the water out of the active part of the core in less than a second, has the advantage that perturbations due to control rod guide tubes can be avoided in the investigated lattices.

The new grids of the reactor installation are made for square lattices with a pitch of 1.303 cm, equal to the one of the fuel pins in the SENA assemblies.

An important number of fuel pins was fabricated in the frame of the programme. Their geometry and their nuclear characteristics were chosen in function of those of the SENA fuel and in function of the results of a series of fuel cycle calculations made in the hypothesis of a plutonium recycling operation in SENA. The UO_2 fuel is 4 % enriched and pelletized. Mixed UO_2-PuO_2 oxides with various uranium and plutonium enrichments were used to constitute the other fuel. Some of these plutonium containing rods were pelletized, the great majority being however vibrocompacted. Two different fabrication methods were used for this vibrocompaction, yielding respectively so-called heterogeneous and homogeneous rods. For the various enrichments a certain number of dismountable fuel pins are available, specially designed for measurement purposes. The active length of the fuel pins is 50 cm, and the overall one close to 75 cm.

I.5. In the overall programme of the critical experiments, to be realized in a period of something less than four years, three important phases can be distinguished.

The first and largest one is devoted to the detailed study of lattices in cold, unpoisoned moderator conditions, the lattices being alternatively constituted by the various available fuel types, arranged in one or, more commonly, in two enrichment zones. The investigated characteristics include both integral ones like k_{eff}, and local ones, such as power distributions or spectral index values.

The second phase of the programme will be relative to the study of lattices with a boron poisoned moderator, the boric acid concentration being taken as a parameter. This work will be done first in a UO_2 lattice and then in a mixed one consisting of a UO_2 and a UO_2-PuO_2 zone. In some cases the average moderator temperature of the SENA reactor at nominal power will be simulated by a moderator quantity reduction obtained by the introduction of aluminium microrods between the fuel rods; these results will allow to check the density coefficient treatment by the codes.

The last phase of the programme will consist in the study of some particular problems in connection with possible difficulties in the calculation of SENA or other reactor situations, when plutonium is being recycled. Some of these situations will be simulated as closely as possible in VENUS. In most cases the moderator will be poisoned.

I.6. In order to determine experimentally the wanted characteristics, such as k_{eff} and reactivity values, power or fission density distributions, spectral indices or disadvantage factors, the techniques and the equipment used in the frame of the VENUS-VULCAIN programme were adopted, developed and extended. As for the development work on the measurement techniques, investigations were mainly done about the use of foils with a view to improve the precision obtained with spectral index measurements. About this technique some complementary work was started in the frame of close contacts with Gulf General Atomic. In the GGA laboratories

time of flight measurements were made in order to determine the thermal neutron spectrum in an erbium nitrate solution - erbium being chosen because of the analogy of its thermal resonance structure with the one of plutonium. In order to allow an interesting comparison between that differential type of technique and an integral spectrum measurement technique as the spectrum index one, the erbium solution was put at the disposal of the Belgian programme. Spectrum index measurements will be done in a container, filled with the solution and located in the BR1 reactor.

In the frame of the programme considerable work was done on the development and the automation of the counting equipment. An automatic, relatively high capacity Y-scanning installation for fuel rods was designed and realized. The Y spectrometry laboratory for counting pellets and foils was also further developed and for the manipulations of plutonium containing pellets and detectors a special laboratory was organized in the LMA building (Laboratory for Mean Activities).

I.7. The present report describes the part of the programme, realized under Euratom contract. This includes the preparation of the reactor and the connected installations, the first phase of the code calibration on the basis of other experimental results, the experimental and theoretical work on an important part of the first phase of the VENUS-programme, relative to the detailed study of the 4 % UO_2 fuel and of the mixed 3 % UO_2 - 1 % PuO_2 fuel, as well as the preparation of the measurements in the GGA erbium solution.

This means that this report contains relatively much description and a relatively few number of conclusions, the work being only in its starting phase. The main conclusion to be presented is that the theoretical methods and codes, after certain changes due to a preliminary calibration on other experimental results, appear to be able to calculate the investigated UO_2 and slightly plutonium enriched UO_2-PuO_2 lattices with a quite satisfactory accuracy, notwithstanding the fact that the involved enrichments are substantially different from the ones delt with in the preliminary

calibration.

The remaining part of the experimental programme will furnish results which will enable to check if this conclusion remains valid for higher plutonium enrichments and for other moderating conditions.

CHAPTER II : DESCRIPTION AND OPERATION OF THE INSTALLATIONS

II.1. General Review

The VENUS critical facility was originally designed to perform critical experiments in the frame of the development of the spectral shift VULCAIN reactor type. After a two year operation for that programme, appropriate modifications were undertaken to adapt the reactor installation to a programme of critical experiments to be realized in the frame of the general Belgian programme on plutonium recycling in light water reactors. In the same time the already existing counting installations were extended and automaticized.

Except for the glove box installations used for plutonium pellet and detector manipulations, which are located in the LMA building, all the involved installations are situated in the BR1 building. There are two counting rooms, one for Y-scanning rods and the other one for Y-spectrometry, and there is the reactor hall itself, comprising three parts :

a) the reactor room, containing the reactor tank, the fast dump system devices and the hydraulic circuit; this room is shielded with heavy concrete and the access to it is allowed by a concrete door;

b) the control room, including the control desk and the racks with all the electronic equipment used for reactor control, health physics control and certain nuclear experiments;

c) the fuel storage room, in which five concrete closets with lead doors contain the fuel pins.

II.2. Reactor Description

II.2.1. Fuel geometry

As the physical characteristics of the studied fuels are detailed in chapter III, this paragraph only deals with their geometry. The dimensions of the fuel pins were chosen in accordance to the ones of the SENA reactor fuel, except for the active length which was taken equal to 50 cm, instead of about 3 m; this change was made in order to get a more compact core shape for the critical configu-

rations in cold conditions and to have more fuel pins with the same amount of fissile material.

The fuel pins contain uranium oxide or mixed uranium-plutonium oxides with various concentrations; they are clad with stainless-steel AISI 304 - or incoloy 800 - tubes. Three kinds of fabrications can be distinguished :

- the common pelleted fuel pins;
- the vibrocompacted fuel pins : they are filled with oxide powder, brought to a high density degree by vibro-compaction;
- the swaged fuel pins : they contain oxide powder too, but the high density is obtained by filling somewhat wider cladding tubes with powder and reducing then the diameter to the desired one by a so-called swaging operation.

All the fuel pins have an active lengtn of 50 cm; at both extremities plexiglass pieces of about 10 cm keep the active part at the correct axial position. The neutron properties of the plexiglass being equivalent to the ones of water, both lower and upper reflectors are rather close to pure infinite water reflectors. The total lengtn of the fuel pins is 74.45 cm. The radial dimensions of the fuel pins are the following ones :

	pelleted fuel	vibrocompacted and swaged fuel
Diameter of the fuel [cm] :	.890	.902 or .960
Inner diameter of the cladding [cm] :	.902	.902 or .960
Outer diameter of the cladding [cm] :	.978	.978 or 1.010
Thickness of the cladding [cm] :	.038	.038 or 0.25

A certain number of dismountable fuel pins are available for activation measurements; they correspond to the standard fuel pins of different types. These pins consist of pellets covered with a double air-tight protection barrier to prevent any plutonium contamination : stacks of five pellets are first clad with small air-tight aluminium tubes, after which the fuel column of 50 cm is obtained by loading ten of these capsules in a stainless steel tube, which is then closed at both ends by removable air-tight stops.

The internal dimensions of the dismountable fuel pins are standardized for practical reasons and the external sizes are the same as for the corresponding standard fuel pins. They are summarized in the following table :

Diameter of the fuel [cm]	: .903
Inner diameter of the Al capsule [cm]	: .906
Outer diameter of the Al capsule [cm]	: .926
Thickness of the Al capsule [cm]	: .010
Inner diameter of the cladding [cm]	: .940
Outer diameter of the cladding [cm]	: .978 and 1.010
Thickness of the cladding [cm]	: .019 and .035

The various geometrical types of fuel pins used in the VENUS programme are shown in figure II.1.

II.2.2. Reactor tank

The reactor tank and its internals appear in figure II.2. It is 1.7 m high and has a diameter of 1.6 m. The upper half part of the reactor tank includes the grids which allow to constitute the reactor core by loading the fuel pins one per one. There are two types of holes in the grids :

- the first type allows to load the fuel pins with a square pitch of 1.303 cm equal to the fuel pitch in the SENA assemblies (square pitches of $\sqrt{2}$ x 1.303 cm and 2 x 1.303 cm are of course also possible)
- the other type allows the introduction of small aluminium rods in the core in order to simulate a temperature of 286° C (nominal operation temperature of the SENA reactor) by decreasing the water quantity and hence its average density in the cell.

There are three grids. Both the lower and upper ones are made of stainless steel; they are as far as possible from the fuel region in order to have unperturbed axial reflectors. For the same reason plexiglass has been chosen for the third grid, which is just above the fuel region in order to guide the fuel pins to their appropriate location in the bottom grid.

The grids are provided with removable parts; they enable the possible location of the Ra-Be start-up neutron source, the neutron generator used for the reactivity measurements by the pulsed neutron technique and removable assemblies for activation measurements between the fuel pins (disadvantage factor determination).

II.2.3. Fast dump system

A schematic view of the reactor tank and the fast dump system is given in figure II.3. The fast dump system allows a fast fall of the moderator (water) out of the core at a scram signal. This system has been designed instead of the commonly used safety rods in order to avoid all perturbations in the regular array of the fuel pins due to the presence of the guiding devices and the holes for the absorbing rods.

The fast dump system comprises a jacket located inside the reactor tank and two dumptanks connected to the reactor tank and located under it. Both dumptanks and the jacket are closed by safety valves. During the normal operation of the reactor, the water is maintained inside the reactor tank by adequate air pressures inside the dumptanks and the jacket.

At a scram signal, all safety valves open, the pressurized air gets out and the moderator falls by gravity. Due to the important opening of the jacket, compared to the ones of the dumptanks, the water enters very quickly into the jacket during the first moments after scram; after this first jump the reactor tank is emptied in a slower way by the water lowering into the dumptanks, which are able to contain all the water present in the reactor.

Various alarms or scram levels are foreseen at the bottom of the jacket and the dumptanks in order to guarantee a fail safe working of the system. Three safety valves are connected to the jacket and two other ones are connected to each dumptank. This repartition has the advantage that the speed characteristics of the fast dump system are not modified if one of the valves does not open.

Two schematic views of a safety valve are given in figure II.4; they represent the close and open positions. The valve works as follows : during normal operation, the valve is closed by the force exercised on the air-tight door by a pneumatic piston through an electro-magnet. On the other hand the door undergoes the air pressure of the jacket or the dumptanks. To obtain the water-scram,

the voltage applied to the magnet is interrupted; the electromagnetic force disappears, so that the air pressure gets the door very quickly opened.
Resetting the valve goes as follows :

- the air pressure of the pneumatic piston is inversed so that the magnet comes in contact with the door,
- the voltage is applied again to the magnet,
- the pneumatic piston is actuated in the normal direction to close the pipe.

The valves are designed in order to guarantee a fail-safe operation. The described fast dump system enables to empty the reactor tank within about one second after the cut-off of the voltage on the magnets.
More details on the characteristics of the safety valves and the fast dump system are given in appendices II.1 and II.2.

II.2.4. Hydraulic circuit

A schematic representation of the hydraulic circuit is given in figure II.5.
In the case of a critical facility such as VENUS, with a maximum power of only about 0.5 kW, there is no cooling problem, so that the hydraulic circuit is very simple.
It allows the following operations :

a) Filling of the reactor tank : three different speeds are possible depending on the position of the water level with respect to the fuel loading :
   - Fast filling up to the lower extremity of the active fuel height
   - Intermediate filling up to a level close to the critical one
   - Slow filling in order to adjust the level when approaching criticality.

b) Demineralization and filtration of the water.

c) Injection of a boric acid solution in the moderator or dilution of this solution by water addition.

d) Mixing inside the storage tank or inside the reactor tank to obtain a high homogeneity degree.

e) Filling and drain of the whole hydraulic circuit.

All these operations are performed by setting the valves in the adequate position by a simple push-button selection and by actuating the corresponding pump.

II.3. Reactor operation and control

The control room including all reactor operation instruments is presented in fig. II.6.

II.3.1. Reactor operation

For a well-known configuration, the reactor can be made and kept critical in two ways; the choice depends on the nature of the measurement.

II.3.1.1. Most of the time the reactor is operated by regulating the water level in order to avoid control rod perturbations in the configuration. The critical level is usually above the fuel region in order to reduce the reactivity effect of a water level variation as much as possible and to obtain the k_{eff} value at nominal level by a period measurement (reactivity excess $\leq 0.3\,\% \frac{\delta k}{k}$ for periods ≥ 10 s).
Due to its importance for precise measurements, great attention is paid to a correct water level determination. Three water level gauges are used :

- Two gauges give a level indication on the control desk of the reactor. The first one gives a rather accurate indication (precision : 0.01 cm), but it cannot follow fast level variations. The second one follows quickly all water level variations, but gives only a very rough indication ($\pm$ 1 cm).
- The third gauge is used as a calibration one; it allows a direct reading of the water level through a glass tube connected to the reactor tank. A reading accuracy of 0.01 cm is obtained by use of a vernier.

II. 3.1.2. When axial buckling measurements are made, the upper reflector has to be infinite, i.e. the moderator has to be at its nominal level; in order to make the reactor just critical in these conditions, regulating rods are to be used. These are made of cadmium clad with a stainless steel tube; they can be moved in empty fuel claddings, which can be loaded in the core as fuel pins. Their position is chosen so that they are not affecting the measurement region.

Up to thirteen cadmium rods can be fixed to each of two available mechanisms; they can be moved at two different speeds : 0.12 cm/s and 1.2 cm/s.

When the regulating rods are used the criticality is reached in two steps : first the water is raised to its nominal level and then the regulating rods are moved up to their critical level.

For both reactor start-up types, a neutron source is used as well to start the chain reaction as to have a flux level before the water reaches the fuel loading. The start-up source is a Ra-α-Be one with an activity of the order of 0.6 Curie. It is moved down from and back in its container from the control desk; it is located in the radial reflector.

II.3.2. Reactor control

The reactivity of the reactor being controlled by the moderator or by regulating rods, the levels of both are given at the control desk in a digital way. For the flux level control, there are 6 control channels, all electronic devices being transistorized. Two start-up pulse channels are used for the low flux levels during the start-up of the reactor (from about 10^2 up to 10^7 n/cm^2 s at the centre of the core). Both consist of a 1" BF_3 counter, connected to a preamplifier, an amplifier with adjustable gain, a linear ratemeter, a logarithmic ratemeter and a periodmeter. They are foreseen with a "Source level" alarm adjusted at 10 c/s, a "period" alarm fixed at 25 s and an output for a pulse counting system. Four ion chambers of the "non-compensated" type are located inside the reactor tank under the bottom grid (see fig. II.3); they are sensitive to fluxes higher than 10^4 n /cm^2 s at the centre of the core. Two of these ion chambers are connected to a logarithmic amplifier, a ratemeter and a periodmeter. These logarithmic safety channels are foreseen with a period-alarm and a period-scram,

respectively fixed at 25 s and 10 s. The two other ion chambers are connected to a linear amplifier with a ratemeter working at four decades corresponding to fluxes of about 5.10^6, 5.10^7, 5.10^8 and 5.10^9 n/cm^2 s in the core. The linear safety channels are foreseen with a level-alarm and a level-scram, fixed respectively at 75 % and 100 % of the scale. All the ratemeters and the periodmeters can be followed on the control desk and may be recorded according to the selection of the operators.

II.4. Safety

II.4.1. Reactor safety

The reactor safety analysis is based on the requirement that no damage of the reactor core should occur even in the case of a power excursion. It has been demonstrated that this criterion is more restrictive than the maximum irradiation dose admitted for the personnel working in the reactor hall during the excursion (12.5 Rem).

The reactor safety is ensured as follows :

II.4.1.1. An analogous study has been performed to define the highest admissible rate of reactivity insertion according to the performances of the fast dump system, electronic devices included. The criterion given above, which corresponds practically to a maximum temperature at the fuel cladding of 100° C, yields that the reactivity insertion rate has to be lower than 0.14 $/s when the water is at its nominal level or 0.30 $/s when it is at a reduced level. The difference between both values results from the effectiveness of the water dump with or without the upper reflector. More details on this study are given in appendix II.3.

II.4.1.2. A series of interdictions and limitations in the reactor control system are imposed; the most important ones are :

- the opening of the reactor shielded-door causes an immediate water dump of the reactor.

- No water can be pumped into the reactor tank if the fast dump system is not operative; this means that all the safety channels must be working, all valves closed and the water below the given levels in the dumptanks and the jacket.
- The filling of water above the safety overflow (at the bottom of the fuel) is possible only through circuits with flows limited according to the analogous study, if there are more than 10 c/s on the start-up channels.
- Adding water above the nominal level is not possible.
- Only one way of reactivity injection at a time is possible : pumping, air injection or regulating rod raising.

II.4.1.3. A general commissioning of the installation did take place before the beginning of the experiments, in order to check that all devices of some importance for control and safety fulfil the specifications. Moreover, during the operation of the facility, several tests are to be made every two weeks and even every day to check that the installation characteristics remain unchanged.

II.4.1.4. For all important changes of the core configuration, a "core certificate" has to be established; this is done in two phases :

- before loading the new configuration, phase I checks that its characteristics fall within the hypotheses and the conditions of the analogous study. This phase is made on the basis of theoretical predictions or of certain experimental results obtained with similar configurations.
- after the first criticality in the new configuration, phase II of the core certificate has to confirm the first phase on the basis of actual experimental results.

II.4.1.5. Finally, adequately chosen personnel and procedures should allow to minimize human errors.

II.4.2. Health Physics

The safety of the personnel presents two aspects :

II.4.2.1. The first one concerns the danger of gamma and neutron radiations, coming from the reactor core.
Inside the reactor room, there are three gamma monitors having three different sensibility ranges : 0.1 mR/h to 1 R/h, 1 mR/h to 10 R/h and 10 mR/h to 100 R/h. They can put in action a klaxon when the reactor room is open (in presence of personnel). There are also two neutron monitors in the reactor room, respectively for thermal and fast neutrons.
In the reactor hall, outside the reactor room, there are two gamma monitors of low range (0.1 mR/h to 1 R/h). An automatic scram of the reactor occurs when both indicate 10 mR/h. There is also a thermal neutron monitor in the reactor hall.

II.4.2.2. The second aspect is the danger of contamination by plutonium. Very severe procedures are applied for the reception and the manipulations of the plutonium fuel elements. They have to be helium-tight and they have to remain so even in case of a manipulation accident. Tests have demonstrated that the fuel elements, manufactured for VENUS, remain helium-tight after a fall from a height of 3 m, a bending of more than 20° , or a shock against a metal corner piece.
Daily checks of the surface of handled fuel elements and of the reactor moderator are made in order to detect any α-contamination.

II.4.3. Population safety

The consequences of an accident of the VENUS reactor, loaded with plutonium fuel, were investigated for the residential area of the CEN/SCK, which is situated at only 200 m from the facility.
The calculation of the maximum credible accident supposes an energy release of 200 MWs and adopts very pessimistic assumptions concerning the melting of the core, the dispersion of fuel and fission gases in the atmosphere and the wind conditions.
From this study it appears that the most restrictive consequences are the inhalation doses of a 6-month child, which are respectively 1.37 Rem of plutonium in the lungs for a wind speed of 85 km/h and 100 Rem of iodine in the thyroid for a wind speed of 3.6 km/h.

This plutonium dose is below the admissible one, but the iodine dose is about 4 times the tolerated one. The superposition of both doses should not be considered, because of the great difference between the wind speeds. It is about certain that the tolerated iodine dose would not be attained due to the speed and the direction of the wind and the fact that the child would not permanently remain in the axis of the plume. Anyway, should the doses become higher than allowed, the residential area should be evacuated; therefore emergency plans exist.

II.5. Installations connected to the critical facility

II.5.1. γ-scanning installation

A main part of the experimental programme is devoted to power distribution determinations. Most of the time, they are obtained by irradiating standard fuel pins and by counting their γ-activities; so plutonium manipulation problems are avoided.
The irradiated fuel pins are counted in an automatic γ-scanning installation controlled by a punched tape with a programme written in function of the kind of measurement and the number of fuel pins. A maximum of 22 fuel pins may be loaded on the machine. The decay correction is applied by comparing all the activities to the activity of a monitor capsule, containing the same fuel. The results are directly punched on tape, which can be introduced in a computer for data processing.
The mechanical part of this installation can be seen in figure II.7. It consists of a shielded room containing two mechanisms : the first one is a storage device, receiving the fuel pins and giving them, one by one, to the second mechanism , which performs the translation of each fuel pin in order to allow its counting at certain preset levels by bringing them before the collimator.
In the figure one sees the cylindrical counting device, consisting of a NaI (Tl) crystal, connected to a classical monochannel analyzer.

II.5.2. Plutonium laboratory

The power distributions can also be measured by counting activated fuel pellets; they are completed by spectral index measurements, mainly with Pu-Al and U-Al foils.
For such experiments dismountable plutonium fuel pins have to be prepared; this work is performed in collaboration with the Hot Laboratory Service of GEX in a special laboratory, located in the LMA building (Laboratory for Medium Activities), which has been appropriately equiped and which is operated by people experienced in handling plutonium material.
A general view of this laboratory is given in fig. II.8; it contains a manipulation glove box, a decontamination glove box and a ventilated hood.
Fig. II.9 presents an internal view of the manipulation glove box, in which small plutonium capsules (containing 5 pellets) and activation detectors are prepared. This glove box also contains a shielded storage place for irradiated plutonium pellets.

In the decontamination glove box the tightness of the capsules is checked and all pieces are decontaminated before they may be used outside the glove boxes.

Finally, the ventilated hood is used for the manipulations of the dismountable fuel pins; they mainly consist in loading and unloading the capsules in and from the cladding tubes.

For the transport of the fuel pins and the detectors, between the BR1 building and the LMA one, special air-tight and lead shielded containers are used.

II.5.3. Y-spectrometry installation

For the activation experiments, the activities of pellets and foils are measured in the Y-spectrometry installation shown in fig. II.10. It consists of four NaI Y-counters connected to monochannel analyzers; they are located inside an insulated room at constant temperature. The monochannel analyzers are connected to an automatic counting system, situated outside the room. The results are punched on

tape to allow direct data handling by a computer.
For the power distribution experiments, the pellets turn around their axis during the counting in order to avoid any effect of the macroscopic radial gradient on the measured activity. This effect is particularly important for the pellets irradiated close to a perturbation or to the reflector.

CHAPTER III : THE FUEL

III.1. Introduction

III.1. An important number of fuel pins was fabricated and put at the disposal of the experimental programme. Not only the number of these fuel pins, but also their variety should allow to study numerous aspects of the presence of plutonium in light water thermal reactors in general and in the SENA reactor in particular and to calibrate accordingly theoretical methods and codes.

As was already pointed out in the introduction of this report, both the geometrical and the nuclear characteristics of the fuel rods were chosen in function of those of the SENA fuel and in function of the results of fuel cycle calculations made in the hypothesis of a plutonium recycling operation in SENA.

As the geometrical characteristics were presented in the previous chapter (II.2.1.), this chapter will be mainly devoted to a discussion of the fabrication of the rods, the choice of the various enrichments and the presentation of some more details on the different available fuel types.

III.2. Fabrication

All the UO_2 and a small fraction of the UO_2 - PuO_2 fuel was manufactured in the form of pellets. Most of these pellets were made to constitute standard, i.e. non-dismountable rods, so that for their fabrication normal tolerances were to be satisfied. The other pellets however were to be used in dismountable rods for measurement purposes, so that for at least an important part of them rather severe dimensional conditions had to be respected, which was not always easy to obtain.

Most of the PuO_2 - UO_2 rods were directly filled with powder. In order to obtain a sufficient fuel density, two different procedures were used : vibrocompaction and swaging (cfr II.2.1.); both kinds of operations do not lead to differences in the nuclear characteristics. Therefore a distinction between them is not necessary

here, so that the swaged rods will be assimilated to the vibrocompacted ones in all further discussions in this report.

Two different types of mixed UO_2 - PuO_2 powders were used. In the first type both the uranium oxide and the plutonium oxide were contained in all grain sizes, whereas in the other powder type the plutonium was only present in the finest of the three considered grain size fractions. The corresponding rods will be called in what follows respectively homogeneous and heterogeneous rods. As a separate final report on fuel manufacturing will be issued soon, we will not enter into details about it in this report.
Let us just remind the fact that the interest of the heterogeneous rods lies in their sensibly lower fabrication cost. Physically the plutonium is then however mainly concentrated at the periphery of the fuel rods; this fact can have some influence on certain neutronic and thermal characteristics and parameters. One of the aims of our critical experiments was the investigation of this neutronic aspect of the heterogeneous rods.

III.3. Some general considerations about the choice of the enrichments

One knows that the basic aim of the programme is to check codes and methods to be used for plutonium recycling calculations for SENA. For this reason the nuclear characteristics of this reactor's fuel throughout a core lifetime were more or less taken into account when choosing the enrichments of the fuel rods for the critical experiments.

For the UO_2 fuel, to be used in the experiments, the adopted U^{235} enrichment was equal to the one of the normal fresh reload uranium fuel in SENA, i.e. 4 % (notation : 4/0). As for the different types of plutonium containing fuel rods, a relatively large number of rods was available for two categories with sensibly different plutonium contents, whereas for the other ones only a limited number of rods were fabricated. The number of the former ones was deliberately chosen rather high in order to be able to perform some parametrical studies on configurations, or important zones in them, for which the ratio between the plutonium and uranium contents increases gradually.

The first of these fuel types is the so-called 3/1 fuel, which is a mixture of 3 % U^{235} enriched UO_2 with 1 % of fissile PuO_2; the non-fissile content of the plutonium is less than 8 %. Very approximately, this kind of fuel is typical for 4 % enriched UO_2 irradiated during more than half a complete SENA corecycle, the plutonium content being in reality sensibly smaller at that stage.
The other fuel in question is the 2/2.7 one, a mixture of 2 % U^{235} enriched UO_2 with 2.7 % of total PuO_2, about 80 % of the latter being fissile. The 2 % figure for the uranium enrichment corresponds to the remaining uranium content in discharged UO_2 fuel, whereas 2.7 % of PuO_2 is an approximate value of the content at which the plutonium could be recycled, when the discharged uranium is to be reloaded and enriched with plutonium.

After the performance of detailed plutonium recycle calculations, it was decided to fabricate on the basis of the obtained results some other fuel types. A first type is the 1.75/3.2 fuel : 1.75 % is the U^{235} enrichment of the discharged uranium in the fuel from which the first plutonium to be recycled would be obtained; it is only in the equilibrium cycles that this value becomes 2 %. The PuO_2 content of 3.2 % was defined on the basis of fuel recycle calculations. Another fuel is the 0.7/5 one, in which the PuO_2 is mixed with natural UO_2; the PuO_2 enrichment of 5.05 % is also a result of series of recycle calculations, carried out in the hypothesis that the discharged UO_2 is not used anymore for reloading. The plutonium in both these fuel types has the same isotopic composition as the one used in the 2/2.7 fuel.

In order to allow a rather direct check of the theoretical treatment of the Pu^{240} resonance at 1.06 eV, it was decided to make a 0.7/x fuel, having the same fissile plutonium content as the 0.7/5 fuel, but containing only a very small quantity of Pu^{240}, instead of 17 % as the plutonium of the 0.7/5 fuel. For that purpose a certain amount of plutonium was used, reprocessed out of irradiated BR1 fuel and containing only about 4 % of Pu^{240}. The enrichment x was defined as 4.37 %.

III.4. Amounts of fissile material involved in the fabrication of the VENUS fuel

The following table presents some information on the amounts of fissile material involved in the programme.

The weight figures are slightly rounded off.

MATERIAL	AMOUNT	OWNERSHIP
U enriched at 4 % U^{235}	571.5 kg (U)	hired from USAEC
U enriched at 3 % U^{235}	162.5 kg (U)	hired from USAEC
U enriched at 2 % U^{235}	189 kg (U)	hired from USAEC
U enriched at 1.75 % U^{235}	~ 22 kg (U)	owned by SCK/CEN
natural uranium	~ 30 kg (U)	owned by SCK/CEN
Pu contained in the 3/1 fuel (isotopic composition : 92.08/7.29/0.60/0.03)	~ 1.7 kg (Pu)	put at the disposal of the programme by EURATOM
Pu contained in the 0.7/4.3 fuel (isotopic composition : 95.65/4.10/0.24/0.01)	0.45 kg (Pu)	owned by SCK/CEN
All other plutonium (isotopic composition : 79.37/17.14/3.05/0.44)	6 kg (Pu)	hired from UKAEA

The uranium enriched at 4, 3 and 2 % was delivered in respectively 3, 2 and 2 batches; there exist very small differences between the enrichments of these different batches for each fuel type. In only one case this difference is not completely negligible : the enrichment of two of the 4 % batches is between 4.008 % and 4.009 %, whereas the third one is 4.04 %; in this last case however the density was slightly reduced in order to have the same amount of fissile material as in the rods made with fuel of the other batches.

III.5. Some more details about the different fuel types

In this paragraph some more details are given on the exact compositions of the different fuel types, especially the mixed oxide ones, the number of available rods and pellets, and the manufacturers. Some figures given for the available number of rods or pellets are still approximate, as all fabrication work was not finished yet when this report was written.

4/0 FUEL

510 pelletized standard rods	4.0086 %	Manufactured by KFK/NMK
505 pelletized standard rods	4.04 %	Manufactured by KFK/NMK
744 pelletized standard rods	4.0084 %	Manufactured by BN
1825 pellets for dismountable rods	4.0086 %	Manufactured by KFK/NMK

3/1 FUEL

- uranium enrichment : 3.0024 % or 3.0005 %
- fissile PuO_2 content : 1 %
- total PuO_2 content : 1.08 %

34 homogeneous vibrocompacted rods, manufactured by the Mixed Group SCK/CEN - BN.

~ 400 heterogeneous vibrocompacted or swaged rods, same manufacturer.

1350 pellets for dismountable rods, manufactured by EURATOM-Karlsruhe.

2/2.7 FUEL

- uranium enrichment : 2.0013 % or 2.0021 %
- fissile PuO_2 content : 2.22 %
- total PuO_2 content : 2.7 %

268 homogeneous vibrocompacted rods, manufactured by the Mixed Group SCK/CEN - BN.

~ 200 heterogeneous vibrocompacted rods, same manufacturer.

379 pellets for dismountable rods, manufactured by BN.

1.75/3.2 FUEL

- uranium enrichment : 1.785 %
- fissile PuO_2 content : 2.61 %
- total PuO_2 content : 3.17 %

~ 65 pelletized standard rods, manufactured by BN.

0.7/5 FUEL

The PuO_2 content is slightly different for the pelletized standard rods and the pellets for dismountable rods.

58 pelletized standard rods :-fissile PuO_2 content : 4.15 %
-total PuO_2 content : 5.04 %

256 pellets for dismountable rods : - fissile PuO_2 content : 4.24 %
- total PuO_2 content : 5.14 %

All this fuel was manufactured by BN.

0.7/4.3 FUEL

- fissile PuO_2 content : 4.20 %
- total PuO_2 content : 4.37 %

4 pelletized rods, manufactured by BN.
1168 pellets for dismountable rods, manufactured by BN.

Still one more category of pellets for dismountable rods is available. They were manufactured by EURATOM-Karlsruhe. Their characteristics are not very different from those of the 2/2.7 fuel :
- uranium enrichment : 2.0013 %
- fissile PuO_2 content : 2.5< %
- total PuO_2 content : 3.06 %

so that they can e.g. be used as filling pellets at the two extremities of the 2/2.7 dismountable rods, at least for certain experiments such as radial power distributions near the mid plane level. The number of pellets available is 167<.

A global review of all the figures given in what precedes shows that an important quantity of fuel is at the disposal of the programme. Making the sum, one finds about 2800 rods, more than 1000 of which contain plutonium, and something less than 7000 pellets for dismountable rods, among which almost 5000 are PuO_2-UO_2 ones.

To conclude this chapter devoted to the VENUS-Pu fuel, a table is given summarising for all the fuel types the linear density in g/cm (mean values) :

TYPE	RODS	PELLETS
4/0	6.33 & 6.36	6.40
3/1	6.60	6.52
2/2.7	6.0	6.07
1.75/3.2	6.43	-
0.7/5	6.57	6.67
0.7/4.3	(6.43)	6.60
2/3.06	-	6.10

CHAPTER IV : THE PROGRAMME

IV.1. Introduction

The general aim of the experimental programme has already been specified in the first chapter: the determination of measurement results, serving as reference data for the calibration of the reactor codes and the theoretical methods and models, used for the study of lattices containing plutonium fuel, more particularly PWR ones.

It has also been seen in chapter II and III that the design of the critical installation in general and of the fuel in particular did take into account certain SENA characteristics. This was not always the case for the programme itself, for which it was rather tried to give it a character as general as possible, without leaving however the scope of the global project. It is in this spirit that the almost four years lasting programme was (and still is) established, continuously discussed and possibly adapted to take into account new aspects or particularities of the type of lattices involved or all other new information of any interest to the programme. Several programme changes were also induced by conclusions resulting from already performed theory-experiment comparisons.

Although the present final report covers only the experiments realized during somewhat more than one year, a period corresponding to about one third of the total one, we thought it would be interesting to outline in this chapter the structure of the complete programme.

IV.2. Some particular aspects

Before going into more details about the actual programme of critical experiments, some involved or related particular aspects are to be put in evidence.

a) **Precision aims of the code calibration**

Quite generally, it can be said that the same precision is wanted for the calculation of plutonium recycle lattices as the one usually required and normally achieved for uranium lattices. Practically, this means 0.5 to 1 % for k_{eff}, 4 % for power distributions, 1 % for reactivity during burnup, 20 % on reactivity coefficients and 10 % on control.

b) **Consequences for the measurement techniques**

It is clear that in order to be able to control if these values can be respected by the calculations, it is necessary to dispose of precise reference data, i.e. accurate experimental results. The experimental precision on the mentioned characteristics k_{eff}, power distribution, etc. should thus be much better than respectively 0.5 to 1 %, 4 %, etc. It is not in all cases and circumstances easy to obtain such a good precision, and further development of the used measurement techniques was (or is) sometimes necessary, the more that the presence of plutonium can also here constitute a complicating factor.

It is in this scope of a further investigation of measurement technique possibilities that a small complementary programme was started in close contact with Gulf General Atomic, aiming at a comparison between an integral spectrum measurement technique (spectrum indices; measurements in MOL) and a differential one (time of flight; GGA measurements). This is done in an erbium nitrate solution medium, the spectrum of which is of the same nature as the one in a plutonium containing lattice, due to the similar resonance structure of plutonium and erbium in the low energy range. In the period on which the present document reports, the measurements were carefully prepared but not yet realized. A description of this preliminary work is given in appendix IV.1.

c) Subcritical measurements

For experiments on plutonium fuel lattices the availability of thrustworthy subcritical measurement techniques can be much more important than for uranium lattices, due to the high cost and hence the generally restricted number of fuel pins at the experimenter's disposal. In the frame of our plutonium recycling programme a considerable effort has therefore been devoted since several years to the development of adequate subcritical techniques, which would even allow the study of highly subcritical fuel loadings. The two first series of subcritical experiments were done on respectively 5 % and 7 % enriched UO_2 fuel pins. Final reports were published, showing how and with which results various measurement and interpretation techniques were investigated. [Ref. IV.1, 2]. A third subcritical programme, using the 4/0 VENUS-fuel, was started at the beginning of 1969, its main aim being the investigation of the use of a long BF_3 detector for reactivity and prompt neutron decay constant (α) measurements. The final intention is to use this technique in VENUS itself for large configurations, which are subcritical due to the presence of a large number of absorbing rods in the lattice or due to an important boric acid concentration in the moderator, or eventually for one zone PuO_2 - UO_2 fuel lattices.

d) Heterogeneous fuel

A particular aspect of the Belgian plutonium programme being the development of the heterogeneous vibrocompacted fuel fabrication technique, it was decided to look through certain experiments for possible incidences of the difference between homogeneous and heterogeneous fuels on their nuclear characteristics.

IV.3. The different phases of the programme

The experiments realized or still to be realized in VENUS can be classified in three large phases.

The first one is relative to lattices with the H_2O moderator at 20° C and not containing soluble poison. This phase - the most extended one of all three - comprises integral and fine structure measurements on the different fuel types in several geometrical arrangements, including the study of the presence of local lattice perturbations. All the experiments reported in the present document belong to this part of the programme.

The second phase will be devoted to the investigation of lattices with a boric acid poisoned H_2O moderator (at various concentrations), with a moderator simulated at SENA nominal power operation temperature (about 285° C) by the introduction of aluminium micro-rods between the fuel rods, or with a moderator combining both these overall perturbations. Most measurements will be of the integral type (critical mass, k_{eff}, buckling values), the main aim being the check of temperature and boron reactivity coefficients. The experiments will be limited to the 4/0 and 2/2.7 fuels and to geometrically simple configurations.

The last phase, finally, will consist in the study of a few configurations in which the characteristics of the first and second phases will be combined, i.e. the moderator will be poisoned and/or simulated at high temperature and the configurations will include local perturbations and various fuel types. It will be tried to simulate as closely as possible a plutonium recycle assembly, as designed for SENA, with its appropriate environment. In a certain sense this part of the work can be considered as a kind of a final demonstration of the possibilities of the codes, calibrated on the basis of the experimental results obtained in the course of the two previous phases.

At the moment of this report's redaction the second and third phases were not started yet, the detailed discussion of their concrete realization already well. About these phases we will however limit ourselves to what was said in this paragraph, whereas in the following one the complete first phase will be further developed.

IV.4. Experiments with unpoisoned, 20° C H_2O as moderator

The first months of the experiments the already available amount of fuel was limited to about 500 4/0 rods and to the 3/1 ones. Therefore it was convenient to start measurements in configurations having a H_2O/UO_2 ratio close to the one of optimal moderation. The VENUS grids allow lattice pitches equal to p_{SENA} = 1.303 cm, $p_{SENA}\sqrt{2}$ = 1.843 cm and 2 p_{SENA} = 2.606 cm, the corresponding H_2O/UO_2 values being approximately : 1.6, 4.5 and 10; these are "effective" ratios : this means that the pure volumetric ratio was corrected for the difference between the actual and the theoretical fuel density. In these conditions the 1.843 cm pitch was chosen for the first four configurations, consisting of one cylindrical or parallelepipedical zone for the two mentioned fuels. In all cases k_{eff} near criticality and the axial and radial bucklings were determined, the moderator being at the nominal level, i.e. the upper axial reflector being infinite.

The critical number of rods being still low for the 3/1 fuel in the case of the 2 p_{SENA} pitch, one zone configurations of cylindrical, respectively parallelepipedical shape were realized and k_{eff} and B^2 were measured.

After these experiments, the for the programme most important lattice pitch (p_{SENA}) was adopted for all other configurations. When defining these configurations, it was tried to separate and insulate as much as possible the different characteristics or properties to be studied; in other words, the nature and the geometry of the configuration were each time chosen in function of an aspect of particular interest. As for the different fuels, it can be said that the three types 4/0, 3/1 and 2/2.7 are investigated rather systematically, analogous measurements being carried out in all three. This is illustrated by the general scheme represented in figure IV.1, where the experiments are grouped in four parts.

The first one shows configurations mainly realized for checking k_{eff}; therefore reactivity and buckling were measured; in those

with a square section, fission density distributions were determined too. The size of the plutonium zones was in the different cases taken as large as the availibility of the involved fuel rods did allow to. From one of the configurations the incidence of the different powder properties ("homogeneous" and "heterogeneous" fuel) on the nuclear characteristics can be deduced for the 2/2.7 fuel. The same aim was pursued for the 3/1 fuel by a series of substitution experiments with small zones (4 x 4 rods) in the center of 3/1 zones; these experiments were carried out in lattices characterized by three different pitches.

The determination of the distribution of the fission density and of the evolution of spectral index values through a boundary between two different fuel zones, more especially a UO_2 and a mixed oxide one, constituted a second kind of experiments.

The third one consisted in a systematical study of the presence of perturbations of varying importance (changing number of cells, going from 1 to 7) and with very different nuclear characteristics : B_4C rods, H_2O gaps and Al rod or plate. In all these cases the reactivity effect due to the perturbations was measured, whereas the power distribution along the axis perpendicular to the perturbation was determined in the most important cases (mainly for all perturbations of 1 and 7 cells respectively).

Some other configurations, finally, were conceived to study perturbations of a particular shape (cross of H_2O, cross of B_4C-rods) or combined perturbation plus boundary situations. Moreover a possible geometry of a SENA assembly in the case of an eventual plutonium recycle operation in that reactor was simulated, mainly to determine the fission density distribution and to measure the reactivity effect of inserted absorbing rods, simulating partially the cruciform control rods of the reactor.

The detailed description of the realization of this programme will be presented in chapter VII; it will however be limited to the experiments carried out under the Euratom contract until 1966, in a few cases completed by some work done afterwards in order to enable a more logical presentation of results in both the present and the ultimate final report.

Practically this means that all configurations containing 3/1 fuel will be discussed in the present report, as well as those composed of 4/0 fuel only, except for the 4/0 configurations with the B_4C crosses in their center.

References

IV.1. J. DEBRUE et al.: Résultats d'expériences sous-critiques réalisées sur des réseaux H_2O-UO_2 enrichis à 5 %; EUR 3378 f.

IV.2. J. DEBRUE et al.: Subcritical Experiments, final report; EN-6908-03.

CHAPTER V : MEASUREMENT TECHNIQUES

In order to determine the wanted characteristics, as well the integral ones such as k_{eff} and bucklings, as the more local ones, such as power distributions near perturbations in the lattice, the measurement techniques developed before in the frame of the VULCAIN critical experiment were used again, some of them after having been more particularly adapted for the study of cores with several zones, containing plutonium.

The description of all these techniques and of the development work done for several of them will be presented in detail in a series of annexes to this chapter. In this text itself we will only outline shortly the nature of the different techniques, as well as the precision with which they allow to obtain the studied characteristics; in general it can be said that the experimental precision is sufficiently good, compared to what is required for testing the theoretical methods.

V.1. k_{eff} and critical mass determination (App. V.1)

For the k_{eff} determination the well known positive period measurement technique is used preferentially, as it yields a very good precision; reproducibility tests, taking not only into account the accuracy of the period measurement itself but also the one associated with other aspects such as the correct water level determination, have shown a precision on k_{eff} of $\pm$ 0.01 Δk_{eff}. In some cases the k_{eff} is determined for very slightly subcritical configurations, using subcritical countings; this technique is based on the knowledge of the upper axial reflector value; the obtained precision, although being somewhat less good than with the period measurement, is more than sufficient for the code calibration purposes.
The determination of a critical mass, normally performed for a cylindrical geometry, is obtained within 0.1 % Δk_{eff} : the main uncertainty in these cases results from the approximate representation of the cylindrical geometry in the reactor.

The relation between the measured period and the associated reactivity worth is given by NORDHEIM's formula (App. V.2).

V.2. One region power distributions (App. V.3)

Axial power distributions are obtained by the fission chamber technique or by the γ-scanning technique; in this last case the γ-activity of the fission products is measured above a certain energy (425 keV). In many cases both techniques have been applied; a good agreement has always been found; in general the dispersion of the measurement points around a best fit curve is better with the fission chamber technique.

Radial power distributions through a one fuel core or zone are obtained by the same type of γ-scanning, choosing the measurement points at the same horizontal level for all the rods. The precision obtained depends on the axial homogeneity degree of the fuel pins; heterogeneous fuel pins are normally not used for such measurements : in such cases the corresponding dismountable pins are preferred, while the achieved accuracy is much higher.

V.3. Buckling determination (App. V.4)

Both the axial and radial buckling values are obtained from a curve, fitting respectively the axial and radial power distributions, discussed in the previous paragraph; in the axial direction, and in the case of rectangular geometries also in the radial one, the fitting curve is a cosine, whereas for cylindrical configurations, the radial distribution is fitted with a J_o Bessel function. In the case of homogeneous fuel (either pelletized or vibrocompacted) the precision on the axial buckling is $\pm$ 1 %, the one on the radial buckling $\pm$ 2 %; this difference is due to the fact that in the second case the number of measurement points is sensibly smaller.

V.4. Reactivity effects of perturbations (App. V.5)

These effects are obtained on the basis of a $\partial\rho/\partial h$ curve, h being the moderator level; determining the critical water level for the two situations between which the reactivity difference has to be found, this difference is obtained by integrating the $\partial\rho/\partial h$ curve between the critical levels. In general the obtained precision is of the order of 0.02 to 0.03 % Δk_{eff}.

V.5. Pu^{239}/U^{235} spectral index determination (App. V.6)

The Pu^{239}/U^{235} spectral index is determined for different fuels because it is very sensitive to spectrum variations in the thermal range, such as those due to the plutonium resonances. When measured for fuel pins located in a zone where the spectrum is the equilibrium one, they can be compared with the theoretical ones, found on the basis of cell calculation spectra.
Experimentally the index is determined by counting the activity of U^{235}-Al and Pu^{239}-Al foils put between fuel pellets, placed in the dismountable rods. In order to get an acceptable precision, the measurements are to be carried out very carefully and appropriate corrections are to be applied. Especially the perturbation created by the presence of the foil in the fuel column has to be defined correctly. The precision actually achieved lies between + 2 % and - 4 %.

V.6. Power sharing between different fuel zones (App. V.7)

It has been seen in one of the preceding paragraphs that inside each fuel zone the relative power distribution can be found with the γ-scanning technique or with the pellet activation one. In order to link these relative distributions in different zones to each other, i.e. to determine the power sharing between these zones, it is necessary to count, either with pellets or possibly with pins, the activity due to the La^{140} peak at 1.6 MeV, at least two weeks after the irradiation. Knowing the La^{140} fission yields for the different fissile uranium and plutonium isotopes, and using the

spectrum index for the determination of the relative importance of the fissions in the uranium and the plutonium in each concerned fuel type, it is possible to convert the measured activity ratios between different types of fuel pins into fission density or power ratios. Normally the resulting global experimental precision on the normalized power distribution is of the order of $\pm$ 2 %.

V.7. Fission density depression inside fuel rods (App. V.6)

This depression can be determined with two different techniques. The first one consists in counting the density of the tracks, created by the fission products in mica foil detectors, put between the fuel pellets. For this technique the irradiation level has to be chosen carefully, in order to have an appropriate track density ($5\ 10^5$ tracks per cm^2). The precision on the individual points is about 2 %; this precision results from an accumulated counting of 3000 tracks. The other method is based on the activation of very thin concentrical rings, forming together a section equal to the one of the fuel pin; the individual counting of these rings gives a step fission density distribution curve; an accuracy of about 2 % is reached on each step result.

CHAPTER VI : CALCULATIONAL METHODS

VI.1. Introduction

For the calculation of slightly enriched UO_2 - H_2O lattices, many codes are available which allow a good evaluation of the nuclear characteristics of these lattices and hence of thermal light water moderated reactors. In these reactors all important materials have 1/v cross sections, so that the accurate knowledge of the spectrum is not very important for the calculation of the various absorption reaction rates and of the reactivity.

The situation is different for UO_2 - PuO_2 - H_2O lattices, due to the important low energy resonances of Pu^{239} and Pu^{240} at respectively 0.3 eV and 1.06 eV. When an important amount of plutonium is present in the fuel, these resonances cause important distortions in the thermal spectrum. This leads to a more important spectrum dependance of the various reaction rates and hence the reactivity. For systems containing plutonium, accurate spectrum calculation methods are thus required, methods developed for UO_2 - H_2O lattices being not necessarily valid for UO_2 - PuO_2 - H_2O ones.

When choosing and developing the calculational models, the following five neutronic differences between uranium and plutonium are to be kept in mind :

1. the existence of the two already mentioned Pu^{239} and Pu^{240} resonances, affecting the thermal spectrum;
2. the difference in magnitude between the thermal cross sections of Pu^{239} and U^{235};
3. the different reactivity worths of absorbing materials in plutonium and uranium lattices;
4. the difference between thermal fission cross sections of U^{235} and Pu^{239} lead to an important discontinuity in the power distribution at the boundary between UO_2 and UO_2 - PuO_2 fuel zones;

5. flux and power peaks are increased near the reflector and near water gaps when plutonium replaces uranium.

VI.2. The calculation codes

Figure VI.1 gives an idea of the structure of the PANTHER code chain, allowing cell, one- and two-dimensional calculations, if wanted with burnup.

Whereas the detailed geometry of lattices and configurations is accounted for in the 1, 2 or possibly 3 dimensional calculations, the basic physical properties are obtained with the cell code PANTHER, which calculates the spectrum and which determines on the basis of this spectrum the few group constants to be used in the dimensional calculations. The dimensional codes, mentioned in the figure, were developed by Belgonucléaire, except for SQUID and EREBUS (ref. VI.1 and 2); they solve the diffusion equation and calculate the reactivity, the power distribution and eventually the core burnup.

The spectrum calculation by the PANTHER code is based on the use of Cadilhac's secondary model in the thermal range, coupled to a multigroup structure similar to the one of the MUFT code (ref. VI.3). The internal structure of PANTHER and the theoretical models at its basis are discussed in detail in Appendix VI.1.

For the non-thermal cross-sections the MUFT-library, normally used in the LEOPARD code, has been adopted. For the thermal cross-sections analytical fittings of BNL 325 curves were chosen :

$$\sigma \sqrt{E} = a + \sum_{i=1}^{n} \frac{c_i}{b_i + (E - e_i)^2}$$

The 2200 m/s values of the fissile isotopes have been chosen as follows (all values in barns) :

isotope (origin)	U^{235} (BNL-Stehn)	Pu^{239} (GfK-J.J. Schmidt)	Pu^{241} (Westcott-1964)
σ_a	679	1031	1376,1
σ_f	578	742	1012,7
α	0.175	0.39	0.3589
ν	2.442	2.89	2.9779
η	2.078	2.0791	2.1913

For Pu^{240} the following absorption cross-section is used :

$$\sigma_a \sqrt{E} = \frac{\Upsilon K}{(\Upsilon + \eta \sqrt{E}) + 4 (E - E_o)^2} \qquad \text{(barns)}$$

with : $\Upsilon = 0.0296$ $\qquad \eta = 0.0024$

$K = 6250$ $\qquad E_o = 1.0575$

For the few group calculations the following group structure is normally used :

I. 10 MeV to 821 keV : in this energy range the inelastic scattering and the fast fissions in U^{238} take place;

II. 821 keV to 5.53 keV : here the neutron removal is primarily due to the important scattering cross section of hydrogen; these two first groups contain the fission spectrum;

III. 5.53 keV to 1.855 eV : in this range the scattering cross section of hydrogen is constant, so that the flux varies according to a 1/E law, except at the resonance positions;

IV. below 1.855 eV : thermal range, chosen intentionally rather wide, in order to include the Pu^{240} resonance at 1.057 eV.

isotope (origin)	U^{235} (BNL-Stehn)	Pu^{239} (GfK-J.J. Schmidt)	Pu^{241} (Westcott-1964)
σ_a	679	1031	1376,1
σ_f	578	742	1012,7
α	0.175	0.39	0.3589
ν	2.442	2.89	2.9779
η	2.078	2.0791	2.1913

For Pu^{240} the following absorption cross-section is used :

$$\sigma_a \sqrt{E} = \frac{\gamma K}{(\gamma + \eta \sqrt{E}) + 4 (E - E_o)^2} \qquad \text{(barns)}$$

with : $\gamma = 0.0296$ $\qquad \eta = 0.0024$

$K = 6250$ $\qquad E_o = 1.0575$

For the few group calculations the following group structure is normally used :

I. 10 MeV to 821 keV : in this energy range the inelastic scattering and the fast fissions in U^{238} take place;

II. 821 keV to 5.53 keV : here the neutron removal is primarily due to the important scattering cross section of hydrogen; these two first groups contain the fission spectrum;

III. 5.53 keV to 1.855 eV : in this range the scattering cross section of hydrogen is constant, so that the flux varies according to a 1/E law, except at the resonance positions;

IV. below 1.855 eV : thermal range, chosen intentionally rather wide, in order to include the Pu^{240} resonance at 1.057 eV.

VI.3. Code calibration

The calibration of the described codes has been undertaken in two phases. First it was done on the basis of the experimental Hanford-BNWL and Saxton results; the main results of this work are presented in Appendix VI.2. Then the testing of the codes was continued, using the VENUS results as reference data. This work is the subject of the following chapters of this report. Let us just remember here that the final purpose is to obtain calculational tools allowing the achievement of the following accuracies :

± 0.5 to 1 %	on k_{eff}
± 5 %	on power distribution
± 1 %	on reactivity during burnup
± 20 %	on reactivity coefficients
± 10 %	on control rod worth

VI.4. Calculation of the nuclear parameters

The various nuclear parameters are calculated by means of the calculational tools indicated in figure VI.1; for each of them a calculational procedure has to be defined.

a) Multiplication factor : k_{eff}

In a first step, a cell calculation with the PANTHER code provides few group constants, which can then be used for the calculations with the one, two or three dimensional diffusion codes, by which the reflector can be explicitly represented for the considered directions. The multiplication factor can also be obtained by a cell calculation, the leakage being taken into account through an experimentally determined material buckling; this procedure can of course only be used for single fuel region lattices. Comparing both methods, the diffusion calculations (1D, 2D or 3D) seem to be mainly advisable for small systems with high leakage. An important trend in function of the geometrical dimensions (B^2) of a series of different critical configurations

appears when comparing the multiplication factors obtained by a cell calculation and by one or two dimensional diffusion calculations : figures VI.2 and 3 illustrate this statement.

b) Power distributions

The comparison of the calculated local power peak values near a reflector or near a water gap with experimental values and also with values obtained with more elaborated calculational tools (e.g. based on transport theory instead of diffusion theory) has led to the decision of using in the diffusion calculations thermal MND cross-sections (ref. VI.4).
Appendix VI.3 summarizes the main differences between conventional and MND thermal cross-section calculations.

c) Control rod worth calculations

In order to meet the 10 % accuracy requirement, if possible with a not too expensive method, a few methods, chosen among the numerous ones described in the literature, were investigated; although the work is still underway, it can be said that with the following two methods rather good results were obtained :

- B_4C rod region few group constants, generated by a PANTHER cell calculation;
- B_4C rod region few group constants, generated by Henry's method (ref. VI.5).

References

VI.1. SQUID : EUR-3682
VI.2. EREBUS : FN-E-88
VI.3. MUFT : WAPD-TM-224
VI.4. R.J. BREEN : Nu Sc Eng 9 (1961)
VI.5. A.F. HENRY : WAPD-218

CHAPTER VII : REALIZATION OF THE PROGRAMME

VII.1. Introduction

The aim of this chapter is to describe the configurations studied in the frame of the Euratom contract, to present the obtained experimental results and the corresponding theoretical ones. All these results were found using the experimental and the theoretical methods and techniques described in the two preceding chapters. In this chapter we will limit ourselves to a mere presentation of results; the discussion on the agreement between experimental and theoretical results will be presented in the next chapter. In a few cases only experimental results are given.

During the realization of the programme a reference number was given to each type of configuration, starting from 1. As in most of these configurations minor variations were made several times in order to adapt them better to each kind of measurement, subnumbers were introduced, the notation being e.g. 1/1. Not for all these configurations a map has been included in this report; only the most important ones were chosen. The configuration numbers, mentioned in the present report, go from 1 to 10; table VII.1 summarizes to which type of configurations they correspond. Rather than discussing configuration per configuration, it will be tried to group the different investigations in the most logical way.

VII.2. k_{eff} and B^2 for one zone configurations

(involved configurations : 1, 2, 3, 4, 5, 6, 8 and 8 bis)

One zone configurations were realized for different fuels (4/0 and 3/1), with different pitches (p_{SENA}, $p_{SENA}\sqrt{2}$, $2\,p_{SENA}$) and in different geometries (cylindrical and rectangular configuration sections). In all cases the nominal moderator level was adopted.

For the cylindrical cases it was of course tried to come with the actual configuration as close to the ideal cylindrical one

as possible. Several measurements were done to study the influence of the imperfect simulation of the cylindrical shape; this was done by slightly rearranging the peripherical rods. It was found that in the case of the SENA pitch the differences were almost negligible, but for the $p_{SENA}\sqrt{2}$ pitch the effect was found to be more important : the resulting possible error on the measured k_{eff} due to this geometrical effect was estimated at $^{+\ 0.04}_{-\ 0.08}$ % $\Delta k/k$. These different conclusions are due to the fact that in the case of the SENA pitch the number of rods to get critical is almost three times larger than in the other case.

For the rectangular configurations, it was tried to realise complete rectangles, i.e. without incomplete rows at the periphery, and as close as possible to a square.

For the 3/1 fuel the case of the SENA pitch could not be done, as the available number of rods was lower than the critical mass; for the 4/0 fuel the 2 p_{SENA} pitch was not considered, as at the time of the measurements not enough of that fuel was available and as, anyhow, the case of that pitch was considered as very secondary, the 3/1 configurations characterized by it giving already a sufficient indication.

Table VII.2 lists for eight configurations the number of rods, the experimental and calculated k_{eff} values and the experimental value of a peripherical rod. This last value is only given in the case of the cylindrical configurations; they are average values, obtained from reactivity measurements done on a few slightly supercritical configurations. Actually the real value of the individual peripherical rods can be very different, due to the importance of their exact localization with respect to the configuration boundary. This can easily be understood when one looks e.g. at the shape of configuration 5, represented in figure VII.1, or even at the one of configuration 8 bis (figure VII.2), where the number of rods is much higher. Figures VII.3 and 4 represent the two cylindrical configurations with the $p_{SENA}\sqrt{2}$ pitch (configurations 1 and 3).

In table VII.2 the just-critical number of rods is given for the cylindrical configurations, whereas for the rectangular ones the experimental k_{eff} values corresponding to the realized complete rectangles are given. As these rectangles' geometry is

of course very simple, no plans are given in this report.

The theoretical k_{eff} values were obtained with one- or two-dimensional calculations, enabling a correct geometrical representation of the radial reflector; axial leakage was accounted for by using the experimental axial buckling value. The table shows a remarkable agreement.

Buckling determination

In six of the eight configurations axial buckling values were determined, as well as the extrapolation lengths. Table VII.3 presents the principal results.

For all B^2_{ax} measurements the two techniques (fission chamber and fission product γ-scanning) were used; the results did agree very well in all cases, so that average values were calculated. After a small correction, applied to take into account the difference between the real fuel length (e.g. 49.50 cm) and the theoretical one (50.00 cm), these average values did lead to the ones given in the first column of the table. Next to them are the corresponding total extrapolation length values.

For five configurations the radial buckling and extrapolation length were determined too. In the case of the rectangular configurations measurements were done for that along two orthogonal axes, as can be seen from the same table VII.3. The γ-scanning technique was used. Summing up B^2_{ax} and B^2_{rad} and applying a correction, when the k_{eff} of the configuration was slightly different from unity, the material buckling was obtained. From these final results (last column of the table) appears clearly that the error margin is sensibly higher for the 3/1 fuel than for the 4/0 one; this is due to the fact that that plutonium bearing fuel was vibrocompacted, and even of the heterogeneous type in some cases.

A close look to all the values given in the table allows several interesting conclusions; one sees e.g. the agreement within error margins of the B^2_{ax} and B^2_{mat} values found for the cylindrical and rectangular configurations of the same type. Furthermore there

is the fact that, at least for all the 4/0 configurations, the axial and radial extrapolation lengths are found to be equal (always within the error margins); this indicates that the presence of both fuel ends in the axial reflector does not change its reflective properties (cfr chapter II : fuel ends in plexiglass).

VII.3. k_{eff} and B^2 for two-concentrical-zone configurations

(involved configurations : 7 and 7 bis)

As not enough 3/1 fuel was available to realize a one zone configuration with the SENA pitch, two-zone configurations, both cylindrical and rectangular, were studied with a central 3/1 zone and a peripherical 4/0 one. They are represented in the figures VII.5 and VII.6. In the cylindrical one the central zone was chosen as large as possible; as can be seen on the figure it was composed of 332 rods. In the rectangular one, on the contrary, a smaller number was chosen (a 14 x 14 = 196 square), in order to allow a more straightforward comparison with later experiments with two types of 2/2.7 fuel, not to be discussed in this report.

All the results are summarized in table VII.4; its presentation is similar to the one previously used for the one zone configurations. This means e.g. that again the B^2_{ax} values were corrected in order to be relative to an exact 50 cm active length.
It can be seen that these B^2_{ax} values are equal to the one found in a pure 4/0 configuration with the SENA pitch (configuration 8). In the radial direction, only the buckling for the central zone was determined.

The theoretical k_{eff} values given in the table result from criticality calculations done with conventional, i.e. non-MND corrected, cross-sections. These values practically do not change, when the MND cross-sections are used in the appropriate way, as described in the previous chapter.

VII.4. Radial fission density distributions in the one- and two-concentrical-zone configurations

(involved configurations : 1, 2, 3, 4, 7 and 8)

For all the configurations for which the B^2_{rad} was given in what precedes, the corresponding experimental fission density distributions are available, as they were used to find the B^2_{rad} values through cosine or J_o fitting procedures. In the case of rectangular configurations, the two orthogonal axes were measured, whereas in the cylindrical ones two appropriate diameters were chosen, in most cases making a 45° angle with each other.

Some of the results are shown in figures VII.7, 8 and 9. In the first and last cases the configuration was cylindrical (configurations 1 and 7) and the fitting did happen with a J_o function; one can distinguish the two sets of points, measured along the different diameters.
Figure VII.8 gives an example of a distribution along an axis of one of the studied rectangular configurations, number 4/1; in this case a cosine fitting was made.

VII.5. Small zone substitution studies

(involved configurations : 4, 6 and 7)

Substitution experiments have been carried out in a relatively small zone of 4 x 4 = 16 rods, located at the center of configurations, essentially composed of vibrocompacted, heterogeneous 3/1 fuel rods. This has been done for the three different pitches.

In the substitution zone not only 4/0 and 2/2.7 fuels have replaced the reference 3/1 fuel, but it was also tried to determine the reactivity difference due to several fabrication procedures used for some of the 3/1 fuel rods. The results are presented in table VII.5. The notation ≃ 0 means that the measured results did not exceed in absolute value 0.004 % Δk_{eff}, which was the experimental precision. The k_{eff} values themselves are not given, as they have no importance here; the configuration types used correspond to the previously discussed cases 4, 6 and 7.

It can be seen that for none of the pitches a difference was measured between the two types of vibrocompacted rods (heterogeneous and homogeneous ones), this conclusion remaining valid when the vibrocompacted rods are compared to the swaged ones with the same cladding thickness. In the case of the swaged rods with a slightly thicker cladding (the same as the one of the 4/0 and 2/2.7 fuels) a reactivity decrease was of course noticed. As for the 4/0 results, they show that this fuel is more reactive than the 3/1 one in the case of the SENA pitch and less for the other pitches; this conclusion is confirmed by the ones obtained from the measurements described in the preceding paragraphs VII.2 and VII.3.

Theoretical calculations, corresponding to these measurements, were made. Special attention was devoted to the comparison between the heterogeneous and the homogeneous vibrocompacted 3/1 fuels. In order to simulate the heterogeneity in the calculation, a radial plutonium distribution model was defined on the basis of some radiographs. For the calculation itself it was necessary to have codes allowing the representation of the fuel zone in the unit cell in several regions. Two codes were used : PANTHER with its Bonalumi option and LASER [Ref. VII.1]. The results found for the k_∞ values are the following ones :

k_∞	P_{SENA}		$P_{SENA}\sqrt{2}$	
	VIB. HOM.	VIB. HET.	VIB. HOM.	VIB. HET.
PANTHER	1.3338	1.3344	1.3937	1.3955
LASER	1.3367	1.3370	1.4089	1.4107

It can be seen from these results that both codes agree rather well. In order to compare these results with the experimental ones, the Δk_∞ values are to be reduced to Δk_{eff} values, taking into account the relative weight of the 16 central rods in a critical loading. In the SENA pitch case, Δk_{eff} is found negligibly small, whereas the case of the $p_{SENA}\sqrt{2}$ pitch leads to a more significant value. Further discussion on these results will be presented in the next chapter.

VII.6. Upper reflector reactivity value

(involved configurations : 3, 4, 5, 6 and 7)

The knowledge of the reactivity value of the upper reflector can be very useful, and is actually in some occasions even required, during the measurements, e.g. when determining the k_{eff} of a slightly subcritical configuration from counting rates at different moderator levels in the upper reflector part.

This value can be obtained from the curve giving $\Delta k/k$ as a function of the water level; it was found that this curve practically does not depend on the type of fuel or the geometrical shape of the configuration, but in the first place on the lattice pitch. So it was determined for the three considered pitches, using each time a large number of period measurements, carried out in several configurations with the same pitch.

The three curves are compared in figure VII.10. The three reflector reactivity values deduced from them are;

p_{SENA}	: 0.22 ± 0.01 % $\Delta k/k$
p_{SENA} 2	: 0.34 ± 0.01 % $\Delta k/k$
2 p_{SENA}	: 0.37 ± 0.01 % $\Delta k/k$

VII.7. Systematical study of local perturbations in 4/0 and 3/1 SENA pitch lattices

The systematical study of local perturbations was done at the center of configuration 8 for the 4/0 fuel and in the central slab of configuration 10 for the 3/1 fuel. In both cases three types of perturbations were considered : an absorbing one (B_4C rods), an overmoderating one (H_2O gaps) and an intermediate one (aluminium plate or rod); the length of the (always linear) perturbation varied from one to seven equivalent unit cells. The study included the determination of the reactivity effect of the perturbations, their influence on power distribution, and, in some cases, their influence on spectral index values.

The choice of these three types of perturbations was decided on the basis of three particular situations which are met when one has to make design calculations for a power reactor. The B_4C rods correspond of course to a situation "control rod in"; as absorbing material B_4C was chosen, rather than the e.g. in SENA used Ag-In-Cd alloy, in order to be sure to test the formalism for the treatment of heavy absorbers, the absorption cross section knowledge being much better for boron than for the elements constituting the mentioned alloy. The B_4C rods, replacing fuel rods in the lattice, have the same characteristics as the 4/0 fuel rods : same active length and same cladding tube; their active diameter is 9.02 mm and their density is equal to 60 % of the theoretical one.

When control rods are removed out of the core and when they do not have followers, water gaps are created. Although there are followers in the particular case of the SENA reactor, this type of perturbation has extensively been studied due to its importance in connection with safety aspects : the correct prediction of power peaking values near highly moderating local lattice perturbations is very important.

A third type of lattice perturbation, met in power reactors is the presence of metal channels surrounding the fuel assemblies; in the case of SENA this metal is stainless steel. The important point about this kind of perturbation however is not the presence of the metal, but in the first place the local changes of the moderation. Therefore an aluminium plate was realized (length = seven pitches) with a thickness, determined such that the quantity of water between it and the adjacent row of fuel rods is the same as in the case of real fuel assemblies between fuel and channel. This thickness was found to be equal to 9.05 mm; for the height of the plate 50 cm was taken; 99.5 % pure aluminium was used.

In order to be able to complete a set of one cell perturbations analogous to the one of seven cells, an Al rod of the same purity as the plate was used; it had a diameter of 9.8 mm and a length equal to the overall length of the fuel rods (74.4 cm).

Before discussing in more detail all the results found in the presence of these perturbations, a paragraph will be devoted to the unperturbed reference configurations.

VII.7.1. Unperturbed reference configurations

The basic reference configuration is a rectangular one consisting completely of 4/0 fuel : 27 x 32 rods. It is the one for which the k_{eff} was given in paragraph VII.2; its number is 8/0. Its width of 27 rods has been kept unchanged in all further configurations to be discussed in this report (8, 9 and 10); this 27 rod side is parallel with the X-axis, adopted for the representation of the configurations on the maps. For the power distribution studies, the rods located on this X-axis are chosen, the perturbation direction coïnciding with the Y-axis.

The radial power distribution along the X-axis is represented in figure VII.11; in fact it served for the determination of the radial buckling in that direction, the result of which was given in table VII.3 : $(4230 \pm 160)\ 10^{-6}\ cm^{-2}$.

Whereas the just quoted 4/0 reference configuration was critical very near the nominal moderator level, configuration 10, used for the corresponding measurements in the 3/1 fuel, was from the beginning chosen large enough to be still critical with 7 B_4C rods (see figure VII.12), so that without perturbation it is critical at a reduced water level. This does of course not matter for the determination of the radial power distribution, which was obtained in the same way as in the case of the 4/0 fuel; the corresponding B^2_{rad} value was found to be equal to $(4000 \pm 80)\ 10^{-6}\ cm^{-2}$, i.e. within the error margins practically the same as for the 4/0 fuel.

The radial distribution in the 3/1 fuel is represented in figure VII.13, where it is compared with two theoretical distributions, one being obtained with conventional cross-sections, the other one with cross-sections modified according to the MND formalism. It is clear that the power peak near the reflector is calculated much better with the second method.

VII.7.2. Reactivity effects

The measurement method of the reactivity effect due to the insertion in the lattice of a perturbation has been described in a previous chapter; it is based on the determination of a $\partial\rho/\partial h$ curve (reactivity variation as a function of water level variation).

The 4/0 configuration in which the perturbations were realized is represented in figure VII.14; its number is 8/4. One sees at the periphery in the Y-direction two small 3/1 zones; they were necessary in order to make the configuration critical with 7 B_4C rods, the available number of 4/0 rods not being sufficient at that moment. In the case of the measurements in the 3/1 zone, a similar thing had to be done with 4/0 rods, as can be seen on the map of configuration 10 (figure VII.12).

The results for all the measured perturbations in both configurations are summarized in table VII.6. The corresponding theoretical values, given in the table, were obtained with four group MND cross-sections, determined with the PANTHER code in its SPECTROX version. For the B_4C perturbations this calculation procedure appeared to be the best one, as will be shown by a detailed discussion, presented in the next chapter.

VII.7.3. Influence of local perturbations on power distributions

All power distributions were determined along the X-axis. First it was checked in the absence of perturbations that this radial distribution is completely independent of configuration changes at the periphery in the Y-axis direction, such as e.g. in the case of configurations 8/0 and 8/4, with respectively (27 x 32) 4/0 rods and (27 x 33) 4/0 rods plus (27 x 6) 3/1 rods (figure VII.14).

The distribution was measured for six perturbations, namely B_4C, H_2O and Al ones, each of them having a size corresponding to one, respectively seven cells. This was done for both the 4/0 and 3/1 fuels. The results are represented in figures VII.15 and 16, on which the experimental and theoretical distri-

butions can be compared. These theoretical distributions were obtained with MND cross-sections, using the SPECTROX version in the PANTHER calculations.

VII.7.4. Influence of local perturbations on the Pu_f^{239}/U_f^{235} spectrum index

The radial evolution of the Pu_f^{239}/U_f^{235} spectrum index has been measured in the 3/1 fuel (configuration 10) in the absence and in the presence of two extreme perturbations (7 H_2O cells and 7 B_4C rods). The results are given in table VII.7. In the case without perturbation, the spectrum is at equilibrium between the positions X = -19 and X = +1; an average value of the spectrum index of 1.91 $\pm$ 0.03 has been deduced. In the table one can see the decrease of the spectrum index near a water region (both the gap and the reflector) and its slight increase near a B_4C perturbation.

VII.8. A cruciform large H_2O perturbation

A large H_2O perturbation in the form of a cross has been realized in a configuration of type 8 : the rods on the two orthogonal axes of a (27 x 33) 4/0 fuel configuration were removed (configuration 8/5). The main aim of this type of experiment was to check the power distribution near the cross. The comparison between the experimental and the theoretical results (MND cross-sections) is shown in figure VII.17.

The k_{eff} value of the configuration with this cross was also determined and can be compared with the k_{eff} value of the unperturbed configuration (27 x 33 rods) and the ones of the same configuration with a 7 H_2O cell perturbation in its center and the Al plate :

Configuration	k_{eff}
without perturbation	1.0042 ± 0.0002
with Al plate	1.0016 ± 0.0001
with 7 H_2O cells	1.0068 ± 0.0003
with the H_2O cross	1.0143 ± 0.0005

VII.9. Study of the boundary between 4/0 and 3/1 fuel zones

Configuration 9, represented in figure VII.18, is essentially composed of two rectangular slabs of respectively 4/0 and 3/1 fuel. Their dimension in the Y-direction is sufficiently important to assimilate the configuration for calculation purposes to two contiguous infinite slabs, so that a one-dimensional calculation model along the X-axis can be adopted. The study was focussed on two important aspects : power distribution and Pu_f^{239}/U_f^{235} spectrum index determination. In paragraph VII.10 the influence of local perturbations at the boundary on the same nuclear characteristics will be described.

VII.9.1. Power distribution near the boundary

For the determination of the power distribution in each zone, two experimental techniques have been used, namely Y-scanning of undismountable fuel rods and pellet activation counting. The results were found to be in excellent agreement. The normalisation of the distributions to each other was carried out as described in chapter V; the normalization factor was obtained through two measurement techniques : pellet (La^{140} activity)and foil (Pu^{239}/Al and U^{235}/Al foils) counting; both techniques did lead to comparable results.

Figure VII.19 presents the resulting, normalized power distribution, as well as the calculated one. On the figure the radial distribution in the case of a one zone configuration (a cosine) is also represented, in order to illustrate the difference between both cases.

VII.9.2. Pu_f^{239}/U_f^{235} Spectrum Index values

The Pu_f^{239}/U_f^{235} spectrum index has been measured at several rod locations along the X-axis, as is shown on figure VII.20; only the values corresponding to the equilibrium spectrum were compared with theoretical ones deduced from the respective cell calculations.

Region	$\left(\frac{\vartheta_f^{239}}{\vartheta_f^{235}}\right)_{EXPER.}$	$\left(\frac{\vartheta_f^{239}}{\vartheta_f^{235}}\right)_{PANTHER}$	$\left(\frac{\vartheta_f^{239}}{\vartheta_f^{235}}\right)_{GMS-1}$
3/0	$1.92 \begin{smallmatrix}+0.04\\-0.08\end{smallmatrix}$	2.07	1.98
4/1	$2.19 \begin{smallmatrix}+0.03\\-0.08\end{smallmatrix}$	2.22	2.12

It can be seen that the difference between the two fuels as calculated with the two theoretical models (PANTHER on one side, the GMS transport DSN code on the other) is only half as important as experimentally established.

VII.10. Local perturbations at the boundary between 4/0 and 3/1 fuel zones

The aim of this study was to combine two difficulties, investigated before separately. Only experimental results are reported. The measurements were done in configuration 9/1, which is the same as configuration 9, represented in figure VII.18, except that the number of fuel rod rows in the Y-direction was larger, in order to remain critical with the B_4C perturbations. The chosen perturbations were limited to the most important ones : 7 B_4C rods, 7 H_2O cells and the Al plate with a length of 7 pitches.

The resulting power distributions are given in figure VII.21, where they can be compared with the distributions in the respectively two zone and one zone cases without perturbations.

For the same perturbation cases, the evolution of the spectrum index Pu_f^{239}/U_f^{235} was determined. The results are summarized in figure VII.22, where the deviation near the perturbations can be seen; again the case of the water gap shows the most important effect.

VII.11. Fission density depressions inside fuel rods

In the central part of the two zones (4/0 and 3/1) of configuration 9, described in the preceding paragraphs, special measurements were done in order to determine the fission density depression inside a 4/0 and a 3/1 fuel rod, both thus being located in a zone where the spectrum is at equilibrium.

Two methods were used : the track counting method, using mica foils, and fissile (U^{235}/Al and Pu^{239}/Al) foils, cut into several concentrical rings. The results obtained for both fuels with these two methods are given in figure VII.25; the curves are given in a discontinuous form, due to the nature of the ring results; the track counting results did of course lead to a continuous curve. Two sets of theoretical results are also presented. One of them was obtained with a GAS-calculation (a DSN transport code) using GAS-1 library constants, whereas the other one was obtained with a WDSN code using THERMOS calculated cross-sections; these last result was kindly made available by CNEN (La Casaccia).

From the figure one can conclude that the two types of experimental results agree rather well with each other, as well as with the WDSN-THERMOS results. The other theoretical results are less satisfying; it is believed that this might be due to an uncorrect thermal scattering matrix for hydrogen in the GAS-1 library.

References

VII.1 C.G. PONCELET : Burnup Physics of Heterogeneous Reactor Lattices; WCAP-6009 (June 1965).

TABLE VII.1 : REVIEW OF THE DISCUSSED CONFIGURATIONS

Number	Pitch	Fuel	Geometry
1	$P_{SENA}\sqrt{2}$	4/0	cylindrical
2	$P_{SENA}\sqrt{2}$	4/0	rectangular
3	$P_{SENA}\sqrt{2}$	3/1	cylindrical
4	$P_{SENA}\sqrt{2}$	3/1	rectangular
5	$2\,P_{SENA}$	3/1	cylindrical
6	$2\,P_{SENA}$	3/1	square
7	P_{SENA}	3/1 and 4/0	two concentrical zones, cylindrical geometry; 3/1 in the center
7 bis	P_{SENA}	3/1 and 4/0	two concentrical zones, square geometry; 3/1 in the center
8	P_{SENA}	4/0	rectangular
8 bis	P_{SENA}	4/0	cylindrical
9	P_{SENA}	3/1 and 4/0	two contiguous rectangular slabs of 3/1 and 4/0
10	P_{SENA}	3/1 and 4/0	rectangular 3/1 zone, completed with two lateral 4/0 zones

TABLE VII.2 : ONE ZONE CONFIGURATIONS

Config. number	Pitch	Fuel	Geometry	Number of rods	k_{eff}, exp.	k_{eff}, theor.	Experimental value of a peripherical rod
8 bis	p_{SENA}	4/0	CYL	824	1.0000	1.0021	0.018 % $\frac{\Delta k}{k}$
8	p_{SENA}	4/0	RECT	27 x 32 = 864	1.0002	1.0004	-
1	$p_{SENA}\sqrt{2}$	4/0	CYL	351	1.0000	0.9973	0.043 % $\frac{\Delta k}{k}$
2	$p_{SENA}\sqrt{2}$	4/0	RECT	17 x 22 = 374	1.0007	0.9977	-
3	$p_{SENA}\sqrt{2}$	3/1	CYL	299	1.0000	0.9994	0.063 % $\frac{\Delta k}{k}$
4	$p_{SENA}\sqrt{2}$	3/1	RECT	15 x 21 = 315	0.9974	0.9982	-
5	$2\ p_{SENA}$	3/1	CYL	363	1.0000	0.9907	0.028 % $\frac{\Delta k}{k}$
6	$2\ p_{SENA}$	3/1	RECT	20 x 20 = 400*	1.0017	0.9985	-

* The actual configuration was composed of 18 x 18 = 324 rods of 3/1 fuel, plus 76 rods of 4/0 fuel at the periphery.

TABLE VII.3 : ONE ZONE CONFIGURATIONS

CONFIGURATION CHARACTERISTICS (pitch - fuel - geometry)	$B_{ax}^{2\,(EXP)}$ (10^{-6} cm^{-2})	$2\,\lambda_{ax}^{(EXP)}$ (cm)	$B_{rad}^{2\,(EXP)}$ (10^{-6} cm^{-2})	$2\,\lambda_{rad}^{(EXP)}$ (cm)	$B_{mat}^{2\,(EXP)}$ (10^{-6} cm^{-2})
P_{SEMA} - 4/0 - RECT $\begin{cases}27\\x\\32\end{cases}$	2435 ± 10	13.67 ± 0.14	$\begin{cases}4230 \pm 160\\3240 \pm 30\end{cases}$	$\begin{cases}13.10 \pm 0.93\\13.48 \pm 0.24\end{cases}$	9910 ± 170
P_{SEMA} √2 - 4/0 - CYL	2569 ± 7	11.98 ± 0.15	8724 ± 40	12.20 ± 0.12	11418 ± 41
P_{SEMA} √2 - 4/0 - RECT $\begin{cases}17\\x\\22\end{cases}$	2584 ± 11	11.80 ± 0.18	$\begin{cases}5236 \pm 64\\3620 \pm 28\end{cases}$	$\begin{cases}12.09 \pm 0.27\\11.67 \pm 0.20\end{cases}$	11481 ± 37
P_{SEMA} √2 - 3/1 - CYL	2582 ± 19	11.82 ± 0.26	10710 ± 300	10.54 ± 0.54	13300 ± 300
P_{SEMA} √2 - 3/1 - RECT $\begin{cases}15\\x\\21\end{cases}$	2603 ± 24	11.58 ± 0.30	$\begin{cases}6158 \pm 147\\4335 \pm 159\end{cases}$	$\begin{cases}12.39 \pm 0.47\\9.02 \pm 0.85\end{cases}$	12980 ± 240
$2\,P_{SEMA}$ - 3/1 - CYL	2590 ± 23	11.73 ± 0.28	-	-	-

TABLE VII.4 : TWO CONCENTRICAL ZONE CONFIGURATIONS (p_{SENA})

CONFIG. NUMBER	OVERALL GEOMETRY	CENTRAL ZONE	OUTER ZONE	k_{eff}, exp.	k_{eff}, theor.	Experimental value of a peripherical rod
7	CYL	332 3/1 rods	580 4/0 rods	1.0009	1.0049	0.016 % $\frac{\Delta k}{k}$
7 bis	SQUARE (30 x 30 rods)	14 x 14 = 196 3/1 rods	704 4/0 rods	0.9965	1.0025	-

CONFIG.	ZONE	$B_{ax}^{2\,(EXP)}$ (10^{-6} cm^{-2})	$2\,\lambda_{ax}^{(EXP)}$ (cm)	$B_{rad}^{2\,(EXP)}$ (10^{-6} cm^{-2})
7	3/1	2438 ± 18	13.62 ± 0.18	5780 ± 140
7	4/0	2399 ± 16	14.14 ± 0.32	-

TABLE VII.5 : SMALL ZONE SUBSTITUTION STUDIES

(4 x 4 = 16 rods zone in the center of 3/1 configurations; the results are Δk_{eff} values in %; the experimental precision is $\pm$ 0.004)

SUBSTITUTION ZONE			P_{SEMA}		$P_{SEMA}/2$		$2\ P_{SEMA}$	
Enrichm.	Fabrication	Cladding thickness	EXP.	Theory	EXP.	Theory	EXP.	Theory
3/1	VIB. MET.	0.25	0	0	0	0	0	0
3/1	VIB. HOM.	0.25	≃ 0	≃ 0	- 0.004	- 0.001	≃ 0	
3/1	SWAGED	0.27	≃ 0		- 0.014	- 0.047	≃ 0	
3/1	SWAGED	0.38	- 0.058		- 0.182	- 0.228	- 0.177	
4/0	PELLETS	0.38	+ 0.094		- 0.237	- 0.270	- 0.566	
2/2.7	VIB. HOM.	0.38	- 0.092		-	-	- 0.090	

TABLE VII.6 : REACTIVITY EFFECTS OF VARIOUS PERTURBATIONS IN 4/0 AND 3/1 FUELS

PERTURBATION NATURE	4/0 FUEL (configuration 8/4)		3/1 FUEL (configuration 10)	
	EXPERIMENT	THEORY (MND; 4 groups)	EXPERIMENT	THEORY (MND; 4 groups)
1 B_4C rod	- 0.59 ± 0.01	- 0.52	- 0.44 ± 0.02	- 0.42
2 B_4C rods	- 0.99 ± 0.01		- 0.79 ± 0.02	- 0.73
3 B_4C rods	- 1.36 ± 0.02	- 1.38	- 1.08 ± 0.02	- 1.01
4 B_4C rods	-		- 1.38 ± 0.02	- 1.30
5 B_4C rods	- 2.03 ± 0.02	- 2.11	- 1.66 ± 0.03	- 1.59
6 B_4C rods	- 2.35 ± 0.03		- 1.92 ± 0.03	- 1.87
7 B_4C rods	- 2.70 ± 0.03	- 2.80	- 2.19 ± 0.03	- 2.14
1 H_2O cell	+ 0.032 ± 0.005	+ 0.048	+ 0.056 ± 0.016	+ 0.042
7 H_2O cells	+ 0.190 ± 0.010	+ 0.25	+ 0.283 ± 0.013	+ 0.33
1 Al rod	- 0.016 ± 0.005		~ 0	
1 Al plate	- 0.200 ± 0.010		- 0.105 ± 0.013	

TABLE VII.7 : Pu^{239}/U^{235} SPECTRUM INDICES

(Configuration 10 : 3/1 fuel, p_{SENA})

Measurement position	No perturbation	7 H_2O cells	7 B_4C rods
reflector			
+ 4	1.65 ± 0.03		
+ 3	1.86 ± 0.03		
+ 2	1.84 ± 0.03		
+ 1			
0	1.90 ± 0.03		
- 1			
- 2		1.91 ± 0.03	1.88 ± 0.03
- 3	1.93 ± 0.03		
- 4		1.89 ± 0.03	1.93 ± 0.03
- 5			
- 6		1.92 ± 0.03	1.90 ± 0.03
- 7			
- 8		1.81 ± 0.03	1.95 ± 0.03
- 9	1.96 ± 0.03	PERTURBATION POSITION	

CHAPTER VIII : COMMENTS ON THE COMPARISONS BETWEEN THEORETICAL AND EXPERIMENTAL RESULTS

VIII.1. Introduction

In this chapter we will shortly comment on the various comparisons between theoretical and experimental results, presented in the preceding chapter. This will be done systematically for each parameter. As was stated before and as can be seen e.g. from table VII.1, only the 4/0 (UO_2) and 3/1 (UO_2 - PuO_2 with about one third of the fissions in the plutonium) fuels are concerned in this discussion.

VIII.2. Multiplication factor calculations

The procedure adopted for the calculation of this parameter has led to very satisfactory results; this appears clearly from the results listed in table VII.2 : the agreement is always better than 0.5 % Δk_{eff}, except in one case, where the disagreement remains however acceptable. This set of results gives us a particular confidence in the ability of our methods to calculate the k_{eff} of configurations, constituted by the considered fuel types. Moreover it is quite important to stress that the various lattices are relevant to quite different moderator to fuel volume ratios, so that the confidence is not limited to the case of PWR lattices, such as the SENA one, but can be extended to BWR lattices. The very large moderator to fuel ratios allow a severe check of the events taking place in the thermal energy range, as in these cases the heterogeneity degree in the cell, i.e. the disadvantage factor, is increased. The one fuel zone lattices constitute of course the best check of the k_{eff} calculation procedure; table VII.4 illustrates however also that the k_{eff} calculated for two zone configurations, are close to the experimental values.

It should be outlined furthermore that the lattice with 4/0 fuel and the SENA pitch is a very important one in the scope of our programme; from table VII.2 it appears that for both the rectangular and the cylindrical geometries the agreement is very close.

VIII.3. Power distribution calculations

Although the procedure applied for power distribution calculations has been described in chapter VI, it is worthwile to summarize here the essential steps :

- the power distribution is calculated by means of diffusion calculations (1D, 2D or 3D), using a few group scheme (4 neutron groups);
- the few group cross sections are generated by a cell calculation taking into account the leakage by means of a total material buckling;
- the few group cross sections attributed to each region correspond to the equilibrium spectrum of the considered region;
- the MND formalism is used for the thermal cross sections, because this formalism leads to a better prediction of the power near water gaps and near the reflector.

The purpose of the various experiments leading to comparisons between experimental and theoretical power distributions is to check how well the methods described previously are able to predict this important nuclear parameter in situations which normally occur in power reactors, in situations specific to the recycling of plutonium in power reactors, and also in more complicated situations, constituting still more severe tests.
A first situation to be investigated is met in lattices with different fuel regions, especially when one of them contains plutonium and another one does not. The study of the power sharing in such cases is quite important for the recycling of plutonium in light water reactors.

Due to the difference in magnitude of the fission cross sections of U^{235} and Pu^{239} an important discontinuity of the power distribution occurs at the boundary between the two kinds of fuel. The study of configuration 9 is representative of this problem. The calculated distribution is in good agreement (fig. VII.19) with the experimental distribution, but one should keep in mind that in the 3/1 fuel only one third of the fissions occur in the plutonium; therefore the further check of this kind of situation in the case of higher plutonium enrichments remains necessary.

The power distributions near various perturbations, created in regular lattices, such as e.g. local B_4C rod or H_2O gap zones, constitute another important problem for the theoretical tools. Their ability to predict accurately such power values should be ensured, as in a power reactor various lattice perturbations exist. Therefore the power distribution has been measured and calculated in presence of various perturbations in the two considered fuels (4/0 and 3/1). From fig. VII.15 and VII.16 it appears that the agreement is satisfactory, except in the presence of the B_4C rods. Fig. VII.17 is relative to a configuration constituting a very severe test of the power distribution calculation procedure; it was more particularly intended to prove the validity of the MND cross section method.

As can be seen, all the calculated local power values are in the range of the required accuracy (5 %). It is important to pay attention to the sense of the disagreement : the calculation overestimates the power peaks near water gaps so that, as far as safety considerations are concerned, the results can be considered as conservative.

VIII.4. Control rod worth calculations

Table VII.6 summarizes the various results obtained for lattices where a certain number of fuel rods were substituted by B_4C rods. The 10 % accuracy goal for control rod reactivity worths is

reached for the listed cases; on the other hand it has been seen that the power distribution around the B_4C rods is not precise enough. As both characteristics are linked in the calculation, further work remains necessary.

VIII.5. Comparison of the neutronic characteristics of homogeneous and heterogeneous fuels

The small zone substitution experiments having shown no reactivity effect when substituting 16 homogeneous vibrocompacted 3/1 fuel rods by 16 heterogeneous ones, a theoretical investigation was carried out to explain this fact. Table VII.5 illustrates that the global theoretical conclusion is the same. From the analysis of the theoretical results it appears that in the case of the heterogeneous fuel, where the plutonium is preferentially located at the periphery, the plutonium isotopes have a larger disadvantage factor than in the case of the homogeneous fuel. The formula

$$\bar{\Phi}_i = \frac{\int_o^r 2\pi r \, N_i(r) \, \Phi_i(r) \, dr}{\int_o^r N_i(r) \, 2\pi r \, dr}$$

shows the importance of the spatial dependance of the concentration on the mean flux in the rod for each isotope i. It is clear that the isotopes which are at the periphery will have a larger mean flux value than the unique mean flux value corresponding to a homogeneous fuel. Furthermore it is clear that in the case of heterogeneous PuO_2 - UO_2 fuel, the change of the disadvantage factor for the four Pu isotopes will have a reactivity effect depending on the Pu composition. This means that, if for certain plutonium compositions compensations occur so that no reactivity difference between heterogeneous and homogeneous fuels is resulting, this will not be necessarily so for other types of plutonium fuels.

CHAPTER IX : CONCLUSIONS

As pointed out in the general introduction to this document, the described results do not constitute a final account on the complete reactor physics programme set up by Belgonucleaire and the SCK/CEN in the field of plutonium recycle studies, but only on the activities until 1968. The present conclusions drawn about the ability of the theoretical methods and codes are limited to fuels without plutonium or with a relatively low plutonium content. Therefore these conclusions have to be considered as incomplete and provisional, when referring to the entire problem of reactor design calculations in the case of plutonium recycling. In order to be able to make a complete and final judgement, higher enriched plutonium fuels, poisoned moderator configurations including plutonium fuel zones, as well as certain particular local features of power reactor cores, will be studied ; the end of this programme will fall in 1971.

Nevertheless, the work reported here has led to conclusions, which are in general very satisfactory and which allow already to have a certain confidence in the results to be obtained further on. In fact, it can be mentioned that, at the moment of the editing of this report, the results obtained in 1969 for the 2/2.7 fuel tend to confirm rather well that confidence.

Basing ourselves only upon the results, discussed in this report and thus relevant to the 4/0 and 3/1 fuels, the following specific conclusions can be drawn :

1) the effective multiplication factor is calculated with a precision better than 1% Δk;

2) in almost all cases the requested 4 to 5% accuracy on calculated power distributions is achieved ; in some specific situations the use of more developed calculational tools seems to be advisable, such as 3 D diffusion codes instead of 2 D ones or codes allowing to take into account the spatial spectrum variation (e.g. near

absorbing perturbations), such as THERMOS or P_1MG codes ;

3) the control rod worth determination should equally be studied further on the basis of other experiments ; the importance of the correct evaluation of the mutual shielding between adjacent absorbing rods in the case of cruciform arrangements is obvious ; on the other hand the newer type of reactor control, the RCC one, has to be investigated too, both for reactivity worth and local power distribution.

APPENDICES

APPENDIX II.1 : TECHNICAL CHARACTERISTICS OF THE SAFETY VALVES

The air-tightness of the door is obtained by pressing a glued rubber disc on a circular knife with a diameter of 13.5 cm, which penetrates the rubber by 0.5 mm. The pressure is chosen to have a good air-tightness without damaging the rubber : the nominal pressure is 15 kg/cm^2, the leakage beginning at a pressure of 10 kg/cm^2.
The electro-magnet is made of "perminox"; its force is comprised between 50 and 60 kg for a 120 mA current. The permanent magnetism force is lower than or equal to 7 kg. During the normal operation, the actual traction force on the electro-magnet is between 21 and 33 kg, thus lying between the magnetic forces with and without current.
Extensive tests have been made using microswitches mounted on the valve and a pulse generator giving 1000 pulses/s. A complete scram circuit has been reproduced on a bench making the following measurements possible :

- the delay time between the scram order and the door opening start
- the delay time corresponding to the complete opening of the valve.

The measurements have been made for dumptank-connected valves and jacket-connected ones in three typical conditions :

- The "operating" condition, characterized by a rubber pressure of 15 kg/cm^2.
- The "leakage" condition, characterized by a rubber pressure of 10 kg/cm^2.
- The "extreme" condition corresponding to no pressure on the rubber.

The results are given in the following table :

Water level in the reactor tank [cm]	Rubber pressure [kg/cm^2]	Valves of the jacket(1)		Valves of the dumptanks	
		Door departure [ms]	Opening [ms]	Door departure [ms]	Opening [ms]
168 (nominal)	15	41 ± 7 (2)	93 ± 2	29 ± 7	66 ± 7
	10	46 ± 6	100± 3	33 ± 5	70 ± 1
	0	70 ± 14	129 ±10	45 ± 7	85 ± 8
118	15	46 ± 8	108 ± 3	30 ± 8	71 ± 6
	10	68 ± 13	133 ±13	40 ± 7	82 ± 4
	0	85 ± 11	155 ± 9	55 ± 11	100 ±10

(1) The difference between a valve connected to a dumptank and one connected to the jacket is due to different air pressures resulting from the corresponding water heights.

(2) The results are the mean delay times for all the experimental valves and the deviations give the range in which all values are comprised.

APPENDIX II.2 : TECHNICAL CHARACTERISTICS OF THE FAST DUMP SYSTEM

The fast dump system has been designed in order to get the reactor under control with a speed comparable to the one obtained with safety rods.

The dump system has the advantage that there remains no criticality risk after the scram, the moderator being out of the core. The design of the fast dump system had to take into account some characteristics of the already existing installation; for this reason it consists of two important parts : the dumptanks, which do not let the water fall at a sufficient speed but which are able to receive the complete water content of the reactor tank, and the jacket, which cannot receive the water of the reactor tank, but enables a fast jump at the beginning of the scram. This fast jump is mainly necessary for a quick elimination of the upper reflector which has a relatively small reactivity effect.

Checks of the effectiveness of the fast dump system have been made in the presence of several configurations consisting of different numbers of dummy rods in aluminium. These rod numbers did more or less correspond to the numbers of fuel rods in the critical configurations to be constituted during the experimental programme.

The reactor control being possible by the water level, checks of the effectiveness of the fast dump system have been made at different levels. Moreover, all the measurements were performed at the center of the core to take account of the fact that the bottom grid delays the water present in the core. A comparison between the fall law in the reflector and in the core illustrates this effect(see fig.II.11).

In order to determine the delay times accurately, electrodes insulated from the reactor structures are loaded at the place of some fuel pins. They have contacts with the water at different levels. An electrical contact between the electrodes and the reactor tank is obtained when the water reaches the contact levels.

A pulse generator giving 1000 pulses per second is connected to the reactor tank.

When the water is at its start level, the pulses are collected by some scalers. At the same time, the scram button cuts the voltage of the scram line and starts all the scalers. The indications of the

scalers give respectively the delay time before the water starts moving and the time needed to reach the different water levels during the water dump. The results are given in fig. II.11.
It can be seen that in the worst conditions the delay time to empty the core is smaller than one second and that the fall law presents only small differences when the amount of rods or the start level change.

APPENDIX II.3 : CALCULATION OF THE HIGHEST ADMISSIBLE REACTIVITY INSERTION RATE.

1. Some core parameters used for the safety analysis

The choice of these parameters was made on the basis of the planned experimental programme.

1.1. Neutron life-time and delayed neutron fraction

Parameter	Fuel 4/0 (*)	Fuel 2/2.7 (*)
l [s]	15.10^{-6}	12.10^{-6}
β_{eff} [%]	0.75	0.55
$1/\beta_{eff}$ [s]	20.10^{-4}	22.10^{-4}

1.2. Temperature coefficient

Range of temperatures	Fuel 4/0	Fuel 2/2.7
< 40° C	$- 0.9.10^{-5}$ \$/° C	$- 1.1.10^{-5}$ \$/° C
from 90° C to 150° C	$- 0.7.10^{-5}$ \$/° C	$- 0.8.10^{-5}$ \$/° C

1.3. Form factor

The highest form factors to be considered for the different fuels are 1.5 axially and 2.4 radially.

1.4. Relation between power density and neutron density

Fuel 4/0 : 1 W/cm^3 of cell corresponds to $7.89.10^5$ n/cm^3 of cell.
Fuel 2/2.7 : 1 W/cm^3 of cell corresponds to $6.38.10^5$ n/cm^3 of cell.

(*) The exact definition of these fuel enrichments is given in chapter III

1.5. Reactivity in function of decreasing water level

Water level [cm]	Fuel 4/0 [$]	Fuel 2/2.7 [$]
168 (nominal)	0	0
165	- 0.1	- 0.2
160	- 0.5	- 0.6
155	- 1.7	- 2.2
145	- 5.8	- 7.7
135	-13.3	-17.5

2. Analogous calculation

The calculation is performed on the analogous computer of the CEN/SCK. It consists in finding which linear reactivity increase is necessary to reach a temperature of 100°C at the outer cladding surface of the hottest fuel pin. The used calculation model is conservative with respect to the actual situation. Indeed, both logarithmic channels are assumed out of service (no period scram) and the thermal model is based on the representation of an adiabatic single cell of unit length, in which the heat transfer takes place only by conduction. For the kinetical neutron treatment, a point model is used with six delayed neutron groups. In these circumstances, an energy of 300 W.s per cm fuel pin is calculated to be necessary to get such a temperature. The calculation has been performed for both 4/0 and 2/2.7 fuels; the results for the 4/0 fuel are somewhat more restrictive than the other ones and are the only ones considered hereafter.

Two water fall laws, corresponding respectively to the nominal level and a reduced one, are combined with the reactivity in function of water level law to give the reactivity decrease in function of the time elapsed after the scram signal (fig. II.12.).

For the analogous calculation, these curves are simplified into a delay time followed by a linear decrease of the reactivity, in such a way that the delay time includes successively : the amplifier delay time, the relais delay time, the fall law delay time and the time at the beginning of the water level decrease when the reac-

tivity change remains small.

The initial flux and the scram levels are used as parameters of the problem; the most restrictive of all the considered cases corresponds to an initial flux of 10^3 n/cm^{2}s and a scram level of 10^{-6} A ($\simeq 5.10^9$ n/cm^2 s) and the corresponding highest admissible reactivity increases are found to be :

0.14 $/s at nominal lvel,

0.30 $/s at reduced level.

APPENDIX IV.1 : SPECTRUM STUDIES IN CONTACT WITH GULF GENERAL ATOMIC

A. Introduction

Already in 1965 several contacts took place between staff members of Gulf General Atomic, San Diego (USA), and some members of the Belgian plutonium project team. In that period G.G.A. had just prepared a "proposal for program to perform experimental and analytical reactor lattice physics studies" [see : GACP-52-225, May 1965], for submission to the USAEC with a view to its realisation in the frame of the Joint U.S.-Euratom R and D Programme.

The main objective of that programme was described as "the systematic measurement and calculation of neutron spectra and transport in typical lattices of direct interest in light water design". As one of the aims of the Belgian plutonium programme was the study of neutron spectra in plutonium fuelled thermal lattices, both theoretically and experimentally, it appeared that a certain collaboration between both programmes could be interesting. The idea was approved by the USAEC and by Euratom in 1966.

The work on the "Lattice Physics Studies" programme started at San Diego on May 1, 1966. Three months later, Dr J.L. Russell Jr of GGA visited Mol during a few weeks. At that occasion the practical collaboration possibilities were discussed and some actions decided. From then onwards regular contacts between both sides of the Atlantic were maintained and at the occasion of mutual visits the progress of the work was discussed.

B. General survey and principal aims of the programme

Since many years before the start of the mentioned "Lattice Physics Studies" programme, time of flight spectrum measurements were being done in the GGA laboratories, so that the experimenters there had acquired quite a lot of experience in the field. On the other hand, the experimental study of neutron spectra was in Mol always done by means of spectrum index measurements with activation detectors.

It was felt that, when both techniques (the differential and the integral one) could be applied in the same or in very similar physical conditions, the comparison and the analysis of the results might lead to interesting conclusions on both of them allowing eventually certain improvements. Furthermore it was hoped that through such comparisons a more precise knowledge of the nuclear characteristics of some frequently used activation detectors could be achieved.

First the possibility had to be created to realize measurement conditions in San Diego and in Mol in such a way that the obtained results would be completely comparable. During Dr Russell's visit to Mol, the design and fabrication of two identical cylindrical containers with boron containing walls were decided; these containers would be filled with liquid solutions, the equilibrium spectrum of which was to be studied. One of these containers was to be used for the time of flight measurements, the other one would be put in a thermal column of the BR1 reactor in Mol for the activation measurements; in the latter case the neutron source would be a highly enriched uranium plate, located just outside the container, on its axis. The originally planned container dimensions were modified later on, due to the fact that they appeared to be too small to allow accurate parallel theoretical spectrum calculations, which GGA wished to carry out; so a new, larger container type was designed in mutual agreement.

As for the programme of the experiments, it was decided to start with measurements in plain water as a reference case. The main measurements would then be done in an erbium nitrate solution in water. The choice of erbium as resonant absorber was justified by the fact that its low energy resonance structure is very similar to the one of plutonium, thus yielding spectra of the same type. The time of flight measurements were done by GGA in this erbium solution, after which this solution was sent to Mol for the activation measurements : in this way it was made sure that the properties of the solution were the same for the two types of measurements.

C. Status of the work at the expiry of the Euratom TRUB-contract

At the end of the period, covered by the Euratom TRUB-contract, everything was ready to start the experiments: the measurement equipment (container and fuel plate), the detectors, the erbium solution and some codes needed for the interpretation of the measurement results. This preliminary work will be described very shortly in what follows.

C.1. Measurement equipment

The most important part of the measurement equipment is of course the cylindrical container itself; it is represented in figure IV.2, which shows also some other details about the whole of the "Integral Spectrum Facility", such as the final location of the container with respect to the BR1 reactor and the position of the U^{235} fission plate. The outer radial dimension of the container was chosen so that it could just be introduced into the Y_6 channel (a horizontal thermal column in BR1); preliminary measurements on the relative importance of the reactor background contribution to the activities measured inside the container did lead to the conclusion that the best localisation of the container was just outside the graphite, as represented in the figure. The B_4C layer all around the container allows only the fast fission neutrons, coming from the fission plate, to enter in the container; those coming from the reflecter are absorbed. The entering fast fission neutrons are then moderated inside the container according to the properties of the solution it is filled with.

Figure IV.3 shows the positioning device of the detector foils, to be put inside the container; in the case represented in the figure, the detectors are arranged for the measurements of two radial flux distributions; analogous possibilities exist for axial distribution determinations.

C.2. Detector choice

It was decided to use an important number of detectors, all based on (n,Y) reactions, at the exception of the fissile ones, for which the U^{235} and Pu^{239} (n,f) reactions were to be counted. These activation detectors include Mn, Dy, Au, In, Lu, Ir, Eu,

For most of them an extensive evaluation work on their nuclear characteristics, essentially resonance parameters, was done in 1967 [SCK/CEN report BLG 421].
These detectors have their main resonances at different energies, so that different energy ranges of the spectrum can be investigated.

C.3. Calculation tools

Also in 1967, a code was written in Mol (CROCUS), allowing the accurate calculation of the cross sections of detectors with important thermal and epithermal resonances, as well as their response functions in given spectra. On the other hand the availability of a code, allowing spectrum unfolding from measured reaction rates, was prepared through contacts with the CNEN-Center of La Casaccia.

C.4. The erbium solution

An erbium nitrate solution of about 105 g/l was prepared by GGA. The time of flight measurements in it were done in San Diego in the course of 1967. Then it was sent to Mol for the activation measurements, as well as the time of flight results. At GGA these results were already compared with the ones calculated with the GATHER code; the difference found was assigned to the cross section parameters used for the calculation, a conclusion that should be confirmed by the activation results.

D. Conclusion

At the moment of this report's redaction an important number of activation measurements have already been performed and a good part of them has been analyzed. Enough results are already available to conclude that this spectrum study programme, a relatively modest part of the whole plutonium programme, will allow to obtain some interesting and concrete results.

APPENDIX V.1 : k_{eff} AND CRITICAL MASS DETERMINATION

A. General method

Most of the critical checks are made once for a cylindrical geometry and once for a rectangular one.

After the approach to criticality, performed by progressive subcritical countings, the k_{eff} or the critical mass determination is generally done in the supercritical state in order to get a better accuracy.

When the configuration has to be purely rectangular, it is practically impossible to find a just critical core; indeed, the approach can only be done by increasing the core size by steps of one row of fuel pins. The problem is thus to find a rectangular core which is somewhat supercritical, the reactivity excess being sufficiently small to enable a period measurement.
In the case of a cylindrical geometry, the approach to criticality is much easier; indeed, the core size can be increased by steps of one fuel pin (in fact, steps of four fuel pins are made for symmetry reasons). The final critical mass is obtained by a supercritical approach on the basis of two period measurements for two slightly different supercritical configurations. In both cases, the reactivity excess is obtained by measuring the asymptotic positive period produced by rising the water from its critical level up to its nominal level(complete upper reflector).
Practically, the counting rates induced by the neutron flux in a BF_3 proportional counter are punched at successive time intervals in a form directly suited for computer analysis.
After disappearance of the transients, the results obey the law :

$$\Phi(t) = \Phi_o . e^{t/T}$$

where T is the asymptotic period.
The value of the period is calculated by a least square fitting of the experimental data corrected for the dead time of the counter (S.C.K.-C.E.N. programme PA 112).

The associated reactivity excess is then calculated on the basis of the NORDHEIM equation as will be described in appendix V.2.

B. Particular cases

When it is not possible to find a core with a sufficiently small reactivity excess, use is made of one of the calibrated curves giving the reactivity excess as a function of the critical level (see fig. V.1).
From a lot of experimental results for different configurations and fuels, it appears that the reactivity excesses for critical levels above the fuel height and the reactivity effect of the upper reflector depend only on the pitch of the core. Such curves are useful to obtain the k_{eff} of a configuration only by a critical level determination.
On the other hand, it may happen that the suitable configuration is slightly subcritical. In that case, the k_{eff} is obtained by performing subcritical countings in presence and in absence of the upper reflector. The inverse counting rate being proportional to the subcriticality, the same kind of extrapolation, as performed in a critical approach, but using the reactivity effect of the upper reflector, gives the magnitude of the subcriticality at nominal level.
An example of such a k_{eff} determination is presented in fig. V.2.

C. Accuracy discussion

C.1. Accuracy of a direct k_{eff} measurement

Reproducibility tests carried out on a well-defined configuration show an accuracy of $\pm$ 0.002 % $\Delta k/k$ on a period measurement.
In general however, the reproducibility of a k_{eff} measurement does not depend only on the period, but also on the critical level determination, the water temperature, etc. An idea of this global reproducibility is given by the dispersion of the points around the curves of figure V.1. Most of the points are close to the curves, within 0.01 % $\Delta k/k$.

C.2. Accuracy of the critical mass determination in a cylindrical geometry

The advantage of the cylindrical geometry is that it allows a one-dimension calculation. Experimentally however, the cylindrical geometry can only be approximated by a broken line. In most cases, several rather close approximations of a circular section are possible, resulting in small differences; this effect can be important for small cores.

Systematical tests have been made for the smallest configuration of the programme, i.e. configuration 3 with about 300 3/1 fuel pins, pitch = $\sqrt{2}$ x SENA pitch.

Several cylindrical configurations of 307 fuel pins, different by their approximation of the circle, have reactivity excesses varying within $\pm$ 0.036 % $\Delta k/k$. Due to the fact that all these configurations have a perimeter rather different from the ideal circular one, a systematical error of the same order (i.e. 0.04 % $\Delta k/k$) can affect the final result, so that the total uncertainty due to geometry is estimated to $^{+\ 0.04}_{-\ 0.08}$ % $\Delta k/k$.

Moreover, during the supercritical approach, the reactivity value of the peripherical fuel pins depends on their exact location at the periphery. This effect leads to one more uncertainty of $\pm$ 0.01 % $\Delta k/k$.

The greater the critical rod number, the smaller these errors become. The following table summarizes the global error, associated with critical mass determination.

TABLE V.1 : ERRORS ON CRITICAL MASS DETERMINATION

Configuration type (fuel, pitch)	Critical number of fuel pins	Reactivity effect of a peripheric fuel pin $\left[\% \frac{\Delta k}{k}\right]$	Global error on the k_{eff} taken equal to 1 $\left[\% \frac{\Delta k}{k}\right]$	Global error on the critical number of fuel pins [%]
4/0, SENA pitch	824	0.018	+ 0.01 - 0.03	- 0.1 + 0.2
4/0, √2 x SENA pitch	351	0.043	+ 0.03 - 0.06	- 0.2 + 0.4
3/1, √2 x SENA pitch	299	0.063	+ 0.05 - 0.09	- 0.3 + 0.5
3/1, 2 x SENA pitch	363	0.028	+ 0.02 - 0.04	- 0.2 + 0.4

APPENDIX V.2 : RELATION BETWEEN THE ASYMPTOTIC PERIOD AND THE REACTIVITY

The relation between the reactivity and the asymptotic period is obtained for each configuration on the basis of the NORDHEIM equation, using six groups of delayed neutrons :

$$\rho = \frac{1}{1 + T} + \frac{T\,\beta_{eff}}{1 + T} \sum_{i=1}^{6} \frac{a_i}{1 + \lambda_i T}$$

where ρ is the reactivity excess in the form of $\delta k_{eff}/k_{eff}$

T is the period

β_{eff} is the total effective fraction of the delayed neutrons

a_i is the relative fraction of each group of delayed neutrons

and λ_i is the corresponding decay constant.

Due to the great differences between the studied configurations from the point of view of geometry and fuel composition, β_{eff}, a_i and λ_i are to be calculated for each configuration. This is done in the following way :

a) the macroscopic neutron constants of the elementary cell are obtained by the PANTHER code (see chapter VI), for four energy groups;

b) the β_i, a_i and λ_i being to be weighted over the whole configuration, the needed flux distributions are calculated with a diffusion code : use is made of the one-dimension PANOPLIE code in the case of a cylindrical configuration and of the two-dimension codes PANDA and SQUID in the case of a rectangular configuration.

The indices i, j and k referring respectively to the delayed neutron group numbers, the fissile isotopes and the energy groups, the following expressions are used :

$$\beta_i = \frac{\Sigma_j\, \beta_{ji}\, S_j}{\Sigma_j\, S_j}$$

where S_j is the total source of neutrons produced by each isotope j :

$$S_j = \Sigma_{k=1}^{4}\, \nu.\Sigma_{fjk}.\phi_k.V$$

$$\beta_{total} = \sum_{i=1}^{6} \beta_i$$

$$a_i = \frac{\beta_i}{\beta_{total}}$$

$$\lambda_i = \frac{\Sigma_j \lambda_{ji} S_j}{\Sigma_j S_j}$$

c) The effective total fraction of delayed neutrons is then obtained by a second diffusion calculation, with the same codes, but where three more groups are introduced in order to calculate separately the flux distributions of the prompt neutrons and the delayed ones. The transfer cross sections relative to the neutrons going from each of these groups to the other ones are calculated taking into account the fraction of the delayed neutrons produced in the corresponding energy range. The β_{eff} is then obtained as follows :

$$\beta_{eff} = \frac{\Sigma_{k=5}^{7} S_k}{\Sigma_{k=1}^{7} S_k}$$

where S_k is the total source of neutrons produced by all the isotopes in energy group k : $S_k = \Sigma_j \nu.\Sigma_{fjk}.\Phi_k.V$

Tables V.2 to V.7 and figure V.3 summarize the results obtained for four typical configurations of the experimental programme related here :

1) a cylindrical configuration of 810 4/0 fuel pins loaded according to the SENA pitch;
2) a cylindrical configuration of 365 4/0 fuel pins loaded according to the $\sqrt{2}$ x SENA pitch;
3) a cylindrical configuration of 281 3/1 fuel pins loaded according to the $\sqrt{2}$ x SENA pitch;
4) and a cylindrical configuration of 365 3/1 fuel pins loaded according to the 2 x SENA pitch.

TABLE V.2 : ABSOLUTE FRACTION β_{ji} PER GROUP AND ISOTOPE

group	U-235	U-238	Pu-239	Pu-240	Pu-241	Pu-242
1	0.000215	0.000204	0.000074	0.000091	0.000091	0.000091
2	0.001424	0.002151	0.000626	0.000775	0.000775	0.000775
3	0.001274	0.002543	0.000443	0.000549	0.000549	0.000549
4	0.002568	0.006092	0.000685	0.000848	0.000848	0.000848
5	0.000748	0.003533	0.000181	0.000224	0.000224	0.000224
6	0.000273	0.001178	0.000092	0.000114	0.000114	0.000114

TABLE V.3 : WEIGHTED ABSOLUTE FRACTION β_i FOR THE CONSIDERED CONFIGURATIONS

group	configuration 1	configuration 2	configuration 3	configuration 4
1	0.000214	0.000215	0.000160	0.000162
2	0.001467	0.001445	0.001135	0.001137
3	0.001350	0.001310	0.000988	0.000983
4	0.002778	0.002668	0.001938	0.001919
5	0.000914	0.000827	0.000607	0.000580
6	0.000327	0.000299	0.000229	0.000220
β_{total}	0.00705	0.00676	0.00505	0.00500

TABLE V.4 : RELATIVE FRACTION a_i FOR THE CONSIDERED CONFIGURATIONS

group	configuration 1	configuration 2	configuration 3	configuration 4
1	0.030398	0.031740	0.031640	0.032405
2	0.208106	0.213589	0.224518	0.227360
3	0.191423	0.193694	0.195347	0.196596
4	0.394031	0.394496	0.383206	0.383750
5	0.129663	0.122310	0.120092	0.115971
6	0.046379	0.044170	0.045198	0.043918

TABLE V.5 : DECAY CONSTANTS λ_{ji} PER GROUP AND PER ISOTOPE (s^{-1})

group	U-235	U-238	Pu-239
1	0.0124	0.0132	0.0128
2	0.0305	0.0321	0.0301
3	0.1114	0.1390	0.1238
4	0.3014	0.3580	0.3254
5	1.1360	1.4100	1.1220
6	3.0140	4.0200	2.6970

TABLE V.6 : WEIGHTED DECAY CONSTANTS λ_i FOR THE CONSIDERED CONFIGURATIONS

group	configuration 1	configuration 2	configuration 3	configuration 4
1	0.0125	0.0125	0.0126	0.0126
2	0.0306	0.0306	0.0304	0.0304
3	0.1130	0.1122	0.1170	0.1164
4	0.3048	0.3030	0.3123	0.3112
5	1.1523	1.1438	1.1384	1.1351
6	3.0740	3.0426	2.9202	2.9119

TABLE V.7 : EFFECTIVE ABSOLUTE TOTAL FRACTION β_{eff} FOR THE CONSIDERED CONFIGURATIONS

Configuration 1	0.00762
Configuration 2	0.00750
Configuration 3	0.00570
Configuration 4	0.00542

APPENDIX V.3 : ONE REGION POWER DISTRIBUTIONS

A. Axial power distribution

The axial power distributions are measured by two different techniques : the fission chamber one and the γ-scanning one.

A.1. Fission chamber method

This method consists in measuring the counting rates of a fission chamber moved step by step along the height of the fuel loading. In VENUS a 20th CENTURY-U^{235} fission chamber is used; it has an external diameter of 3 mm and an active length of 1 cm. It is fixed to a regulating rod drive mechanism, which allows to move the chamber from the reactor control room. The active part of the chamber is guided inside a tube (identical to a fuel pin cladding), which is loaded in the reactor just as a fuel pin. The installation of the fission chamber and its vertical movement inside the core are illustrated in figure V.4.
During the measurements, the reactor is kept critical and stable by small movements of a regulating rod, compensating the small reactivity effects due to the shifts of the fission chamber itself.
The counting rates of the fission chamber are normalized by means of the counting rates of a BF_3 proportional counter, which is fixed during the measurements, so that the small neutron flux variations induced by the reactivity adjustments are taken into account.
A great effort has been devoted to obtain the precise positioning of the chamber in the core : the chamber is located with an accuracy of $\pm$ 1 mm with respect to the fuel mid-plane and its axial movements are reproducible within $\pm$ 0.1 mm.
When doing the measurements themselves, the reactor power is chosen in order to have a statistical accuracy better than 2 % for the fission chamber and 1 % for the BF_3 monitor.

A.2. Y-scanning method

A fresh fuel pin (i.e. a pin having a natural or residual activity which is negligible, or low but well-known) is put in the configuration at the position of interest and irradiated. The irradiation is performed at a constant flux level of about 10^8 n/cm^2 s : the irradiation time is always the same (arbitrarily chosen as one hour), in order to have always the same fission product Y-spectrum and the same Y-activity decay law. A few hours after the irradiation, the Y-activity is measured, the irradiated fuel pin being moved step by step in front of a 2" x 2" NaI (Tl) crystal, which "sees" the rod through a collimating window in a lead shielding; this shielding protects the crystal against the Y-activity of the rest of the fuel pin. The resolution of the collimator may be changed : resolutions of 1 cm or 2 cm are generally used.

In order to get results independent of the radial distribution of the fission products inside the fuel pin (due to a macroscopic radial flux gradient and eventually to a heterogeneous radial distribution of the fissile material), the fuel pin turns slowly around its axis during the measurements.
The relative positions of the fuel pin, the shielding and the crystal are schematicly given in figure V.5.

As it has been seen in chapter II, the Y-scanning installation is completely automatized. The translation mechanism is designed so that it gives a positioning accuracy of the fuel pin with respect to the collimator of about 1.5 mm, the reproducibility of the localizations being better than 0.5 mm.
The NaI crystal is connected to a classical Y-spectrometry analyzer and an automatical counting system with punch recording.
As there is generally no modification of the self-absorption along the axis of the fuel pin, the gross Y-activity measured above 0.425 MeV gives directly the axial power distribution without any error. Except for the heterogeneous fuel pins discussed hereafter, the Y-scanning method gives an accuracy of the order of 1.5 %.

Remark about the influence of the heterogeneity of the fuel on the measured axial power distribution

Figure V.6 compares the distributions of the γ-activity measured respectively for a 3/1 vibrocompacted heterogeneous fuel pin and for a 4/0 pelleted one (considered as homogeneous). Both have been irradiated closely together in an axially constant flux in the BR1 reactor. The results for the 4/0 fuel give an information about the statistical counting accuracy, whereas those for the 3/1 fuel show clearly the heterogeneity incidence.
The following comments can be made :

- the γ-activity of the heterogeneous fuel pin does not show any global variation indicating a systematical error on the measurement of the axial power distribution;
- especially for the low energy γ-ray activities the deviations due to the heterogeneity are much more important than the statistical ones (4/0 results);
- these deviations decrease for γ-rays of higher energy : this is due to the facts that self-absorption is smaller for γ-rays of higher energies and that the heterogeneity concerns the plutonium which is mainly present at the radial periphery of the rod.

It has to be noted that the fast decrease of the γ-activity at both extremities of each fuel pin does not correspond to a variation of the fission density (or of the fuel density), but is due to the actual resolution of the collimator. Indeed, although the collimator window has only a width of 2 cm, experiments performed with a point source show that 78 % of the measured activity corresponds to the considered 2 cm of the pin, the other 22 % coming from the 2 cm next to it, 1 cm at each side. This explains the decreasing values at the fuel pin ends. This phenomenon does not affect however the axial power distribution further than 4 cm from both extremities.

A.3. Comparison of both methods

Figure V.7 gives an example of a comparison between axial power distributions obtained by both methods; it can be seen that the agreement is very good.

B. Radial power distribution

As for the axial power distribution, two experimental techniques are used, but both are based on fuel activation : γ-scanning of irradiated fuel pins and counting of irradiated fuel pellets.

B.1. γ-scanning method

The method is just the same as for the axial power distribution, but instead of counting several points of one fuel pin, one has to count one point of several fuel pins choosing them on the same level. For the sake of precision, especially in the case of heterogeneous fuel, each fuel pin is measured at three different levels near the fuel mid-plane and the values are averaged in order to find a unique radial distribution.

In general, it is again the gross γ-activity above 0.425 MeV which is measured, as for the axial measurements. The advantage of this method is the low irradiation level, enabling the use of the same fuel pins already two weeks later with reasonable residual activities. It is particularly interesting for repeated irradiations, when the amount of available fuel pins does not allow to store a lot of fresh fuel pins for the measurements.

The data are punched by the γ-scanning installation in such a way that they can be introduced directly in the computer for analysis. The measured γ-activities are reduced to a relative power distribution normalized to a given monitor fuel pin, taking into account all counting corrections, such as background, dead time, decay, residual activity, etc. (S.C.K.-C.E.N. computer programme FA 157). An accuracy of the order of 1.5 % is obtained, as for the axial power distribution; this precision is less good in the case of heterogeneous fuel.

B.2. Pellet activation method

The method consists in the measurement of the γ-activity of a given fission product produced by activation of fresh fuel pellets contained in dismountable fuel pins. These dismountable fuel pins being designed to have physical characteristics as close as possible to the ones of the standard fuel pins (see chapter II), the use of this method does not disturb the power distribution of the investigated configuration.

The following decay-chain is used :

$$\text{Fission} \rightarrow Xe^{140} \xrightarrow[(16\ s)]{} Cs^{140} \xrightarrow[(66\ s)]{} Ba^{140} \xrightarrow[(12.8\ d)]{} La^{140} \xrightarrow[(1.67\ d)]{} Ce^{140}(\text{stable})$$

The La^{140} is produced with a yield of about 6 % per fission and it emits 0.94 γ-ray of 1.6 MeV per disintegration.

Thirteen days after an irradiation of two hours at a flux of about 10^9 n/cm^2 s, the $Ba^{140} \rightarrow La^{140}$ chain reaches its radioactive equilibrium and the La^{140} decreases with an effective half-life of 12.8 days. The pellets are counted on a γ-spectrometry installation, composed of four counters with NaI crystals, using a threshold adjusted just below the 1.6 MeV γ-ray. The certainty, that only the La^{140} is measured, in this way, has been achieved by checking the half-life of the Ba^{140} during a long time : a value of 12.86 days, in agreement with literature, has been obtained.

A cycle routine is followed for counting, so that the punched results can directly be analyzed on a computer (S.C.K.-C.E.N. programme PA 114). This programme calculates the relative γ-activities of the pellets and the errors on these values after applying a statistical rejection criterion to the results corrected for dead time, background, natural activity, decay and pellet weight.

An error of the order of 1 % is generally found for this kind of measurement; this error is confirmed by the dispersion of the points around the best fitted curves, when bucklings are calculated.

B.3. Comparison of both methods

The two different ways applied to measure the radial power distribution are compared in figure V.8. Two series of 7 standard fuel pins and 7 dismountable ones have been irradiated at both sides of a water gap. The results allow to conclude that the relative activity distribution does not change, neither between pellets and different types of fuel pins, nor with changes in the counting method, such as a different γ-ray energy discrimination.

APPENDIX V.4 : BUCKLING DETERMINATION

In the one-region configurations, the power distribution is generally measured in three orthogonal directions, in order to obtain the axial buckling (B^2_{ax}), the radial buckling (B^2_{rad}) and the total buckling (B^2_{tot}), which is the sum of the other ones. At the critical state, the total buckling is equal to the material buckling (B^2_m). The axial buckling is always obtained by a cosine fitting, the radial one by a cosine or a J_o Bessel function, depending on the geometry (respectively rectangular or cylindrical). For these fittings a computer programme has been written (RA-51). This programme carries out a least square fitting to find the best set of parameters to be introduced in the formulas of the flux distribution:

- for a cosine distribution : $\phi(x) = \phi_{max} . \cos \left[B_x (x - x_o) \right]$

  where : - x is the abscisse in the investigated direction

  - ϕ_{max} is the maximum of the distribution
  - x_o is the eventual deviation of the maximum-position from the reactor axis
  - $B_x = \frac{\pi}{X}$ is the square root of the buckling in this direction and X is the corresponding extrapolated size.

- for a J_o-distribution : $\phi(r) = \phi_{max} . J_o \left[B_r (r - r_o) \right]$

  where : - r is the radius along which $\phi(r)$ is measured

  - ϕ_{max} is the maximum of the distribution
  - r_o is the eventual deviation of the maximum-position from the reactor axis
  - $B_r = \frac{2.405}{R}$ is the square root of the radial buckling for the cylindrical core and R is its extrapolated radius.

In order to avoid any influence of the reflector peaks, the analysis is carried out in successive steps by reducing the number of experimental points symmetrically, starting from both extremities. After a few number of steps, the buckling value remains constant and its statistical error reaches its minimum value.

Figure V.9 illustrates the different steps of the buckling determination for an axial power distribution of 50 points. Of course, the results are not significant anymore when the number of points becomes too small (< 10).

The accuracy of an axial buckling measurement is usually $\leq$ 1 %, independent of the used technique, and the accuracy on a radial buckling measurement is $\leq$ 2 %.
The accuracy is of course less good in the case of heterogeneous fuel pins; then the precision is respectively $\leq$ 3 % and $\leq$ 4 %.

APPENDIX V.5 : REACTIVITY EFFECT MEASUREMENT

A. Introduction

The reactivity effect of a perturbation is defined as the k_{eff} variation of a reactor loading induced by the introduction of this perturbation. If it is smaller than 0.3 % $\Delta k/k$, it is always possible to determine it by a positive period measurement as described in appendix V.1.

For greater reactivity effects, the subcritical techniques cannot always be used or are not accurate enough to allow a check of the calculated reactivity effects. On the other hand, performing the check with critical mass determinations with and without the perturbation has the disadvantage that the neutron leakage is changed simultaneously with the perturbation insertion.

Another possibility is to start with a perturbated configuration, critical at a reduced level, to extract the perturbation by small steps of $\simeq$ 0.3 % $\Delta k/k$, to determine the corresponding reactivity effect by period measurement and to sum all the results between the critical level with the perturbation and the critical level without it.

The "$\partial\rho/\partial h$ method" described in what follows is in fact a more practical form of this method.

B. Method

First the variation of the reactivity effect associated with a small increment of the water level is measured in function of the critical level. The variation of the critical level is obtained by introducing an increasing number of perturbations and the water level increment is given by plunging a constant volume in the reactor tank (a sealed tube moved by a regulating rod mechanism).

A relatively small number of measurements is enough to define the $\partial\rho/\partial h$ curve with a good accuracy, due to the fact that the results can be fitted by an analytical curve. Indeed, applying the one neutron group theory to a given loading, the reactivity can be described as follows :

$$\rho = \frac{k_{eff} - 1}{k_{eff}} = \frac{\dfrac{k_\infty}{1 + M^2B^2} - 1}{\dfrac{k_\infty}{1 + M^2B^2}} = 1 - \frac{1 + M^2B^2}{k_\infty}$$

The reactor height (or immersed fuel) can be introduced through the axial buckling :

$$\rho = 1 - \frac{1 + M^2B^2_{rad} + M^2 \dfrac{\pi^2}{(h+\lambda)^2}}{k_\infty}$$

Working always at critical levels below the upper limit of the active part of the fuel rods, i.e. not changing λ, one obtains by derivation of the preceding formula :

$$\frac{\partial \rho}{\partial h} = \frac{2M^2 \pi^2}{k_\infty} \times \frac{1}{(h+\lambda)^3}$$

The complete $\frac{\partial \rho}{\partial h} = f(h)$ curve can thus be obtained by a least square fitting of the experimental points and the best values of $\frac{2M^2 \pi^2}{k_\infty}$ and λ are determined.

The axial extrapolation length λ can also be defined on the basis of axial buckling measurements; but, up to now, the fitting has always been better with a smaller extrapolation length than the one given by the buckling determination. The only explanation of this fact seems to be the lack of precision due to the one group theory approximation.

An example of such a measurement is given in figure V.10.

The curve being known, the reactivity effect of a given perturbation is easily obtained by measuring the critical levels with and without this perturbation and by integrating the $\partial\rho/\partial h$ curve between both :

$$\int_{h_o}^{h_i} \frac{\partial \rho}{\partial h}\, dh = \frac{M^2 \pi^2}{k_\infty} \left[(h_i + \lambda)^{-2} - (h_o + \lambda)^{-2} \right]$$

C. Accuracy

The precision on each measured point, used for the $\frac{\partial \rho}{\partial h}$ fitting, depends mostly on the knowledge of the water level increment; it is of the order of 5 %.

A $\frac{\partial \rho}{\partial h}$ curve is generally fitted on about 15 points; this reduces the uncertainty on the $\frac{M^2 \pi^2}{k_\infty}$ parameter to 1.5 %.

The final uncertainty on the reactivity effects is usually found between 0.015 and 0.035 % $\Delta k/k$; it depends mostly on the water level measurements for small perturbations and on the $\frac{M^2 \pi^2}{k_\infty}$ parameter for greater ones.

APPENDIX V.6 : SPECTRAL INDEX MEASUREMENTS

A. Introduction

We define a spectral index as the ratio between the reaction rates of two isotopes irradiated in the same spectrum. It can be expressed as follows :

$$\frac{\int_o^\infty \Phi(E)\,\sigma_i(E)\,dE}{\int_o^\infty \Phi(E)\,\sigma_j(E)\,dE} = \frac{\dfrac{\int_o^\infty \Phi(E)\,\sigma_i(E)\,dE}{\int_o^\infty \Phi(E)\,dE}}{\dfrac{\int_o^\infty \Phi(E)\,\sigma_j(E)\,dE}{\int_o^\infty \Phi(E)\,dE}} = \frac{\hat{\sigma}_i}{\hat{\sigma}_j}$$

where : - $\Phi(E)$ is the neutron spectrum;

- $\sigma_i(E)$ and $\sigma_j(E)$ are the differential cross sections of the considered isotopes for the measured reactions;
- $\hat{\sigma}_i$ and $\hat{\sigma}_j$ are the effective cross sections for the given spectrum according to the WESTCOTT notations.

The most important spectral index for uranium-plutonium fuel is the ratio between the Pu^{239} and U^{235} fission rates, because most of the fissions are induced in those isotopes and because this ratio is very sensitive to spectrum variations in the thermal energy range.

B. Experimental method

The measurement is based on the activation of two kinds of fissile foils :

- a U/Al alloy with 20 % uranium, enriched at 93 % of U^{235}. The uranium content of the foil is 7.65 mg/cm^2 and its thickness is 0.127 mm.

- a Pu/Al alloy with 20 % plutonium, containing 97 % of Pu^{239}. The plutonium content is 4.55 mg/cm^2 and its thickness is 0.076 mm.

The experimental method consists in comparing the foil activities after an irradiation in the investigated spectrum with the activities of the same foils irradiated in a pure Maxwell spectrum, which is available in the graphite thermal column of the BR1 reactor.
The spectral index is obtained by the expression :

$$\left(\frac{\hat{\sigma}_f^{239}}{\hat{\sigma}_f^{235}}\right)_R = \frac{\left(\frac{A_o^{239}}{A_o^{235}}\right)_R}{\left(\frac{A_o^{239}}{A_o^{235}}\right)_T} \times \left(\frac{\hat{\sigma}_f^{239}}{\hat{\sigma}_f^{235}}\right)_T$$

under the following conditions :

a) the same foils are irradiated successively in the investigated spectrum (R) and in the thermal column (T), so that it is not necessary to take into account eventual weight differences;

b) the activities A_o correspond to zero thickness foils, i.e. they are corrected for the perturbations due to the presence of the foil as well in the investigated medium (the fuel) as in the thermal column; this important point will be discussed below;

c) as the foils are irradiated between fuel pellets, the measured activity contains a parasitical activity of about 5 % due to the fission products coming from the adjacent pellets. The correction is made on the basis of the activity of an aluminium foil, irradiated in the same conditions as the fissile ones;

d) the γ-activities of the foils are measured through a β-shielding made of a 5 mm thick aluminium plate and with a threshold adjusted at 0.765 MeV to avoid any self-absorption effect;

e) both types of foils are irradiated simultaneously and are counted between 2 and 7 hours after the end of the irradiation.
During this period, their γ-activities follow the law :

$$A(t) = A(t_o) \times \left(\frac{t}{t_o} \right)^{-\alpha}$$

where α is a constant for a given fuel. The α's of U^{235} and Pu^{239} being somewhat different, all the activities have to be reconverted into activities at a well-defined moment after the irradiation.

f) the γ-spectra and the decay laws are assumed to be independent of the neutron spectrum in which the foils are irradiated.

The $\left(\frac{\delta_f^{239}}{\delta_f^{235}} \right)_T$ ratio is obtained on the basis of the best values of the fission cross sections (ref. V.1) and of the neutron temperature of the thermal column, which is practically equal to the graphite temperature

Isotope	σ_f (2200 m s^{-1})	g (293 °K)	δ_f (293 °K)	$\left(\frac{\delta_f^{239}}{\delta_f^{235}} \right)_T$
Pu^{239}	(743.1 ± 3.5) b	1.049	(779.5 ± 3.7)b	1.381 ± 0.008
U^{235}	(578.3 ± 1.6) b	0.976	(564.4 ± 1.6)b	

C. Foil perturbation

C.1. In the thermal column

In order to estimate the perturbation of an absorbing foil in a moderator, the following formula is used, according to the work of SHOOK et al. (Ref. V.2) :

$$\frac{\text{actual activity}}{\text{zero thickness activity}} = \frac{\frac{1 - 2E_3(\tau)}{2}(1+\varepsilon)}{1 + \frac{1 - 2E_3(\tau)}{2} g}$$

where τ is the optical thickness of the foil

ϵ is a correction taking into account the edge effect on the self-shielding in the foil;

g is another correction taking into account the edge effect on the external flux depression.

The spectrum of the thermal column being maxwellian, the perturbation calculation performed at one energy is sufficiently accurate : a value of 0.956 is found for the U/Al foil and 0.955 for the Pu/Al one. This proves that the presence of the foils in the thermal column does not modify the ratio $\left(\frac{A_o^{239}}{A_o^{235}}\right)_T$; this is mainly due to the fact that both types of foils have the same optical thickness.

C.2. <u>In the fuel</u>

Irradiated between the fuel pellets, the foils create a perturbation depending on the difference between the macroscopic cross sections of the foils and the fuel. Due to the complexity of the neutron spectrum and the cross sections, a calculation in function of energy is necessary :

$$\frac{\text{actual activity}}{\text{zero thickness activity}} = \frac{\int_o^\infty \phi(E) \frac{\overline{\phi}(E)_{foil}}{\phi(E)} \sigma_f(E)\, dE}{\int_o^\infty \phi(E)\, \sigma_f(E)\, dE}$$

where - $\phi(E)$ is the mean, unperturbed neutron spectrum inside the fuel pin, as calculated e.g. by a theoretical code;

- $\sigma_f(E)$ is the differential fission cross section of the considered isotope U^{235} or Pu^{239};

- $\frac{\overline{\phi}(E)_{foil}}{\phi(E)}$ is the flux perturbation induced by the foil.

For the fuels and the foils considered here, calculations have been made for the four following cases :

Type of foil	Type of fuel	$\frac{\text{actual activity}}{\text{zero thickness activity}}$	Correction factor
U/Al	4/0	0.989	1.011
Pu/Al	4/0	0.930	1.075
U/Al	3/1	0.998	1.002
Pu/Al	3/1	0.948	1.054

Due to the importance of the perturbations created by the Pu/Al foils, an experimental check of the calculation method was made for the most unfavourable case : a Pu foil inside the 4/0 fuel. For that purpose, a special 4/0 capsule was filled with Pu/Al foil sandwiches of increasing thickness, aluminium foils having been introduced in order to allow for the correction for the fission products coming from the adjacent pellets or foils. The correct position of the foils has been checked by radiography; indeed a good contact between the detectors themselves and between the foils and the pellets is very important to avoid streaming effects.
The internal arrangement of the capsule is given in fig. V.11, where the macroscopic gradient, obtained by counting the pellets, and the mean activities of the foil sandwiches are shown. After correction for the macroscopic gradient, these activities can be compared to the calculated results (fig. V.12).
The calculated curves are normalized to unity for the actual thickness of the foils, so that the reading of the curves for the zero thickness gives directly the correction factor. On the other hand, the experimental results are normalized so that the mean theory to experiment ratio is equal to unity.

The ratio $\frac{\overline{\phi}(E)_{\text{foil thickness x}}}{\phi(E)_{\text{zero thickness}}}$ has been calculated in function of energy by two methods :

a) the "DUNN" method

In reference V.3, the author shows that MONTE CARLO calculations are necessary to perform a correct interpretation of disadvantage factor measurements; this is particularly due to the fuel discontinuity introduced by the foils. He shows however that a simplified calculation method allows an adequate estimation of the perturbation, assuming an isotropic flux and neglecting the edge effects :

$$\frac{\text{Act.(x thickn.)} - \text{Act.(0 thickn.)}}{\text{Act.(x thickn.)}} \simeq x \left[\Sigma_{abs.}(\text{fuel}) - \Sigma_{abs.}(\text{foil})\right] \text{Log } \frac{D}{x}$$

where D is the foil (or fuel) diameter and x the foil thickness.

Comparisons between the simplified calculation and the MONTE CARLO one shows that the first one is sufficiently accurate for perturbations below 10 %.

b) the "SHOOK" method

Shook's formula (see 3.1) has also been used, even for the fuel. Indeed the authors of reference V.4 show that the use of this calculation method may be generalized to moderators containing absorbing or multiplying solutions.

As it can be seen in the figure, both methods give the same results above 0.1 mm of Pu/Al; moreover their shape is in good agreement with the experimental points. Below 0.1 mm however they give different results; unfortunately there are no experimental results in this thickness range to allow the choice of the better method. The "SHOOK" method being in fact only intended for situations where the foil is more absorbing than the medium, the "DUNN" method is to be used in general. The small disagreement between both methods is taken into account for the experimental error estimation.

D. Experimental accuracy

The experimental error has to be estimated on the basis of the following items :

- the knowledge of the fission cross sections for the reference spectral index calculated for the thermal column : $\pm$ 0.6 %;
- the accuracy of the ratio between the foil activities has been estimated by reproducibility tests : $\pm$ 1 %;
- the accuracy of the perturbation calculations is estimated at $\pm$ 1 %;
- an additional uncertainty has to be added to take into account the choice of the calculation method : $^{+\ 0\ \%}_{-\ 2\ \%}$.

According to these figures, the experimental value of the $\frac{\sigma_f^{239}}{\sigma_f^{235}}$ spectral index is obtained with a global uncertainty of $^{+\ 2\ \%}_{-\ 4\ \%}$.

APPENDIX V.7 : POWER SHARING DETERMINATION

A. Introduction

In a core with fuels of various compositions, the distribution of the fission density or of the power density has to be measured in two phases, when the activation technique is used. Indeed, the proportionality coefficient between the investigated density and the γ-activity of the fuel differs from one fuel to another one. The first phase is an individual measurement of the γ-activity distribution in each region and the second one is the determination of the so-called power sharing factor, which allows the normalization of the γ-activity distributions. The power sharing factor can be obtained by two practically independent methods.

B. Activation of fissile foils

When the reactor core is composed of two fuel regions, the simultaneous irradiation of two couples of U/Al and Pu/Al foils in each region allows the determination of the ratio between the fission densities for each isotope in the two regions as well as the $\frac{Pu^{239}}{U^{235}}$ spectral indices in each region.

The ratio of the total number of fissions in the two regions can easily be obtained by combining these ratios with the corresponding atomic densities. In the case of a 3/1 fuel region adjacent to a 4/0 one e.g., the total fission ratio is expressed as follows :

$$\frac{F_{3/1}}{F_{4/0}} = \frac{F^{235}_{3/1} + F^{238}_{3/1} + F^{239}_{3/1} + F^{240}_{3/1} + F^{241}_{3/1}}{F^{235}_{4/0} + F^{238}_{4/0}} =$$

$$\left[\frac{N^{235}_{3/1}}{N^{235}_{4/0}} \times \frac{\left(\hat{\sigma}_f^{235}\right)_{3/1}}{\left(\hat{\sigma}_f^{235}\right)_{4/0}} + \frac{N^{239}_{3/1}}{N^{235}_{4/0}} \times \frac{\left(\hat{\sigma}_f^{235}\right)_{3/1}}{\left(\hat{\sigma}_f^{235}\right)_{4/0}} \times \left(\frac{\hat{\sigma}_f^{239}}{\hat{\sigma}_f^{235}} \right)_{3/1} \right] \times C$$

where : - F is the fission density [fiss./cm^3],

- N is the atomic density [at./cm^3],

- and C a correction factor taking into account the contributions of the isotopes other than U^{235} and Pu^{239}:

$$C = \frac{\left[1 + \frac{F^{238}_{3/1} + F^{240}_{3/1} + F^{241}_{3/1}}{F^{235}_{3/1} + F^{239}_{3/1}} \right]}{\left[1 + \frac{F^{238}_{4/0}}{F^{235}_{4/0}} \right]}$$

The first factor is experimentally obtained and the C factor is established on the basis of theoretical data; it leads to a correction of about 3 ‰.

In order to obtain the power density ratio, the energy yield per fission of each isotope has to be introduced in the preceding expression. The following values are adopted (ref. V.4) :

$$p^{238} \simeq p^{235} = (201.7 \pm 0.6) \text{ MeV/fiss.}$$

$$p^{241} \simeq p^{240} \simeq p^{239} = (210.7 \pm 1.2) \text{ MeV/fiss.}$$

C. Activation of fuel pellets

Pellets of the different fuel types are simultaneously irradiated in the corresponding regions and the γ-activity of the La^{140} produced in each pellet is measured after a cooling time of at least 13 days.

Again, taking the example of a 3/1 fuel region and a 4/0 one, the fission density ratio is obtained as follows :

$$\frac{F_{3/1}}{F_{4/0}} = \frac{\gamma\text{-Act.}^{140}_{3/1}}{\gamma\text{-Act.}^{140}_{4/0}} \times \frac{f_{4/0}}{f_{3/1}} \times \frac{A}{B}$$

where : - $\frac{f_{4/0}}{f_{3/1}}$ is a small correction factor to take into account the different flux depressions in the fuel pellets and their influence on the self absorption of the La^{140} γ-activity; this correction factor is of the order of 0.3 % and has been neglected.

- A is a correction factor, which accounts for the difference between the La^{140} yields for the U^{238} fissions and the U^{235} ones in the 4/0 fuel :

$$A = \frac{1 + \frac{F^{238}_{4/0}}{F^{235}_{4/0}} \times \frac{\gamma^{238}}{\gamma^{235}}}{1 + \frac{F^{238}_{4/0}}{F^{235}_{4/0}}}$$

- B is a correction factor equivalent to A but for the isotopes of the 3/1 fuel :

$$B = \frac{\left[1 + \frac{N^{239}_{3/1}}{N^{235}_{3/1}} \times \left(\frac{\hat{\sigma}_f^{239}}{\hat{\sigma}_f^{235}}\right)_{3/1} \times \frac{\gamma^{239}}{\gamma^{235}}\right]\left[1 + \frac{F^{238}_{3/1} \times \gamma^{238} + F^{240}_{3/1} \times \gamma^{240} + F^{241}_{3/1} \times \gamma^{241}}{F^{235}_{3/1} \times \gamma^{235} + F^{239}_{3/1} \times \gamma^{239}}\right]}{\left[1 + \frac{N^{239}_{3/1}}{N^{235}_{3/1}} \times \left(\frac{\hat{\sigma}_f^{239}}{\hat{\sigma}_f^{235}}\right)_{3/1}\right]\left[1 + \frac{F^{238}_{3/1} + F^{240}_{3/1} + F^{241}_{3/1}}{F^{235}_{3/1} + F^{239}_{3/1}}\right]}$$

In the expressions A and B, the fission densities of U^{235} and Pu^{239} are experimentally obtained by foil activation; the other fission densities are established theoretically. The $\frac{\gamma^{239}}{\gamma^{235}}$ ratio, where γ^{239} and γ^{235} are the La^{140} yields per fission of the corresponding isotopes, is taken equal to 0.826 ± 0.011 (ref. V.5). $\frac{\gamma^{238}}{\gamma^{235}}$ has been measured for U^{238} fast fission and U^{235} thermal fission : $\frac{\gamma^{238}}{\gamma^{235}} = 1.055$ (ref. V.6).

Finally, the contribution of the Pu^{240} and Pu^{241} isotopes being small, it may be assumed that $\gamma^{241} \simeq \gamma^{240} \simeq \gamma^{239}$.

The $\frac{A}{B}$ ratio corresponds to a global correction of about 9 % in the case of the 3/1 and 4/0 fuels.

As for the foil activation method, the power density ratio may be obtained by introducing the yields in energy per fission in both expressions A and B. Here too, it may be assumed that $p^{238} \simeq p^{235}$ and $p^{241} \simeq p^{240} \simeq p^{239}$.

D. Accuracy

For the foil activation method, the power sharing ratio is the result of combining atomic densities and spectral indices; the global uncertainty is thus obtained by combining the corresponding uncertainties. This leads to a global experimental error of about 5 %.

For the pellet activation method, the most important uncertainties are the statistical counting error, which is usually reduced to about 0.5 % by accumulating a great amount of countings, and the error on the $\frac{\gamma^{239}}{\gamma^{235}}$ ratio. A global uncertainty of about 1 % is generally obtained with this method.

E. Comparison of both methods

The foil activation method has two important disadvantages : relatively large statistical errors and possible systematical errors due to the perturbations introduced by the foils inside the fuel. Nevertheless it is interesting to do, in parallel with the pellet activation measurements, a few foil activation measurements in order to make a cross check between both types of results. Both methods are indeed practically independent, because the spectral index, obtained with the foil activation, enters only as a correction factor in the pellet activation analysis.

A lot of power sharing ratios have been measured in a slab configuration with 3/1 and 4/0 fuels, including several perturbations at the

boundary between the fuel regions. All the results are given in fig. V. 13: an asymptotic worth of the power sharing ratio appears when the neutron spectrum reaches its equilibrium at both sides of the boundary. The figure shows also that the results obtained by the two techniques are equal within their error margins.

APPENDIX V.8 : RADIAL POWER DISTRIBUTION INSIDE FUEL RODS

Two different techniques are used for the determination of the radial power distribution inside fuel pins :

A. The track detector technique

A.1. Method

This method consists in inserting mica foils between the fuel pellets. During the irradiation, the fission products emitted by the pellet sides are collected by the mica foil, in which their mean path is of the order of 10 μ. After irradiation, the fission product tracks are enlarged by putting the mica in fluorhydric acid, so that the counting with a microscope becomes easy. The irradiation and etching conditions have been optimized so that :

- the counting precision is good,
- the tracks are sufficiently distant from each other,
- the track sizes are great enough to avoid any confusion with eventual damages of the mica foils.

A track density of 5.10^5 tr/cm^2 is found to be the best one. The track counting is carried out with a microscope which enables the measurement along the diameter of the foil with a resolution of 0.3 mm. Each time the mean result of two opposite radii is adopted in order to avoid any influence of macroscopic flux gradients.

A.2. Precision

The precision on each measured point is about 2 %; therefore a total counting of about 3000 tracks is needed; for central points the precision reaches 1 %, due to a greater number of counted tracks. The influence of the fuel discontinuity, due to the presence of the mica on the measured fission depression, seems to be negligible. Indeed, for the involved mica thickness, which is of the order of 0.05 mm, the thermal flux peaking for both the 4/0 and 3/1 fuels is only about 2 %, assuming for the calculation that there is no neutron absorption in the mica foil.

A.3. It has to be noted that this technique allows also the absolute measurement of the fission density when a calibration is carried out in a well known thermal flux (Ref. V.7).

B. The ring activation technique

B.1. Method

This method consists in irradiating, between fuel pellets, U/Al and Pu/Al foils of the same kind as those used for spectrum index measurements, but cut into small concentric detectors : a central circular one and several rings.
The relative γ-activities of these detectors are a measure of the radial distribution of the fission density for the activated isotope. If these radial distributions are normalized by means of the spectrum index measured inside the fuel, it is possible to obtain the radial variation of this index through the fuel pin.

B.2. Calibration of the counting device

The measurements are performed with a NaI well crystal. Due to the different sizes of the rings, it had to be checked if the sensitivity of the crystal does not change with the diameter of the detector. Therefore, a large square U/Al foil has been irradiated in a flat flux, the size of the foil being large enough to avoid any edge effect. After having checked that its specific activity was really constant by counting small detectors cut along the diagonal of the square foil, a series of concentric detectors was cut and counted in the same way as for a depression measurement. The specific γ-activities of the concentric detectors did not show any radial variation of the crystal sensitivity within the experimental error (about 0.5 %).

B.3. Precision

An estimation of the experimental accuracy has been made on the basis of reproducibility tests; an uncertainty of about 2 % has been obtained for each step value.

A test of an eventual streaming effect, due to a bad flatness of the concentric detectors during the irradiation, has been carried out by comparing the sum of the activities of a series of concentric detectors with the one of a complete detector irradiated close to the first ones. An agreement better than 1 % was found.

C. Comparison of the two techniques

The differential curves given by the track detector technique, have been integrated between the different ring diameters to enable a comparison of the techniques. The agreement is very good for the 4/0 fuel and somewhat less good for the 3/1 fuel, but remains in any case within the experimental uncertainties (see Chapter VII).

References

V.1. WESTCOTT, et al., A Survey of values of the 2200 m/s constants for four fissile nuclides, Atomic Energy Review, 3, 2 (1965)3.

V.2. SHOOK, D.F., et al., Thermal neutron flux perturbation by dysprosium-aluminium foils in water and uranyl fluoride-water solutions; Nuclear Science and Engineering 26 (1966) 453.

V.3. DUNN, F.E., Flux dipping and flux peaking in foils used in thermal disadvantage factor measurements; Transactions of the American Nuclear Society 9, 1 (1966).

V.4. WALKER, W.H., Mass balance estimate of the energy released per fission in a reactor; AECL-3109 (1968).

V.5. OKAZAKI, A., WALKER, W.H., Measurement of the yields of I^{135} and Ba^{140} in the fission of U^{233}, U^{235}, Pu^{239} and Pu^{241}; Canadian Journal of Physics, vol. 43 (1965).

V.6. ACCINI, F., CIUFFOLOTTI, L., The Ba^{140} yields for thermal and fast fission in U^{235} and U^{238}; C.I.S.E.-R-171.

V.7. DE COSTER, M., LANGELA, D., Détermination expérimentale précise du taux de fission dans des crayons combustible au moyen de détecteurs; Communication au Groupe de Travail Dosimétrie, EURATOM (Janv. 1969).

APPENDIX VI.1 : THEORETICAL METHODS USED IN PANTHER CALCULATIONS

A. Thermal spectrum calculation [3] [4] [5] *

The treatment of the thermal energy range in the PANTHER code includes the thermal spectrum calculation on the basis of CADILHAC's method and the averaging of the thermal group constants over the cell spectrum; the cut-off energy can be chosen from 0.625 eV to 1.855 eV. The heterogeneity of the lattice is taken into account : three formalisms are available.

Adequate numerical methods have been proposed by combining the multigroup approximation and P_N or S_N transport methods but they lead to excessive running times for routine calculations for thermal spectrum calculations.

In the stationary case, with no external sources, and assuming an isotropic emission density, the Boltzmann transport equation can be written in the integral form :

$$\Phi(\bar{r}, E) = \int dV \left[\varkappa(\bar{r}, E) \cdot \frac{1}{4\pi |\bar{r} - \bar{r}'|^2} \exp\left(- \int_{\bar{r}'}^{\bar{r}} \Sigma \, ds \right) \right] \quad (1)$$

$\Phi(\bar{r}, E)$ is the scalar flux and $\varkappa(\bar{r}, E)$ the isotropic emission density.

If the system can be divided in N homogeneous regions where the flux can be considered as constant, the relation (1) can be replaced by the N relations

$$\Phi_j(E) = \sum_{i=1}^{N} \frac{P_{j,i}(E)}{\Sigma_i(E)} \varkappa_i(E) \qquad j = 1,N \quad (2)$$

---

* Numbers between square brackets refer to the bibliography, given at the end of this appendix.

Φ_j and $\varkappa_j$ are the volume averaged flux and emission density and Σ_j the total cross-section in zone j. $P_{j,i}(E)$ is the probability that a neutron uniformly and isotropically born in zone j, collides for the first time in zone i :

$$P_{j,i}(E) = \frac{\Sigma_i(E)}{V_j} \iint \frac{\exp\left(-\int_{\bar{r}_i}^{\bar{r}_j} \Sigma \, ds\right)}{4\pi \, |\bar{r}_i - \bar{r}_j|^2} \, dV_i \, dV_j \qquad (3)$$

where r_i denotes a point in zone i and r_j a point in zone j.

The reciprocity relation is an immediate consequence of this expression and reads :

$$\Sigma_i \, P_{i,j} \, V_i = \Sigma_j \, P_{j,i} \, V_j \qquad (4)$$

The study of neutron thermalization will establish a relation between the slowing-down density q and the neutron flux Φ, whereas the study of the geometrical heterogeneity will define the collision probabilities. The fundamental equations to be solved are :

$$\boxed{\Sigma_j \, \Phi_j \, V_j = \sum_{i=1}^{N} P_{i,j} \, \varkappa_i \, V_i} \qquad j = 1,N \qquad (5)$$

B. Treatment of thermalization : the Cadilhac model

Let us consider, in an infinite homogeneous system, the function :

$$G(E) = \frac{d}{dE}\left(\frac{\Phi(E)}{M(E)}\right)$$

M(E) being the Maxwellian flux at the temperature T of the system and K the Boltzmann constant.

$$M(E) = \frac{E}{(KT)^2} \exp\left(-\frac{E}{KT}\right)$$

The flux being Maxwellian in an infinite non absorbing medium, the function C(E) can be interpreted as the departure, due to the absorptions, of the neutron distribution from the equilibrium Maxwellian spectrum. By using the principle of detailed balance, q is related to C by an integral Hermitian operator. The idea of Cadilhac was to consider the inverse operator J [7] :

$$C = \frac{d}{dE}\left(\frac{\phi(E)}{M(E)}\right) = J\, q(E) \qquad (6)$$

J is an Hermitian positive definite operator. In the synthetic model proposed by Cadilhac, J is a differential second order operator. As it is self-adjoint it is written :

$$J(E) = j(E) - \frac{d}{dE}\left(k(E)\frac{d}{dE}\right) \qquad (6')$$

This form of J is shown to be rigorous in two extreme cases; the monoatomic hydrogeneous gas and the heavy free gas, and it can represent with a very good approximation all usual moderators.

In the "Generalized Heavy Free Gas", model of Horowitz the operator J(E) reduces to :

$$J(E) = j(E) \qquad (6'')$$

This is called the primary model.
In the secondary model, j(E) and k(E) are non zero functions related to the scattering law $S(\alpha, \beta)$ of the system. The relation however is not univocal and Soulé has studied the best way to adjust j and k on the physical model. In order to take into account the asymptotic behaviour of j(E) and k(E) at high energies, two new functions are introduced :

$$\left.\begin{aligned} H(E) &= \xi\, \Sigma_s(\infty)\, .\, M(E)\, .\, k(E) \\ G(E) &= \xi\, \Sigma_s(\infty)\, .\, M(E)\, .\, EKT\, .\, j(E) \end{aligned}\right\} \qquad (7)$$

For high values of E, G and H have finite limits; besides, the relation between ϕ and q becomes :

$$\phi(E) = \frac{1}{\zeta \Sigma_s(\infty)} \left[G(E) \frac{q(E)}{E} - H(E) \frac{dq(E)}{dE} \right] \qquad (8)$$

C. Treatment of heterogeneity

The knowledge of collision probabilities in each spatial homogeneous region for the neutrons born in every region which cross the other regions without colliding, can be simplified in a periodical lattice by considering an elementary cylindrical cell preserving the area of the moderator according to the Wigner - Seitz model.

By combining flux boundary conditions with the collision probabilities for the lattice cell effective collision probabilities can be obtained as proposed by Clayton [8]. When considering an elementary cell with a certain number of regions of volume V_j, P_{ik} can be considered as the probability that a neutron born in V_i, or in any of its images V_i^m in the lattice will undergo its next collision in V_k :

$$P_{ik} = P_{ik}^c + \sum_{m \geq 1} P_{ik}^m \qquad (9)$$

where P_{ik}^m is the collision probability in V_k for a neutron born in V_i^m and P_{ik}^o is the collision probability in V_k for a neutron born in V_i, in the absence of lattice.

Then :

$$\Sigma_j(E)\, V_j \,.\, \phi_j(E) = \sum_{i=1}^{N} P_{ij}^o(E) \,.\, \varkappa_i(E)\, V_i + \Theta_j(E) \quad .$$

where :

$$\Theta_j(E) = \sum_{m \geq 1} \left(\sum_{k=1}^{N} P_{kj}^m \varkappa_k V_k \right) \qquad (10)$$

is obviously the contribution to the collision density from emission in the images of the lattice cell. This contribution may be considered as the collisions in the cell due to the boundary flux.

The calculation of these effective collision probabilities is quite different whether the fuel is surrounded by a large weakly absorbing moderator where the diffusion approximation is valid, or if the cell dimensions are small and the fuel strongly absorbing, where the transient solutions of the transport equations are prevailing.

When the outer moderator is weakly absorbing the collision probabilities method may be applied to the remainder of the cell excluding the moderator, and Θ_j is interpreted as the collision in V_j due to neutrons leaving the moderator. Another type of collision is used in the moderator and therefore the specification of Θ_j constitutes the boundary conditions for the inner region of the cell. This is the basis of the SPECTROX method proposed by Leslie, which is a generalization of the Amouyal-Benoist moderator treatment and which gives good results for light water moderator cells, despite the arbitrariness of some of its calculational prescriptions.

As indicated by Sauer [17] the success of the Amouyal method, replacing the extrapolation distance into a black body found by diffusion theory by the extrapolation length derived by means of transport theory of the cylindrical Milne problem with sources at infinity, is due to the fact that the artificial boundary condition used at the fuel boundary approximately compensates for the error caused by cell cylindrization.

In the other case, an approximate boundary condition on the flux must be specified and effective collision probabilities can then be defined.

C.1. Treatment of heterogeneity with weakly absorbing outer moderator (Amouyal and Benoist : SPECTROX)

The fundamental equations (5) can be written :

$$\Sigma_j V_j \phi_j = \sum_{i=1}^{N} P_{ij} \kappa_i V_i + S_M \cdot j_M^- P_{Bj}$$

where j_M^- is the inward current per unit area at the moderator inner surface S_M, and P_{Bj} the probability for a neutron crossing the moderator inner surface to collide for the first time in V_j, according to a given angular distribution.

Beside these N fundamental equations (N being the number of regions inside the moderator), the conservation equation in the moderator

$$\left(\pi_M - \Sigma_{s_M} \phi_M \right) V_M = \Sigma_{a_M} V_M \phi_M + S_M j_M(E) \qquad (11)$$

and the global conservation equation in the inner region

$$\sum_{k=1}^{N} \Sigma_{ak} V_k \phi_k - \sum_{k=1}^{N} \left(\pi_k - \Sigma_{sk} \phi_k \right) V_k = S_M j_M \qquad (12)$$

a last relation between j_M, j_M^- and ϕ_M is needed for the solution of the N+3 unknowns ϕ_i (i = 1, 2,...,N) ϕ_M, j_M and j_M^-.

Leslie [4] has developed the SPECTROX method based upon a successive collision probabilities treatment of the fuel and the use of diffusion approximation in the moderator. The method has been generalized to include many similar treatments. If r_1 is the fuel radius, r_2 and r_3 the inner and outer radius of the moderator, the SPECTROX assumption for the spatial dependence of the neutron flux, justified by the Tretiakoff [9] expansion of the moderator flux in terms of buckling eigenfunctions, leads to the moderator energy dependent mean flux :

$$\phi_M (E) = \phi (r_2, E) \left[1 + \frac{r_2}{\Lambda} h \left(\frac{r_3}{r_2} \right) \right] \qquad (13)$$

with

$$h(y) = \frac{y^2}{y^2 - 1} \left[\frac{y^2}{y^2 - 1} \ln y - \frac{3}{4} + \frac{1}{4 y^2} \right] \qquad (14)$$

The underlying assumptions are, beside the treatment of moderator by diffusion approximation, the boundary conditions :

$$\left.\begin{aligned} \frac{d\phi}{dr} \left(r = r_3 \right) &= 0 \\ \frac{d\phi}{dr} \left(r = r_2 \right) &= \frac{1}{\Lambda} \phi (r_2) \end{aligned}\right\}$$

A relation between j_M and j_M^- is provided either by the diffusion theory or by the blackness concept leading to :

$$j_M^- = \frac{3}{4} \left(\Lambda \Sigma_{tr_M} + H \right) j_M \qquad (15)$$

with $H = 2/3$ in diffusion theory (16)

$= H \left(r_2 \Sigma_{tr_M} \right)$ in Kushneriuk's method for a gray body

$= \frac{4}{3} - \lambda_{bb}$ in Amouyal - Benoist's method [5]; λ_{bb} is the extrapolation length of a black body in an infinite medium.

With the help of Fick's law the desired supplementary equation is found :

$$j_M^-(E) = \frac{1}{4} \phi_M(E) + \left[\frac{3}{4} H(E) - \frac{r_2}{4D_m} h \left(\frac{r_3}{r_2} \right) \right] j_M(E) \qquad (17)$$

The treatment of a void between fuel and moderator will not increase the complexity of the problem if the probabilities P_{Bi} can be related to the corresponding probabilities for a neutron coming to the surface S_1 of the fuel rod, which have been extensively studied and tabulated.

The flux shape in the moderator near S_M has been defined by the extrapolation length Λ. The parameter of the anisotropy is then

$\frac{3}{2} H \frac{\lambda_M}{\Lambda}$ if λ_M is the moderator mean free path.

The current of neutrons entering the rod per unit height is written as :

$$2 \pi r_1 j_1^- = J_1^- = \frac{\pi}{2} r_1 \phi_M + X J_1 \qquad (18)$$

with

$$X = \frac{3}{4} H n \left(\frac{r_1}{r_2} \right) - \frac{r_1}{4D_M} h \left(\frac{r_3}{r_2} \right)$$

According to Newmarch's treatment with linear anisotropy [6] the expression for n(x) is :

$$n\left(\frac{r_1}{r_2}\right) = \frac{2}{\pi}\left\{ \mathrm{Sin}^{-1}\frac{r_1}{r_2} + \frac{r_1}{r_2}\left[1 - \left(\frac{r_1}{r_2}\right)^2 \right]^{1/2} \right\}$$

while Amouyal and Benoist find with the assumption of isotropy :

$$n\left(\frac{r_1}{r_2}\right) = \frac{r_1}{r_2}$$

Two cases are to be distinguished in the determination of P_{11} and P_{B1} according to whether $\Sigma_1 \cdot r_1$ is smaller or greater than 1.

In the first case, the spatial uniformity of the flux can be assumed.

Stuart and Woodruff [12] showed that the anisotropy of the incident neutrons can be ignored, as different angular distribution laws lead to quite similar results. Moreover as the fuel does not contain light elements the anisotropy of the scattering can also be ignored in the calculation of P_{B1} and P_{11} which are thus known. It should be emphasized that neglecting the anisotropy is only a simplification which is thought not to produce any appreciable error.

Expressing the fundamental equation for a non absorbing rod immersed in a homogeneous infinite medium with the same composition we have the condition that :

$$P_{B1} = 2\left(1 - P_{11}\right)\Sigma_1 \cdot r_1 \qquad (19)$$

In the second case the use of numerous spatial homogeneous subregions can be avoided by considering the successive collision probabilities P_k in the rod for a neutron entering the rod according to a given angular distribution.

By equating the total collision rate in the rod to the sum of successive collision rates, the mean flux in the fuel and the current entering the fuel are related by :

$$\left(\frac{1}{G} - Kz \right) \Sigma_1 V_1 \phi_1 = J_1^- + \frac{1}{G^2} \left[P_o (P_1 - P_2) * \left\{ P_1 z (P_o J_1^-) \right.\right.$$

$$\left.\left. - z (P_1 P_o J_1^-) \right] + \ldots \right\} \qquad (20)$$

with

$$L_1(\phi) = \int_o^\infty \Sigma_{s1} (E' \rightarrow E) \phi_1 (E') dE' - \Sigma_{s1}(E) \phi_1(E)$$

$$z = \frac{L_1}{\Sigma_1} - \frac{\Sigma_{a1}}{\Sigma_1}$$

$$K = \frac{P_o}{G^2} \left(P_1 + 2P_1 P_2 + 3P_1 P_2 P_3 + \ldots \right)$$

$$G = P_o \left(1 + P_1 + P_1 P_2 + \ldots \right)$$

The assumption has been made that the operator z is sufficiently weak to neglect its powers. This assumption can become inaccurate at resonance peaks.

If all P_i ($i \geq 1$) are equal or if z can be permuted with P_i (both conditions proving rather well fulfilled), equation (20) reduced to :

$$\left(\frac{1}{G} - Kz \right) \Sigma_1 V_1 \phi_1 = J_1^- \qquad (21)$$

The same procedure leading to equation (19) gives now :

$$G = 2r_1 \Sigma_1 \qquad (22)$$

Equation (21) requires all probabilities P_j. Practically one equals all probabilities P_j ($j \geq M$) to a probability P'_M defined so as to fulfil equation (22).

When $M \rightarrow \infty$, K tends to a limit which can be considered as the exact limit. Owing to the fact that transport theory entails $K = 2/3$ when $\Sigma_1 r_1 = 0$, Leslie found the following analytical form for $K(\Sigma_1 r_1)$:

$$K(x) = \frac{1}{2} + \frac{3}{16} x + \left[6 + 2.8 \times 4.4 \left(1 - e^{-2x} \right) \right]^{-1}$$

The flat flux approximation corresponds to the assumption

$$P_1 = P_2 = P_3 \ldots$$

The system to be solved is then :

$$\left.\begin{aligned} J_1^- &= \frac{\pi}{2} r_1 \Phi_M + XJ_1 \\ J_1^- &= \left(\frac{1}{G} - Kz \right) \Sigma_1 V_1 \Phi_1 \\ V_1 \varkappa_1 &= \Sigma_1 V_1 \Phi_1 - J_1 \\ V_M \varkappa_M &= \Sigma_M V_M \Phi_M + J_1 \end{aligned}\right\} \qquad (23)$$

One finds :

$$L_M \Phi_M = \varkappa_M - \Sigma_{sM} \Phi_M = \Sigma_{aM} \Phi_M - \frac{\pi r_1}{2 V_M} \frac{1}{K - X} (\Phi_M - \Phi_1)$$

$$= G_{MM} \Phi_M + G_{1M} \Phi_1$$

$$L_1 \Phi_1 = \varkappa_1 - \Sigma_{s1} \Phi_1 = \Sigma_{a1} \Phi_1 + \frac{\pi r_1}{2 V_1} \frac{1}{K - X} (\Phi_M - \Phi_1)$$

$$= G_{M1} \Phi_M + G_{11} \Phi_1$$

A system of two coupled differential equations is to be solved, with the boundary conditions :

$$\Phi_i = 0 \qquad E = 0$$

$$i = 1,M$$

$$\Phi_i = \Psi_i \qquad E = E_c$$

In the generalized heavy gas formalism :

$$L = \xi \Sigma_s \frac{d}{dE} \left\{ \frac{1}{G(E)} \left[EKT \frac{E}{dE} + (E - KT) \right] \right\}$$

the system can be solved by the integration method proposed by Leslie [4] .

In Cadilhac's formalism however, the introduction of new functions is suggested :

$$U_i = \Phi_i \left[1 + \frac{H_i}{\zeta \Sigma_{si}} \left(g_{ki} \frac{\Phi_k}{\Phi_i} + g_{ii} \right) \right] \qquad (24)$$

$$= \Phi_i B_i$$

and the system to be solved is (y = E/KT) for i = 1, k = M and i = M, k = 1

$$\frac{d}{dy} \left\{ \frac{1}{G_i(y)} \left[y \frac{dU_i}{dy} + (y - 1) U_i \right] \right\}$$

$$= \frac{1}{B_i} g_{ii} U_i + \frac{1}{B_k} g_{ki} U_k$$

According to the definition of U_i, an iteration procedure is necessary here in secondary models of thermalization, i.e. when $H \neq 0$, but could be avoided by a different definition of functions U_i, as shown in the next section.

C.2. Treatment of heterogeneity with isotropic boundary flux (Bonalumi)

If J^- is the current of neutrons entering the cell and P_{Bi} the probability that such a neutron will suffer a collision in V_i, $\Theta_i = J^- * P_{Bf}$ As the net current entering the cell :

$$J = \sum_{i=1}^{N} \left(\Sigma_i \Phi_i - \pi_i \right) V_i \qquad (25)$$

must be zero, one finds the following expression for the effective collision probabilities :

$$P'_{ki} = P^o_{ki} + \frac{(1 - P^o_k)}{\sum_{j=1}^{N} P_{B_j}} P_{Bi}$$

where $P^o_k = \sum_{i=1}^{N} P^o_{ki}$ is the non escape probability for V_i.

An additional assumption is to be made on the angular distribution of the boundary flux for the calculation of P_{Bi}. Askew and Brissenden [13] have proposed a general boundary condition in which a fraction ζ of the neutrons reaching the boundary are reflected as from a mirror, the rest being scattered back into the moderator with a cosine distribution in the azimuthal direction which is independent of the path of the neutron before it strikes the boundary.

A "white" boundary condition at the outer cylindrical cell boundary, corresponding to $\zeta = 0$, has been imposed, corresponding to a situation in which the neutrons reaching the cell boundary recoil in an inward direction, all such directions being equally probable or in other words that the cell boundary flux is isotropical.
In this case it is proved by Case [14] that

$$P_{Bi} = \frac{4V_i}{S} \Sigma_i \left(1 - P_i^o \right)$$

where S is the surface area of the boundary.

As the approximate method to calculate collision probabilities in annular systems proposed by Bonalumi [15] and improved by Jonsson [16] does not entail explicit integrations but leads to accurate results by an elaborate procedure easily adapted to machine calculations, use has been made of it.

The first step is the calculation of transmission probabilities $(1 - G_{ij})$ in V_j for a neutron entering the inner boundary of this region with an angular distribution corresponding to uniform birth inside $r_i \leq r_{j-1}$.
Assuming the radial isotropy of the virgin flux the neutron balance leads to analytical formulas in terms of V_i and Σ_i for G_{ij}.

P_{11} in the central cylinder is tabulated [9] and P_{1j} are obtained by recurrence.

Considering Cadilhac's equation the 2N equations to be solved are then written as :

$$\left.\begin{aligned} \Phi_j \Sigma_j V_j &= \sum_{i=1}^{N} P_{ij} \left(\Sigma_{si} \Phi_i + \frac{dq_i}{dE} \right) V_i \\ \frac{d}{dE}\left(\frac{\Phi_j}{M_j}\right) &= j_j \cdot q_j - \frac{d}{dE}\left(k_j \cdot \frac{d}{dE} q_j \right) \end{aligned}\right\}^{j = 1,N}$$

or, in matrix form with $u = \frac{\Phi}{M}$

$$A \cdot u = B\, q'$$

$$u' = J\, q - (K\, q')'$$

The capital letters denote square matrices, whereas the smaller represent vectors. The elimination of the slowing-down densities q leads to a system of N differential equations, which can be easily solved numerically in the case of two media, by writing :

$$\left.\begin{aligned} q_i' &= \sum_{j=1}^{2} G_{ij} \Phi_i \\ u_i' &= j_i q_i - k_i' q_i' - k_i (q_i')' \end{aligned}\right\} \quad j = 1,2$$

and introducing the new functions :

$$U_i = \sum_{j=1}^{2} B_{ji} \Phi_j$$

with

$$\left.\begin{aligned} B_{ij} &= \delta_{ij} + H_j \frac{G_{ij}}{\Sigma_{sj}} \\ \sum_{j=1}^{2} g_{ji} W_j &= \sum_{j=1}^{2} G_{ji} \Phi_j \end{aligned}\right\} \quad i = 1,2$$

therefore, the problem is reduced to solving a system similar to (23). When the number of regions becomes larges an iterative method is preferred.

D. Non-thermal spectrum calculation [1] [2]

The basis of the calculation procedure is the P1 or B1 approximation to the Fourier transform with respect to space of the one-dimensional Boltzmann equation.

The moderation is accounted for by hydrogen and non-hydrogeneous components. Within the given approximations (P1 or B1), hydrogen moderation may be treated either generally or according to the Selengut-Goertzel (S.G.) approximation.

Non-hydrogeneous or heavy element slowing-down may be computed by either the Fermi (F) or Greuling-Goertzel (G.G.) approximations.

Five equations are simultaneously solved :

$$\left[\Sigma_a^s(u) + \Sigma_{in}(u) \right] \Phi(u) - \epsilon_1 * B * J(u)$$

$$= f_o(u) + \int_o^u \Sigma_{in}(u',u) * \Phi(u)\, du' - \frac{\partial \eta}{\partial u} - \frac{\partial \rho}{\partial u} \qquad (26)$$

$$\left[\gamma(u) * \Sigma(u) - \sum_i \bar{\mu}_i * \Sigma_s^{oi} \right] * J(u) = - \frac{B}{3} \Phi(u) - \frac{2}{3} * \delta_1 * \frac{\partial p}{\partial u} \qquad (27)$$

$$\frac{\partial \eta}{\partial u} = - \eta(u) + \Sigma_s^{OH} * \Phi(u) \qquad (28)$$

$$\delta_1 * \frac{\partial \rho}{\partial u} = - \frac{3}{2} \rho(u) + \Sigma_s^{OH} * J(u) \qquad (29)$$

$$\delta_2 * \lambda * \frac{\partial q}{\partial u} = - q(u) + \sum_{i \neq H} \xi^i * \Sigma_s^{oi} * \Phi(u) \qquad (30)$$

The different approximations mentioned previously can be obtained by forcing various terms to assume certain values according to the scheme :

δ_1 \ $\gamma(u)$		$\gamma(u)$	1
0	$\delta_2 = 0$	B.1. S.G. F	P.1. S.G. F
	$\delta_2 = 1$	B.1. S.G. G.G.	P.1. S.G. G.G.
1	$\delta_2 = 0$	B.1. F	P.1. F
	$\delta_2 = 1$	B.1. G.G.	P.1. G.G.

The "two step search" defined by Strawbridge is included [18].

The various cross-sections for each nuclide are tabulated from 54 MUFT groups.

The multigroup MUFT calculations are reduced to few group results (three groups or one group).

The cut-off energy between the fast and thermal energy ranges is variable.

E. The burn-up equations [1]

PANTHER considers only these groups of related elements :

a. uranium-238 through plutonium-242;
b. promethium-149 and samarium-149;
c. iodine-135 and xenon-135;
d. one pseudo-element accounting for all other fission products.

An exact solution for these nuclide chains is used based on Laplace transforms of the set of differential equations.

U-238 CHAIN

The first nuclide chain is linear (I isotopes)

$$\frac{dN_i}{dt} = - A_i N_i + C_{i-1} N_{i-1} \qquad i = 1,I$$

$$A_i = \int \sigma_a^i(E)\, \phi(E)\, dE + \lambda^i$$

$$C_i = \int \sigma_c^i(E)\, \phi(E)\, dE + \lambda^i$$

Using the Laplace transform :

$$\begin{vmatrix} p + A_1 & & \\ - C_1 & p + A_2 & \\ & - C_I & p + A_I \end{vmatrix} * \begin{vmatrix} N_1 \\ \\ N_I \end{vmatrix} = \begin{vmatrix} N_{01} \\ \\ N_{0I} \end{vmatrix}$$

and the Cramer rule :

$$N_i(p) = \sum_{l=1}^{i} \frac{N_i^o \prod_{r=1}^{i=1} C_r}{\prod_{j=l}^{i} \left(p + A_j \right)} \quad ;$$

hence, the time-solution is :

$$N_i(t) = \sum_{l=1}^{i} \sum_{u=l}^{i} \frac{N_i^o \prod_{r=1}^{i-1} C_r}{\prod_{\substack{j=l \\ j \neq u}}^{i} \left(A_j - A_u \right)}$$

FISSION PRODUCTS

The fission product chain differential equations are :

$$\frac{dN_1}{dt} = - A_1 N_1$$ U-238 chain

$$\frac{dN_2}{dt} = - A_2 N_2 + C_1 N_1$$

.....

$$\frac{dN_F}{dt} = - A_F N_F + C_{F-1} N_{F-1}$$

$$\frac{dN_p}{dt} = - A_p N_p + B_{Fp} N_F$$

.....

$$\frac{dN_{p+k}}{dt} = - A_{p+k} N_{p+k} + C_{p+k-1} N_{p+k-1} + B_{Fp+k} N_F$$ Fission products

Using the Laplace transform :

$$\begin{vmatrix} p + A_1 & & & & \\ - C_1 & p + A_2 & & & \\ & - C_{F-1} & p + A_F & & \\ & & - B_{Fp} & p + A_F & \\ & & - B_{Fp+1} & - C_p & p + A_{F+1} \\ & & - B_{Fp+k} & & - C_{p+k-1} \quad p + A_{p+k} \end{vmatrix} \begin{vmatrix} N_1 \\ \\ \\ N_F \\ N_p \\ \\ N_{p+k} \end{vmatrix} = \begin{vmatrix} N_{01} \\ \\ \\ N_{OF} \\ N_{OP} \\ \\ N_{OP+k} \end{vmatrix}$$

the following transformed equation results :

$$N_{p+k}(p) = \sum_{l=P}^{P+k} \frac{N_{ol}^{l} \prod_{r=1}^{k-1} C_r}{\prod_{i=1}^{p+k} \left(p + A_i \right)}$$

$$+ \sum_{n=1}^{F} \left\{ \sum_{l=1} \frac{N_{ol} \prod_{r=1}^{n-1} C_r}{\prod_{i=1}^{n} \left(p + A_i \right)} \right\} * \left\{ \sum_{l=P}^{P+k} \frac{-B_{mP+k} \prod_{r=1}^{p+k-1} C_r}{\prod_{i=1}^{P+k} \left(p + A_i \right)} \right\}$$

The time solution is :

$$N_{p+k}^{F}(t) = \sum_{l=1}^{F} \sum_{u=1}^{F} \frac{N_{ol} \prod_{r=1}^{F-1} C_r \exp\left(- A_u t \right)}{\prod_{\substack{i=1 \\ i \neq u}}^{F} \left(A_i - A_u \right)}$$

$$* \left(\sum_{l=p}^{p+k} B_{Fl} \frac{\prod_{r=1}^{p+k-1} C_r}{\prod_{i=1}^{k} \left(A_i - A_u \right)} \right)$$

$$+ \sum_{l=P}^{P+k} \sum_{v=1}^{P+k} \frac{B_{Fl} \prod_{r=1}^{P+k-1} C_r \exp\left(- A_v t \right)}{\prod_{\substack{i=1 \\ i \neq v}}^{k} \left(A_i - A_v \right)}$$

$$* \left(\sum_{i=1}^{F} \frac{N_{ol} \prod_{r=1}^{F-1} C_r}{\prod_{i=1}^{F} \left(A_i - A_v \right)} \right)$$

The criticality search can be performed using buckling, boron-10 or H_2O/D_2O ratio adjustment.

F. Bibliography

[1] P. DE MYTTENAERE, N. MEYVAERT & J. QUENON.
PANTHER - Internal Report BN 6603 04 (Modifications 2).

[2] P. DE MYTTENAERE & J. QUENON.
Application des modèles de ralentissement neutronique à l'équation du transport dans l'approximation P-1 et B-1.
Internal report BN 6509 10.

[3] P. HAUBERT & N. MEYVAERT.
Approximate treatment of neutron thermalization in heterogeneous systems.
ANS meeting, San Diego, February 7-9, 1966.

[4] P. HAUBERT.
Application of Cadilhac's formalism to the determination of neutron spectra in heterogeneous systems.
Symposium on Advances of Reactor Theory, Karlsruhe, 27-29 June, 1966.
EAES.

[5] P. HAUBERT.
Thermal neutron spectra in uniform lattices - use of Cadilhac's formalism.
EUR 3350 e.

[6] G.D. JOANOU, C.V. SMITH & H.A. VIEWEG.
GATHER II, an IBM 7090 FORTRAN II programme for the computation of thermal neutron spectra and associated multigroup cross-sections
GA 4132.

[7] M. CADILHAC.
Méthodes théoriques pour l'étude de la thermalisation des neutrons dans les milieux absorbants infinis homogènes.
C.E.A. - R 2368 (1964).

[8] A.J. CLAYTON.
The programme PIP1 for the solution of the multigroup equations of the method of collisions probabilities.
AEEW - R 326 (1964).

[9] D.C. LESLIE.
The "SPECTROX" method for thermal spectra in lattice cells.
Reactor Science and Technology (Journal of nucl. energy parts A/B vol. 17, 293.306 (1963)).

[10] AMOUYAL & BENOIST.
Interprétation des résultats obtenus par Kushneriuk et Mc Kay.
Additif au C.E.A. 571 - JPM 246 (1957).

[11] D.A. NEWMARCH.
A modification to the diffusion theory of the thermal flux structure in a reactor to account for the effect of air channels.
J. Nucl. En. 2, p. 52 (1955).

[12] G.W. STUART & R.W. WOODRUFF.
Method of successive generations.
Nucl. Sc. & Eng. 3, 339 (1958).

[13] J.R. ASKEW & R.J. BRISSENDEN.
Some improvements in the discrete ordinate method of B.G. Carlson for solving the neutron transport equations.
AEEW - R 161.

[14] K. CASE, F. DE HOFFMANN & G. PLACZEK.
An introduction to the theory of neutron diffusion.
Los Alamos Sci. Lab. (1963).

[15] R. BONALUMI.
Neutron first collision probabilities in reactor physics.
Energia Nucleare - vol. 8 n° 5 - Maggio, 1961.

[16] A. JONSSON.
One group collision probability calculations for annular systems by the method of Bonalumi.
Reactor Sci. & Technol. vol. 17 - pp 511-518 (1963).

[17] A. SAUER.
Thermal utilization in the square lattice cell.
Journal of Nucl. Energy, parts A/B, 1964, vol. 18 - pp. 425-447.

[18] STRAWBRIDGE.
N.S.E., July, 1965.

APPENDIX VI.2 : PANTHER CALIBRATION ON THE BASIS OF AMERICAN EXPERIMENTAL RESULTS

In order to test the validity of the PANTHER code and to compare its different options, it has been used for the calculation of an important number of uranium and uranium-plutonium configurations, experimentally studied in the USA (Hanford and Saxton). These configurations include :

3 UO_2 cores enriched to 5.74 %
6 PuO_2-UO_2 cores, with a PuO_2 content of 1.5 %
5 PuO_2-UO_2 cores, with a PuO_2 content of 6.6 %.

More details about these configurations are summarized in tables I and II.

The results obtained with the PANTHER code have been compared with the available experimental results and also with the results calculated with more powerful codes like LEOPARD and the transport code LASER. These comparisons were relative to the overall disadvantage factors, the disadvantage factors at certain energies, the average and effective microscopic cross sections, the thermal absorption balance and, mainly, to the effective and infinite multiplication factors (k_{eff} and k_∞).

All the results obtained for both these factors are presented in table App. VI.3; all configurations were experimentally determined to be just critical. It can be seen that in almost all the cases the Bonalumi option of the PANTHER code gives the best results.

TABLE APP. VI.1 : FUEL CHARACTERISTICS OF THE STUDIED HANFORD AND SAXTON CONFIGURATIONS

	UO_2 (5.74 %) (Westinghouse)	PuO_2-UO_2 (1.5 %) (Hanford)	PuO_2-UO_2 (6.6 %) (Westinghouse)
Rod diameter (cm)	0.906	0.945	0.856
Uranium enrichment (w/o)	5.74	0.2	0.7
PuO_2 content (w/o)	-	1.5	6.6
Pu-239 in (w/o)	-	91.5	90.49
Pu-240 in (w/o)	-	7.8	8.57
Pu-241 in (w/o)	-	0.7	0.89
Pu-242 in (w/o)	-	~ 0	0.04

TABLE APP. VI.2 : LATTICE CHARACTERISTICS OF THE STUDIED HANFORD AND SAXTON CONFIGURATIONS

FUEL	PITCH (in)	VOLUMETRIC RATIO (H_2O/FUEL)	EXP. B^2 (m^{-2})
UO_2 (5.74 %)	0.52	1.50	117.6
	0.56	1.93	127.1
	0.792	5.07	136.8
PuO_2 - UO_2 (1.5 %)	0.55	1.10	48.0
	0.60	1.56	65.1
	0.71	2.71	78.5
	0.80	3.79	14.9
	0.90	5.14	60.9
	0.93	5.58	55.2
PuO_2 - UO_2 (6.6 %)	0.52	1.68	108.8
	0.56	2.16	121.5
	0.735	4.70	159.6
	0.792	5.67	159.3
	1.04	10.80	128.4

TABLE APP. VI.3 : MULTIPLICATION FACTORS k_∞ AND k_{eff}

Lattice Pitch (in)	SPECTROX with thermalization in the fuel		Amouyal & Benoist without thermalization in the fuel		Bonalumi without thermalization in the fuel		Results LEOPARD or LASER	
Westinghouse UO_2 (5.7 %)	k_{eff}	k_∞	k_{eff}	k_∞	k_{eff}	k_∞	k_{eff}	k_∞
0.52	1.0020	1.4233	1.0037	1.4259	1.0026	1.4244	0.9936	1.4235
0.56	1.0127	1.4532	1.0151	1.4567	1.0135	1.4545	1.0012	1.4486
0.792	1.0083	1.4339	1.0140	1.4421	1.0068	1.4325	0.9968	1.4287
Hanford PuO_2 - UO_2 (1.5 %)								
0.55	1.0013	1.2082	1.0032	1.2106	1.0029	1.2102	0.9932	1.2080
0.60	1.0050	1.2640	1.0069	1.2663	1.0057	1.2649	0.9954	1.2642
0.71	1.0103	1.2916	1.0126	1.2943	1.0093	1.2904	0.9990	1.2916
0.80	1.0092	1.2644	1.0119	1.2677	1.0065	1.2612	0.9974	1.2638
0.90	1.0084	1.2090	1.0117	1.2128	1.0034	1.2032	0.9976	1.2074
0.93	1.0087	1.1893	1.0122	1.1933	1.0030	1.1827	0.9961	1.1831
Westinghouse PuO_2 - UO_2 (6.6 %)								
0.52	1.0020	1.3990	0.9968	1.3911	0.9964	1.3906	0.9932	1.4018
0.56	1.0170	1.4460	1.0123	1.4390	1.0113	1.4373	1.0048	1.4494
0.735	1.0117	1.5209	1.0138	1.5223	1.0071	1.5131	1.0043	1.5241
0.792	1.0138	1.5157	1.0180	1.5201	1.0091	1.5079	1.0072	1.5189
1.04	1.0162	1.4101	1.0283	1.4251	1.0077	1.3983	1.0106	1.4133

APPENDIX VI.3 : THE MND FORMALISM

The diffusion equation for the thermal neutrons can be written in the two following ways :

$$- D \nabla^2 \Phi + \Sigma_a \Phi = \nu \Sigma_f \Phi \quad \text{(conventional)}$$

$$- \frac{\bar{D}_{Max}}{(\frac{1}{v})_{Max}} \nabla n + \frac{\Sigma_a}{(\frac{1}{v})} n = \frac{\nu \Sigma_f}{(\frac{1}{v})} n \quad \text{(MND)}$$

where the various symbols have their usual meaning (cfr ref. VI.4).
The comparison of both formalisms has indicated the following differences :

A. Influence on the thermal spectrum

The MND (Mixed Number Density) formalism leads to a softening of the spectrum in the fuel regions and to a hardening of the spectrum in regions with $B^2 < 0$ (water gaps, reflector).

B. Influence on the leakage

In a fuel region the leakage is mainly due to fast neutrons; the softening of the spectrum due to the use of the MND cross sections leads to a decrease of the leakage in the fuel regions.

In the moderator regions, on the contrary, MND cross sections lead to an increase of the fast leakage and a decrease of the thermal leakage.

C. Influence on the multiplication factor

From the comparison of the two group formulation of the multiplication factor for both formalisms it can be concluded that $(k_{eff})_{MND} > (k_{eff})_{conv.}$; indeed, with conventional thermal cross sections we have :

$$k_{eff} = \frac{\nu \Sigma_{f1}}{D_1 B^2 + \Sigma a_1 + \Sigma_{R1}} + \frac{\Sigma_{R1}}{D_1 B^2 + \Sigma a_1 + \Sigma_{R1}} \cdot \frac{\nu \Sigma_{f2}}{\Sigma a_2 + D_2 B^2}$$

and with MND thermal cross sections :

$$k_{eff} = \frac{\nu \Sigma_{f1}}{D_1 B^2 + \Sigma a_1 + \Sigma_{R1}} + \frac{\Sigma_{R1}}{D_1 B^2 + \Sigma a_1 + \Sigma_{R1}} \cdot \frac{\nu \Sigma_{f2}}{\Sigma a_2 + D_{Max} \frac{v_{Max}}{v_2} B^2}$$

D. Influence on the boundary conditions

Both formalisms have different boundary conditions; between two zones 1 and 2 they are :

with the conventional formalism : $\varphi_1 = \varphi_2$

$$D_1 \frac{\partial \varphi_1}{\partial r} \Big|_N = D_2 \frac{\partial \varphi_2}{\partial r} \Big|_N$$

and with the MND formalism : $n_1 = n_2$

$$D_{1\,Max} v_{1\,Max} \frac{\partial n_1}{\partial r} \Big|_N = D_{2\,Max} v_{2\,Max} \frac{\partial n_2}{\partial r} \Big|_N$$

It is seen that with the MND formalism, the flux continuity condition at the interface between the two zones is replaced by the neutron density continuity condition. The flux discontinuity which appears then with MND cross sections will be particularly important, when the difference between the neutron velocities, characteristic for the equilibrium spectra in the two regions, is important.

ACKNOWLEDGEMENTS

The authors wish to stress the highly valuable assistance they received from an important number of technical agents and specialists; it is clear that the work described in this report could only be realized on the basis of their permanent and dutiful collaboration.

More particularly the authors want to acknowledge the contribution of the following persons :

R. GASPARON (GEX (LMA) - MOL)
J. GOOLENAERTS (SCK/CEN)
V. GRAILET (SCK/CEN)
A. SCHONENBERG (SCK/CEN)
L. TRUYENS (SCK/CEN)
P. VANDERHEYDEN (SCK/CEN)
J. VAN DIJCK (SCK/CEN)
L. VERBRUGGEN (SCK/CEN)
F. VREYS (SCK/CEN)

*

Furthermore they are very grateful to all Sections and Departments of both Belgonucléaire and the SCK/CEN which have contributed in some way to the realization of the programme by putting at its disposal their staff and their equipment. This is mainly the case for the Belgonucléaire Computer Department and for the LMA-Service of GEX in Mol in connection with the plutonium manipulation activities.

Special thanks are due to Mr L. BUVE (SCK/CEN) for the care with which he made the figures of this report.

*

Last but not least, the authors wish to thank Euratom for its important financial contribution which made it possible to give the programme its important size. These thanks go in the first place to Messrs P. KRUYS and A. COLLING for their unfailing interest in the programme.

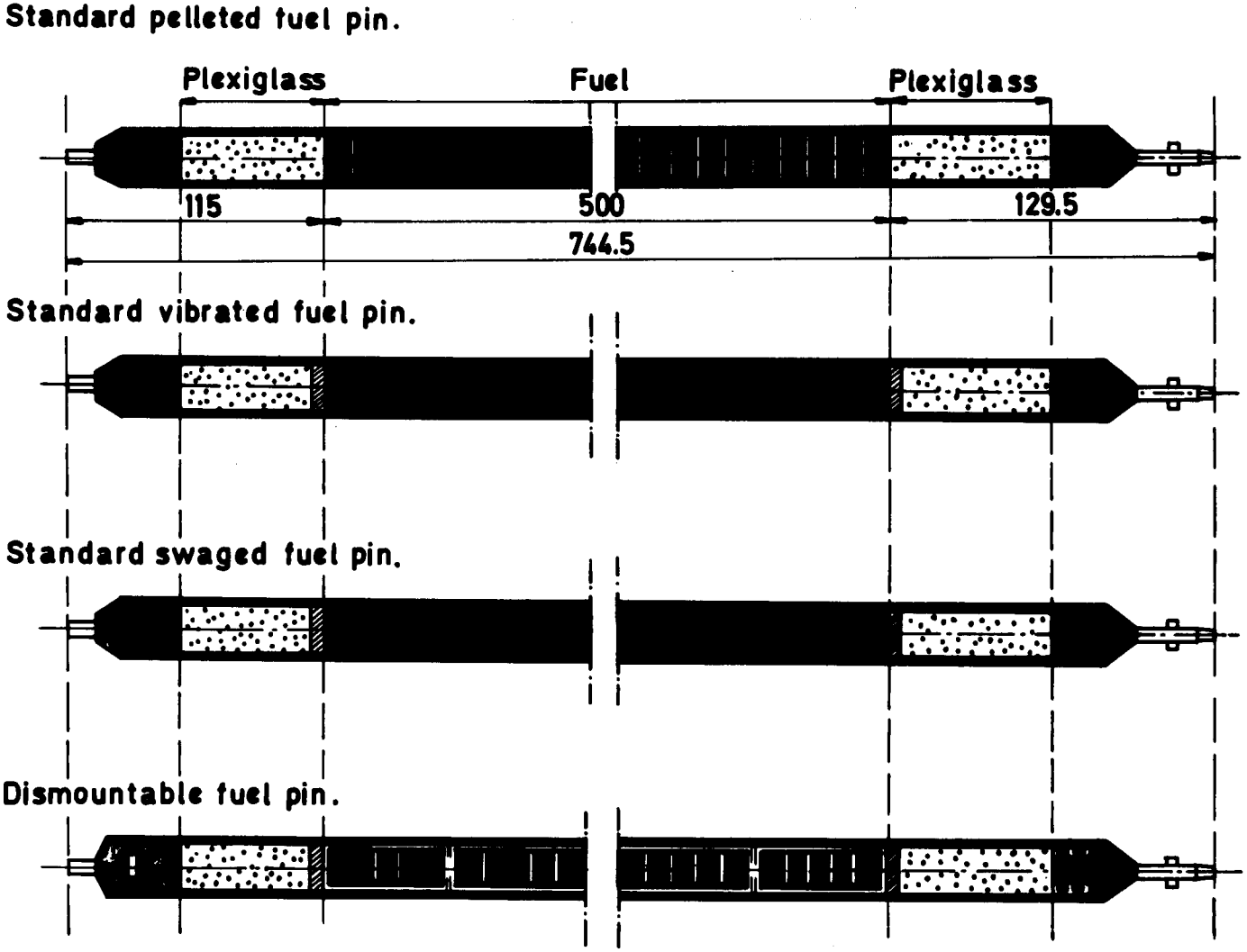

Fig. II. 1. VARIOUS TYPES OF FUEL PINS USED IN THE VENUS CRITICAL EXPERIMENTS

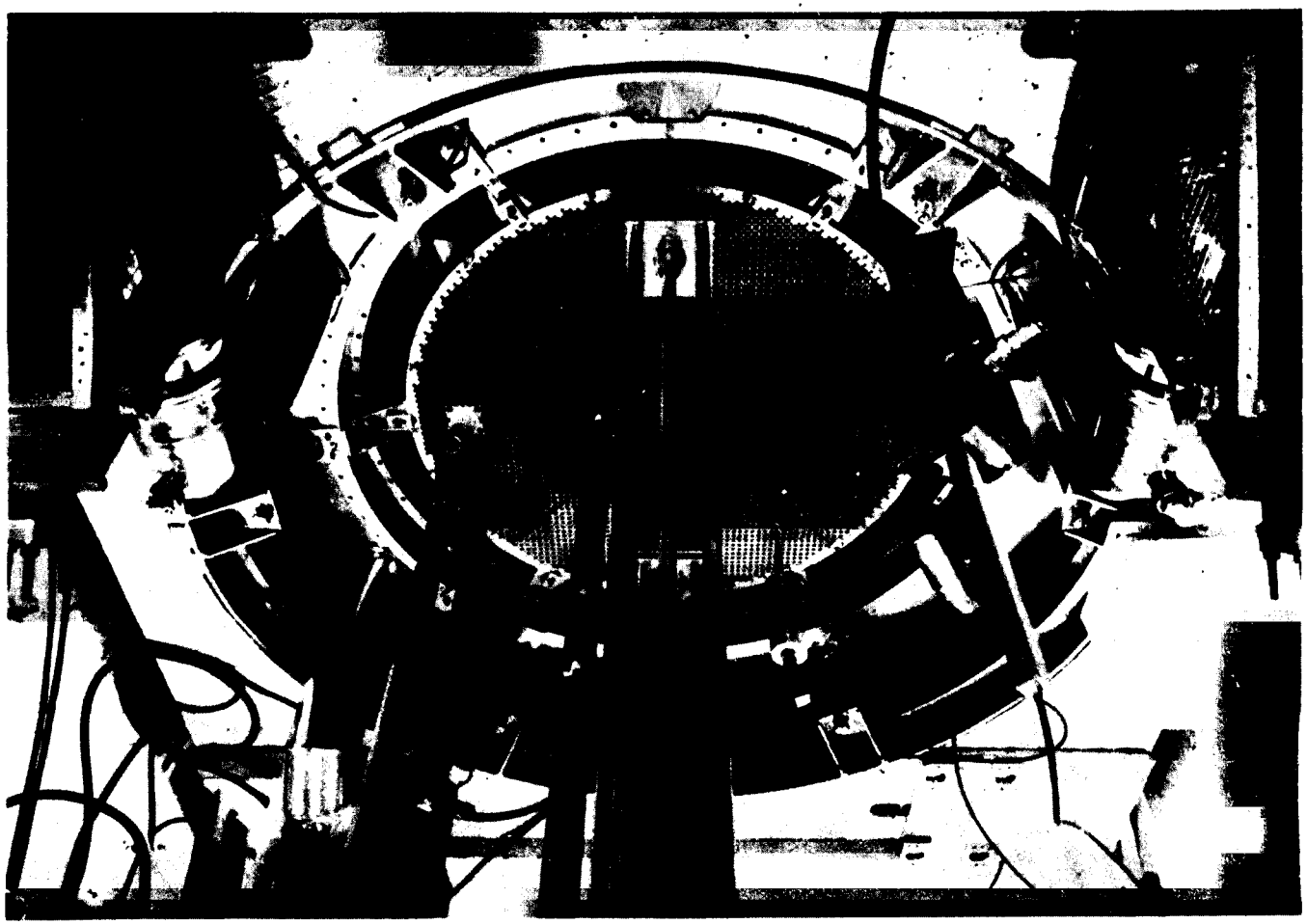

Fig. II 2. TOP VIEW OF THE VENUS REACTOR TANK AND ITS INTERNALS.

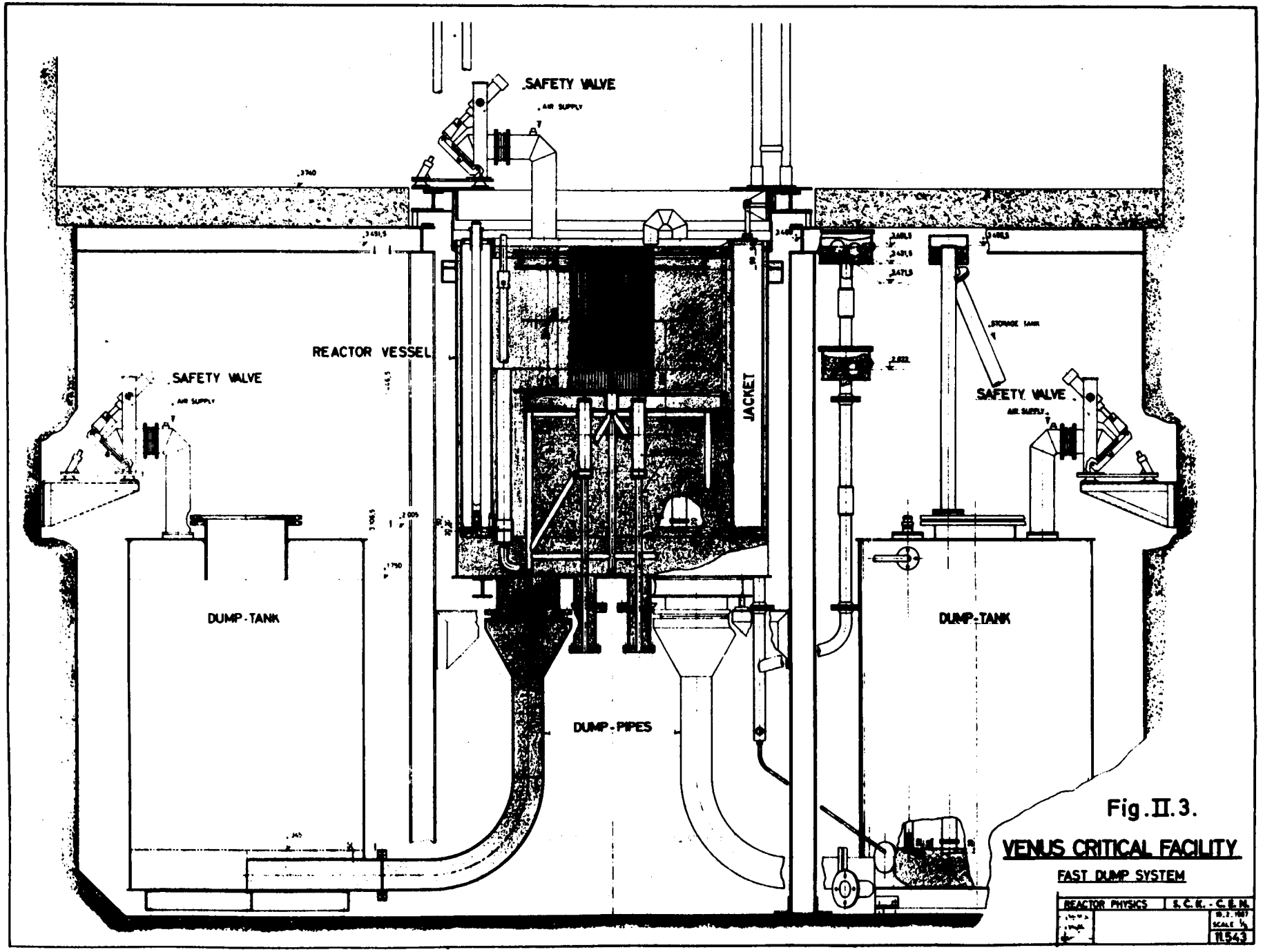

Fig. II. 3.

VENUS CRITICAL FACILITY

FAST DUMP SYSTEM

REACTOR PHYSICS	S.C.K. - C.E.N.
	11.543

Fig.II.4. SCHEMATIC VIEWS OF A VENUS SAFETY VALVE.

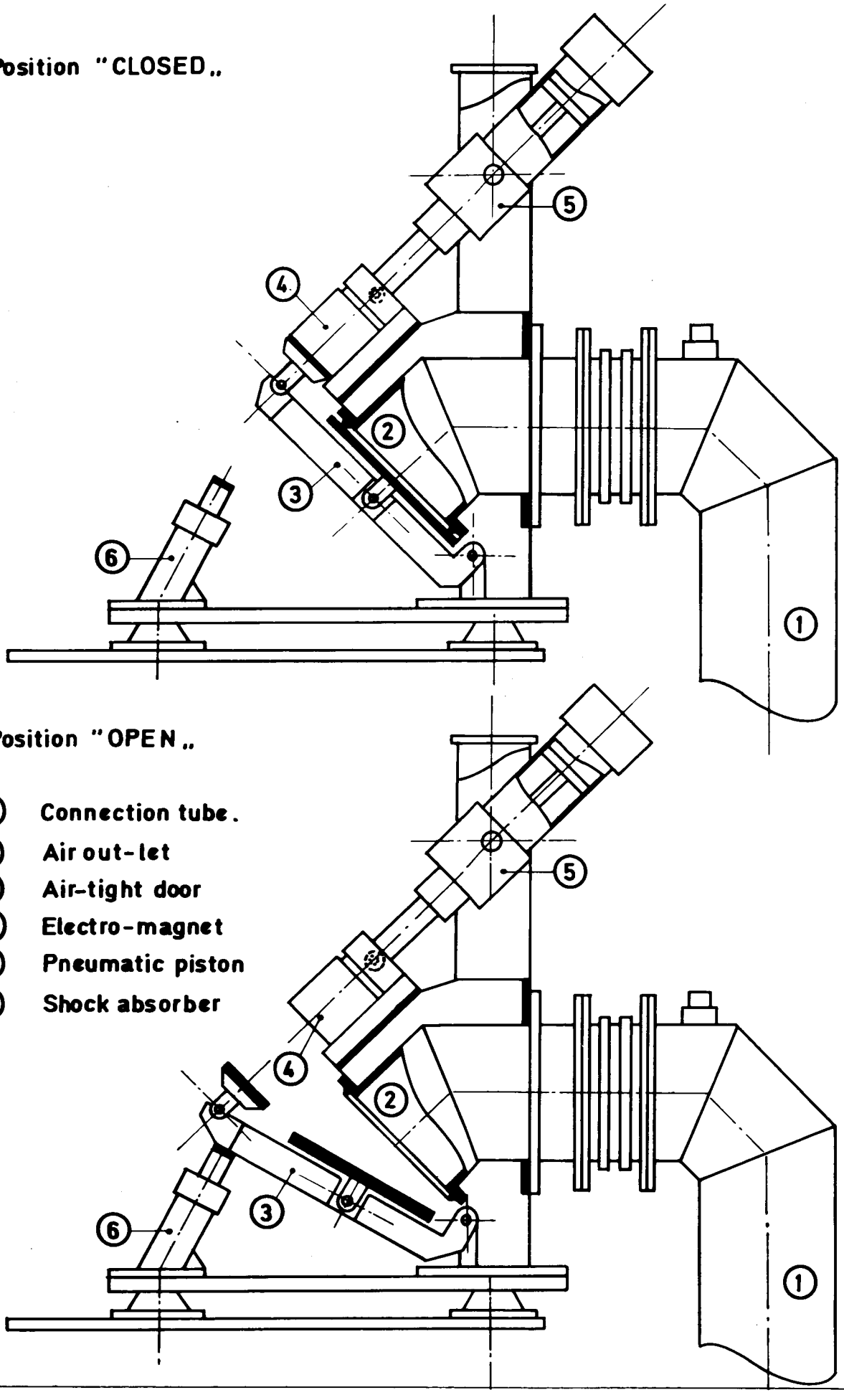

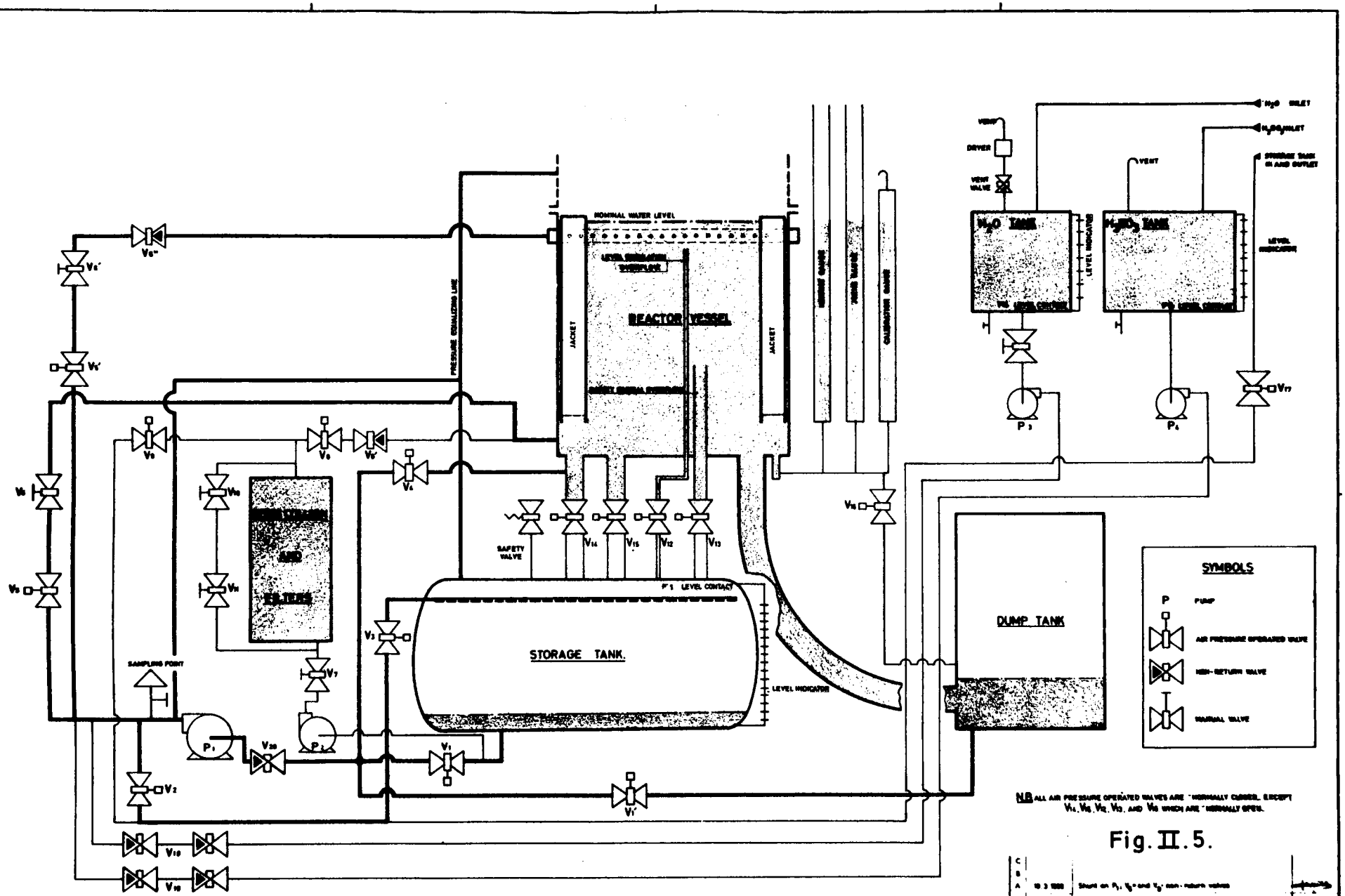
NOMINAL WATER LEVEL
REACTOR VESSEL
JACKET
JACKET
PRESSURE EQUALIZING LINE
SAFETY VALVE
STORAGE TANK.
DUMP TANK
LEVEL INDICATOR
SAMPLING POINT
DRYER
VENT
VENT VALVE
SYMBOLS
P PUMP
AIR PRESSURE OPERATED VALVE
NON-RETURN VALVE
MANUAL VALVE
N.B. ALL AIR PRESSURE OPERATED VALVES ARE "NORMALLY CLOSED, EXCEPT V14, V9, V12, V13, AND V8 WHICH ARE "NORMALLY OPEN.
Fig. II.5.
REACTOR PHYSICS
S.C.K. - C.E.N.
VENUS PLUTONIUM
HYDRAULIC CIRCUIT
11.540

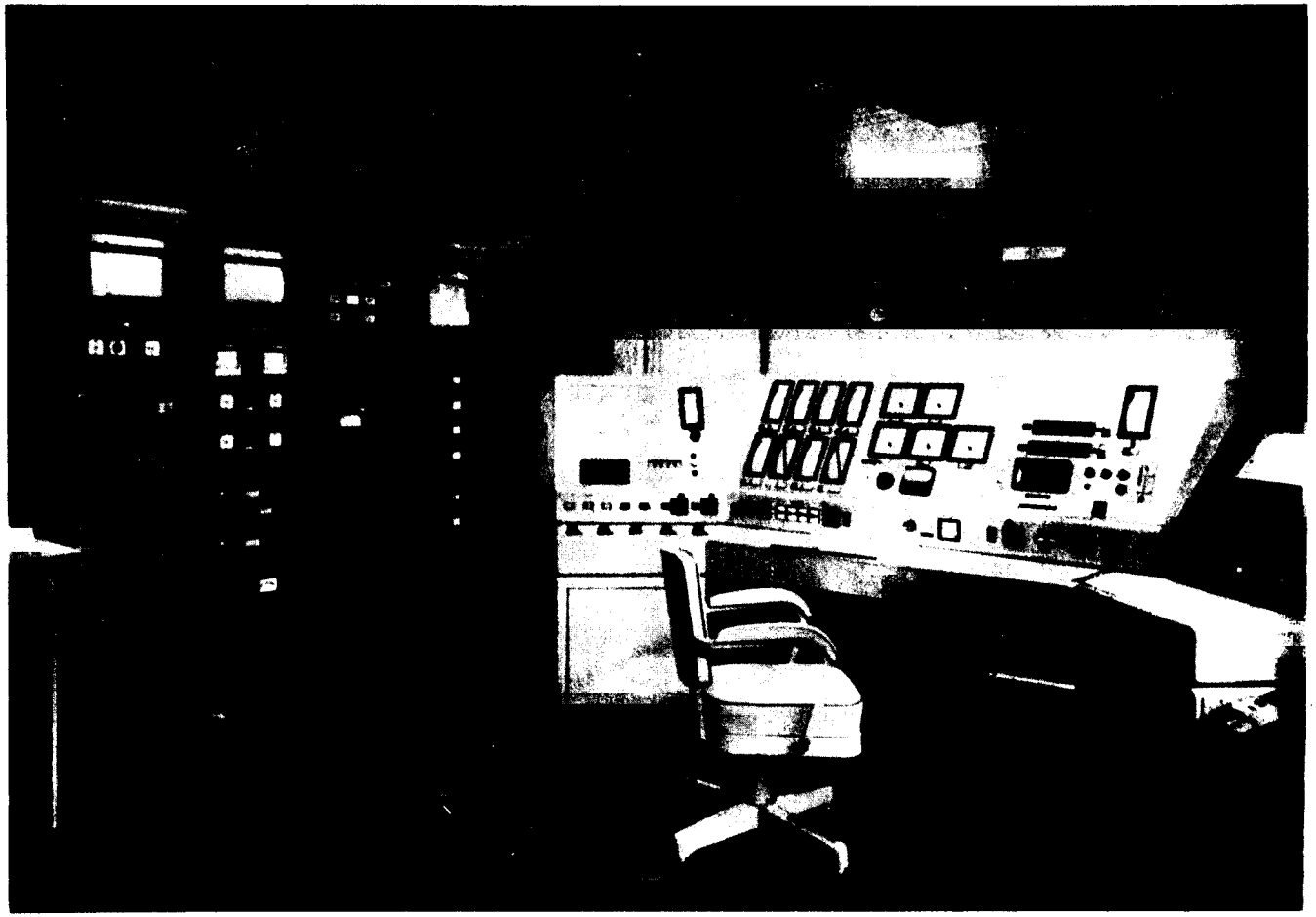

Fig. II 6. VIEW OF THE VENUS CONTROL ROOM.

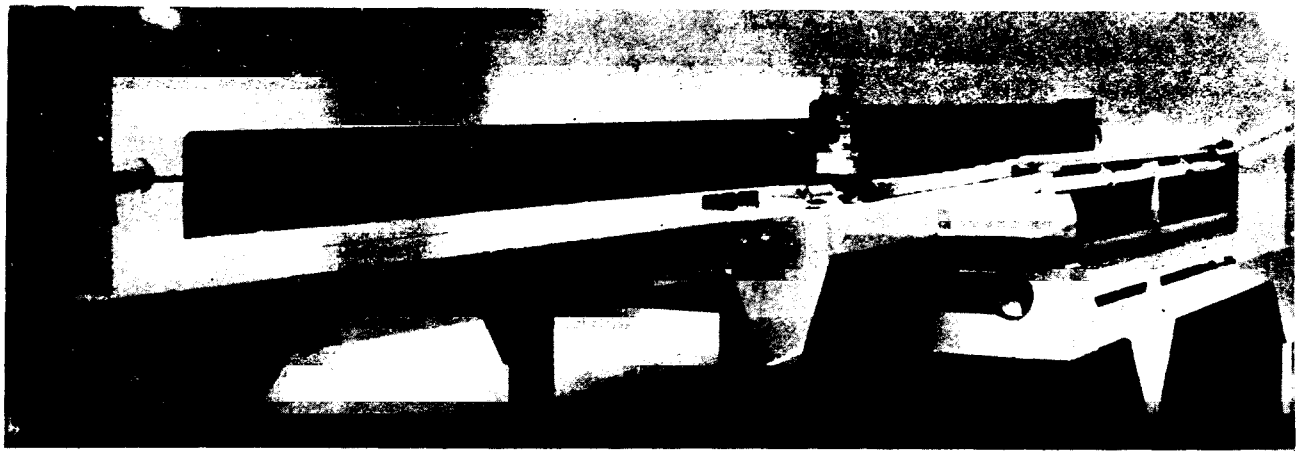

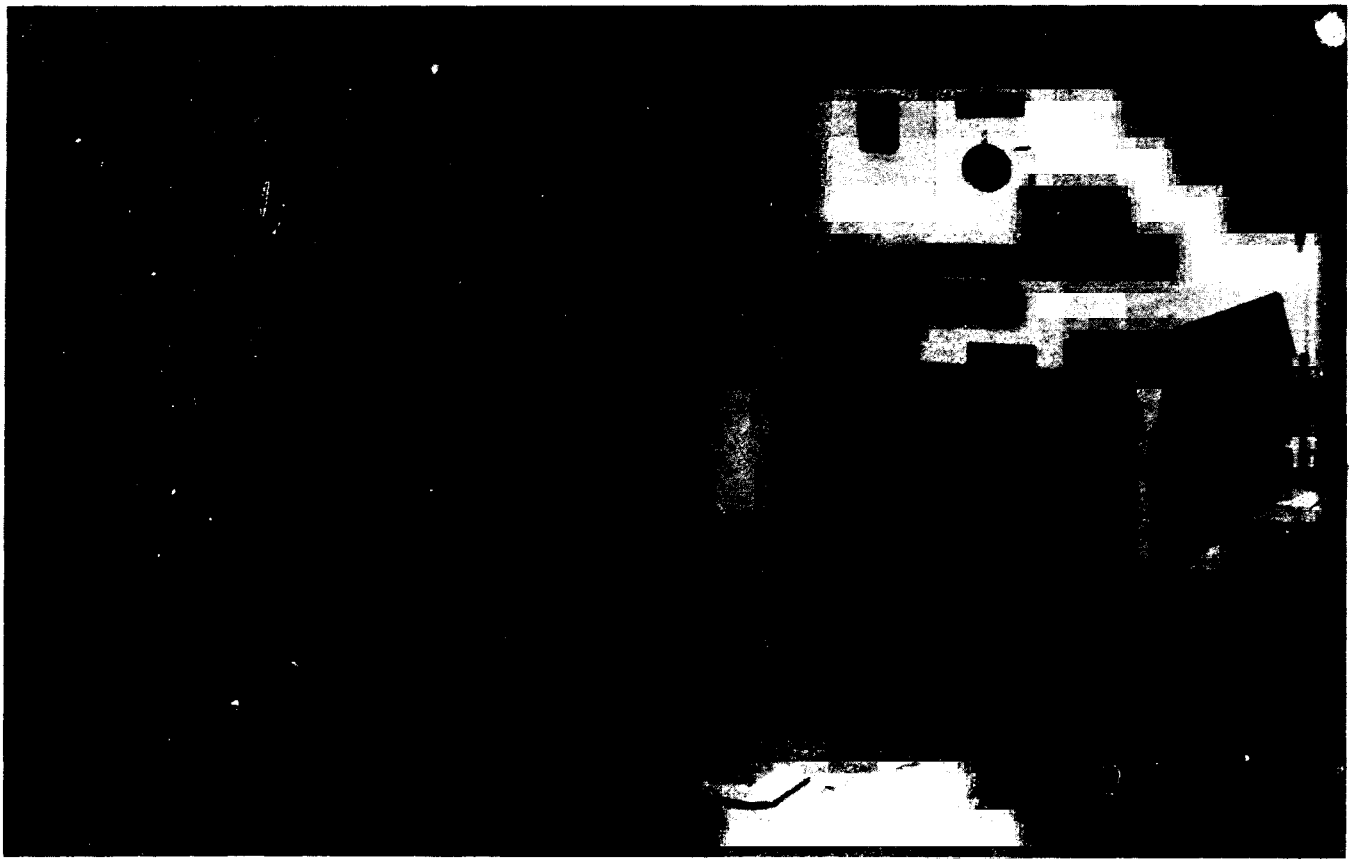

Fig. II 7. INTERNAL AND EXTERNAL VIEWS OF THE δ-SCANNING INSTALLATION

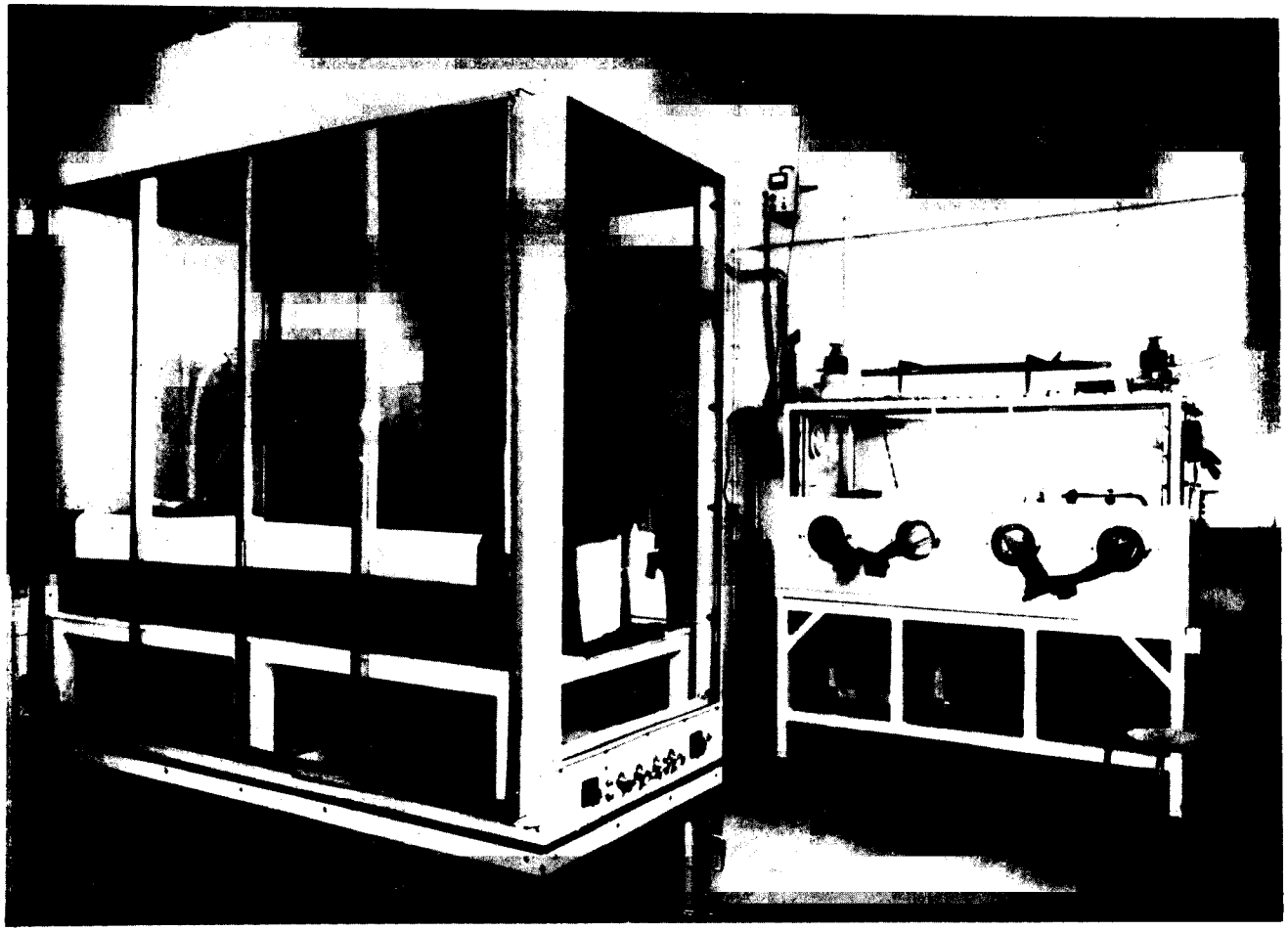

Fig. II 8. GENERAL VIEW OF THE PLUTONIUM LABORATORY ASSIOCIATED WITH THE VENUS CRITICAL FACILITY (LMA LABORATORIES).
(manipulation glove-box on the right, decontamination glove-box on the left with ventilated hood in front of it.)

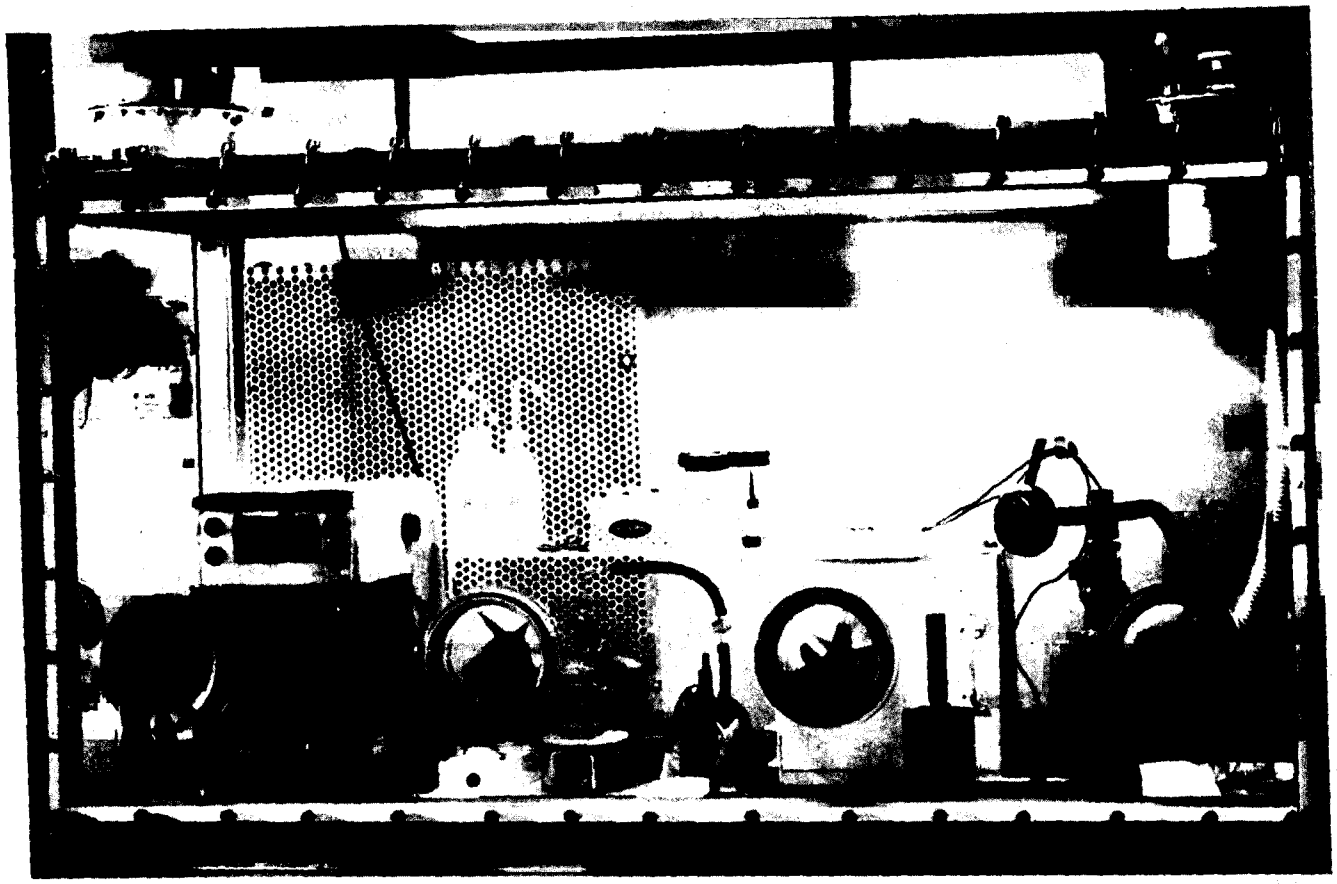

Fig. II 9. DETAILED VIEW OF THE MANIPULATION GLOVE-BOX IN THE LMA PLUTONIUM LABORATORY.

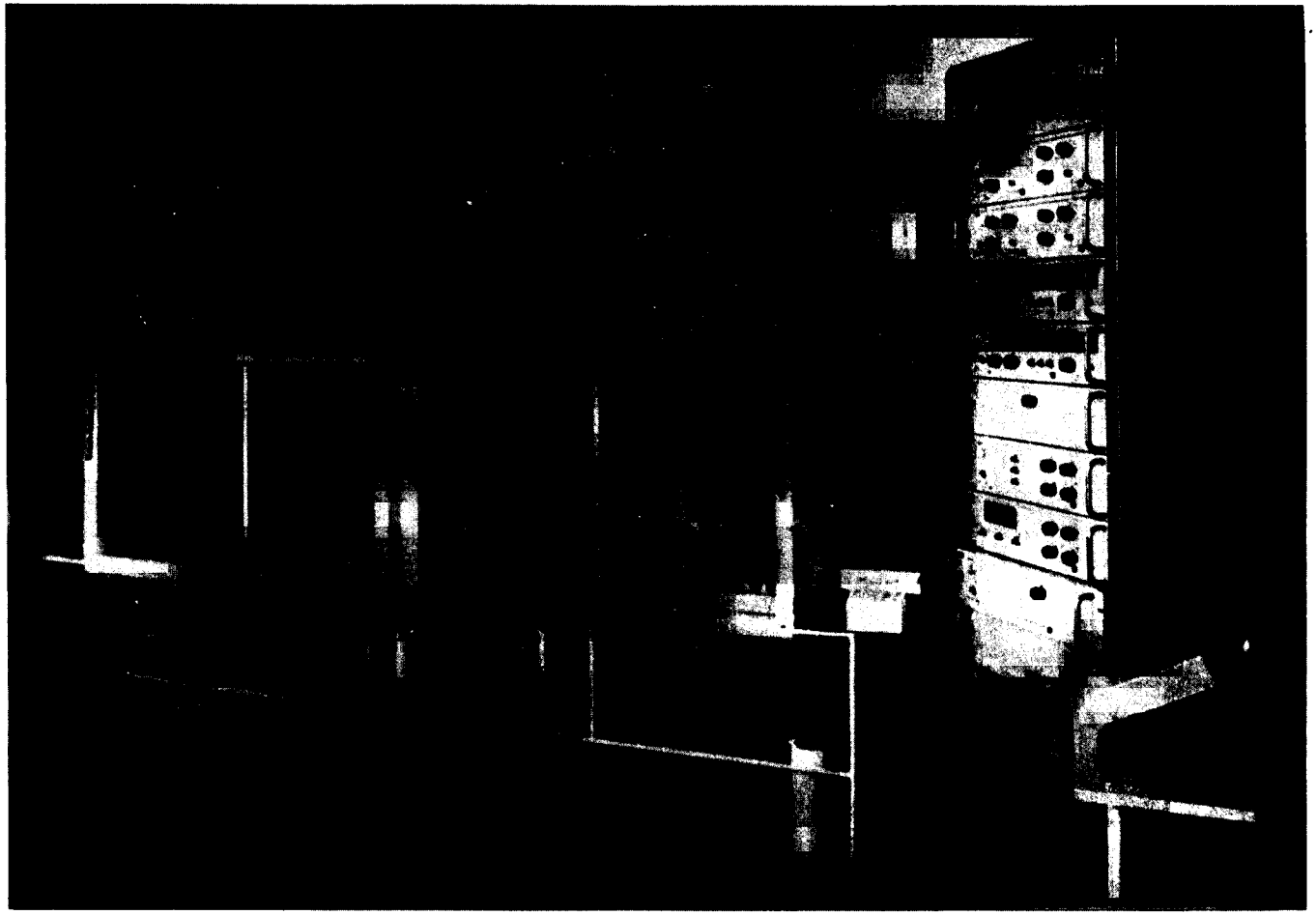

Fig. II 10. INSTALLATION FOR δ-SPECTROMETRY MEASUREMENTS.

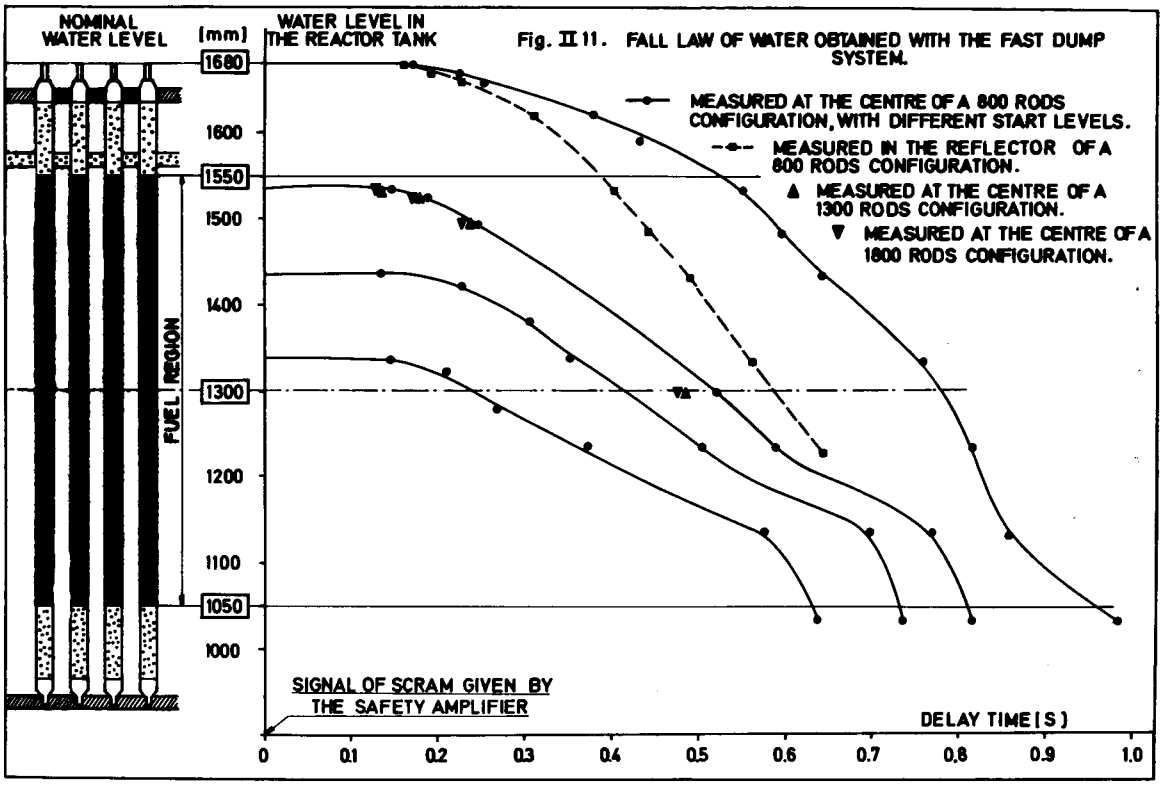

Fig. II 11. FALL LAW OF WATER OBTAINED WITH THE FAST DUMP SYSTEM.

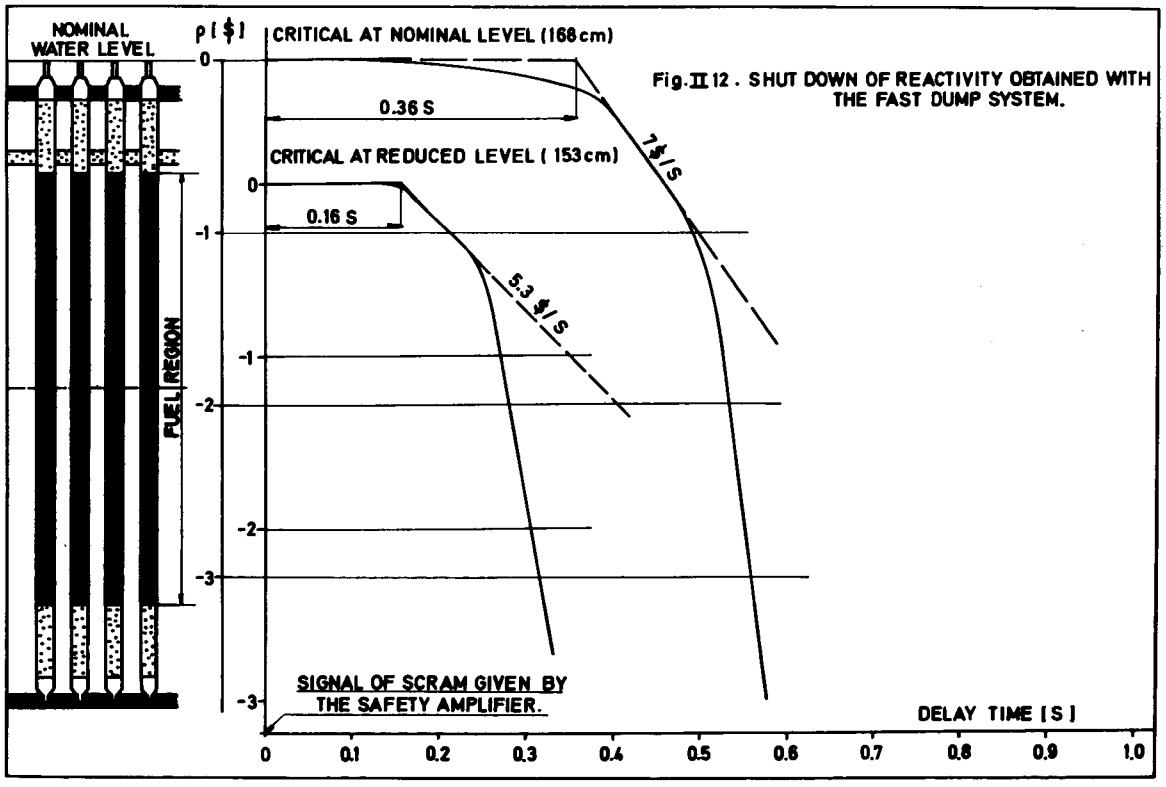

Fig. II 12. SHUT DOWN OF REACTIVITY OBTAINED WITH THE FAST DUMP SYSTEM.

CRITICALITY STUDIES

(REACTIVITY; FISSION DENSITY DISTRIBUTIONS)

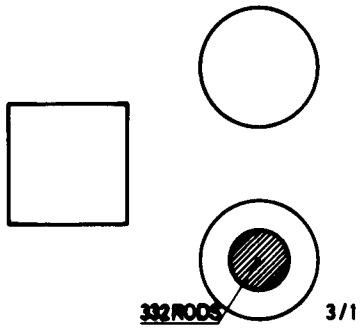

BOUNDARY STUDIES

(FISSION DENSITY DISTRIBUTIONS AND SPECTRAL INDICES)

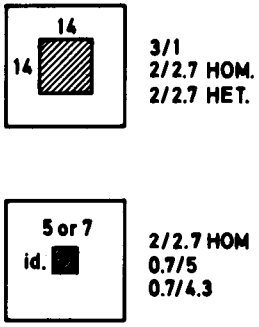

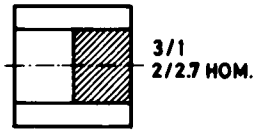

SYSTEMATICAL PERTURBATION STUDIES (B_4C, H_2O, Al)

(FISSION DENSITY DISTRIBUTIONS, REACTIVITY EFFECTS)

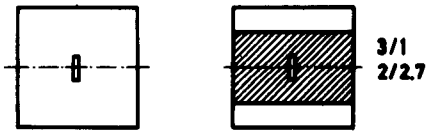

SOME PARTICULAR PERTURBATION CASES

(FISSION DENSITY DISTRIBUTIONS AND/OR REACTIVITY EFFECTS)

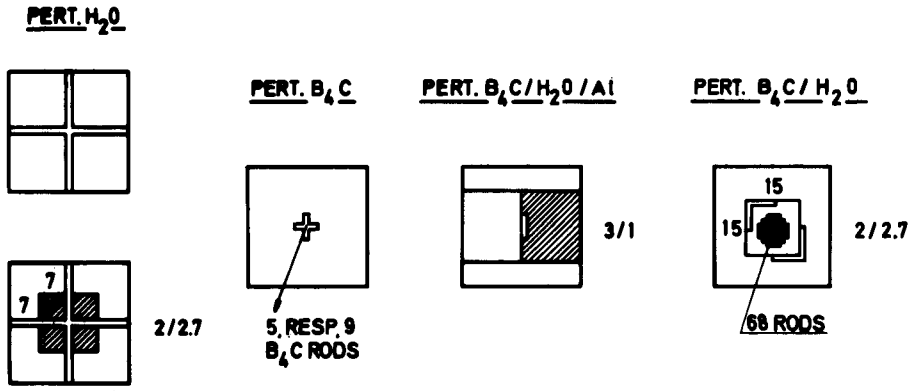

Fig. IV 1.

VENUS-Pu CONFIGURATIONS

- PITCH: p_{SENA} = 1.303 cm
- MODERATOR: UNPOISONED H_2O AT 20°C
- MODERATOR LEVEL AT CRITICALITY:
  NOMINAL OR NEAR TO IT
- FUEL: BLANK = UO_2 (4/0)
  = PuO_2/UO_2
- WIDTH OF ALL PERTURBATIONS: 1 PITCH
- DIMENSIONS, WHEN GIVEN: IN ROD NUMBERS

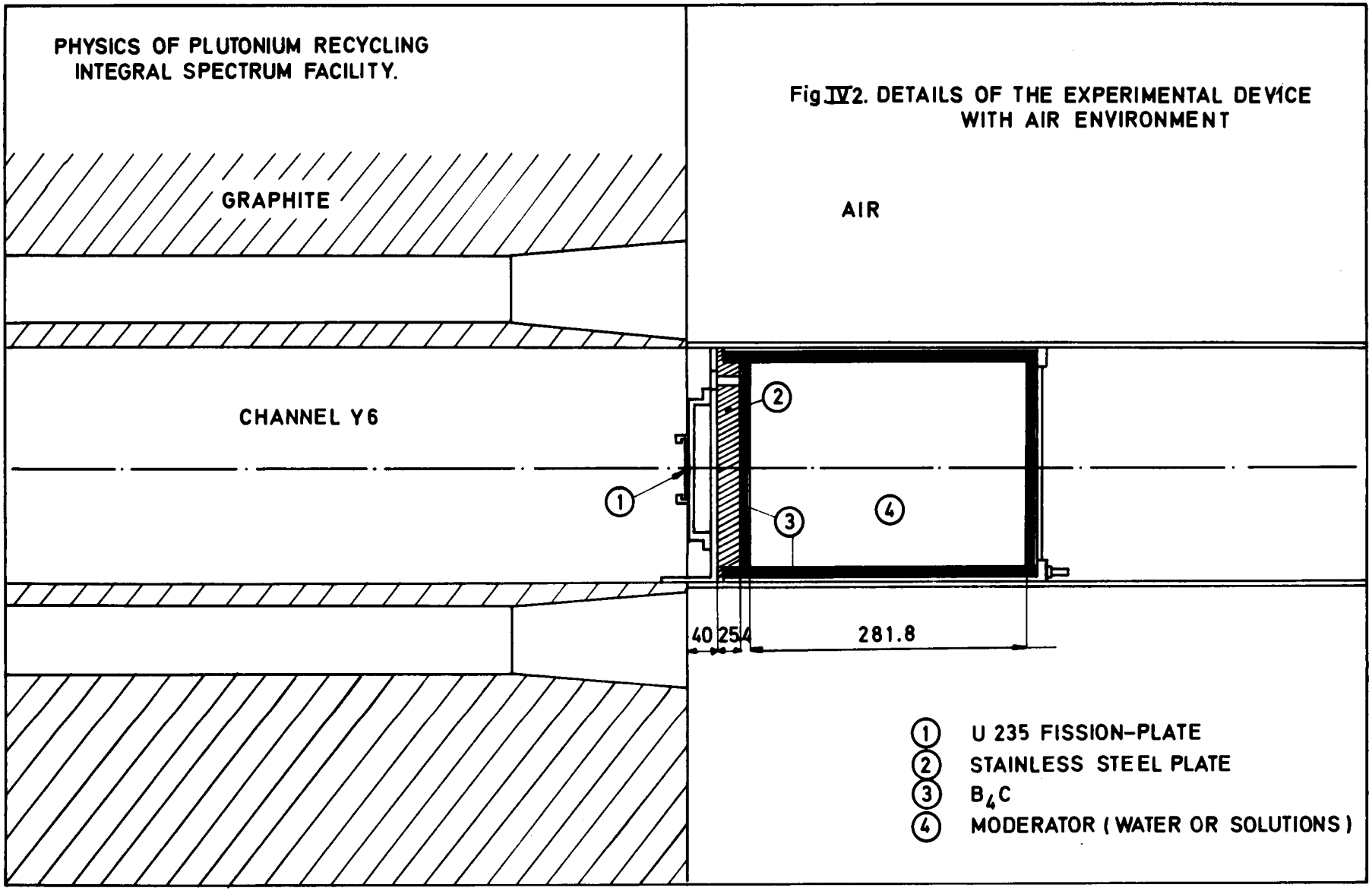
PHYSICS OF PLUTONIUM RECYCLING
INTEGRAL SPECTRUM FACILITY.
Fig IV2. DETAILS OF THE EXPERIMENTAL DEVICE
WITH AIR ENVIRONMENT
GRAPHITE
AIR
CHANNEL Y6
1
2
3
4
40
25.4
281.8
1 U 235 FISSION-PLATE
2 STAINLESS STEEL PLATE
3 B_4C
4 MODERATOR (WATER OR SOLUTIONS)

PHYSICS OF PLUTONIUM RECYCLING
INTEGRAL SPECTRUM FACILITY

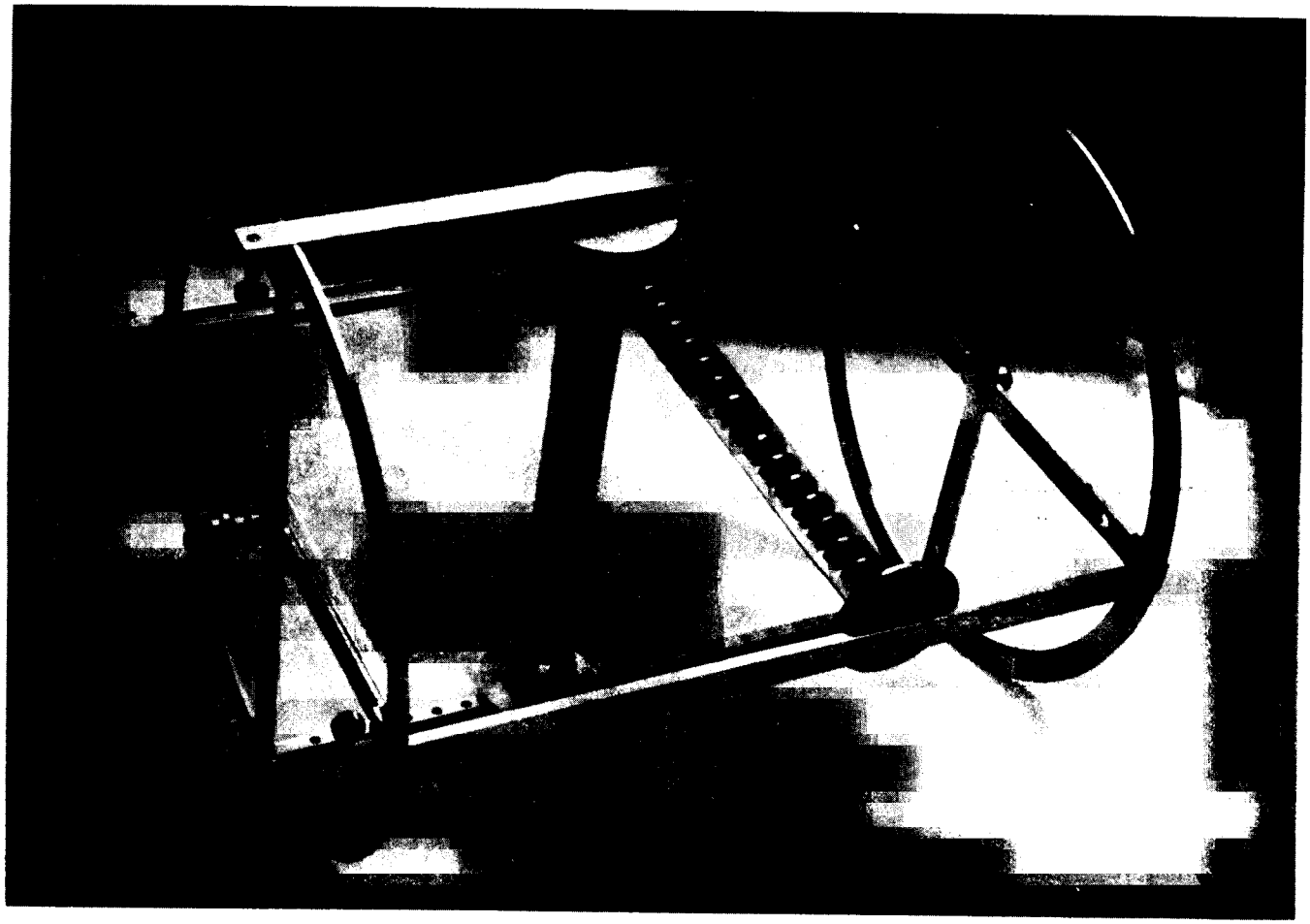

Fig. IV 3 . POSITIONING DEVICE OF THE FOILS USED FOR THE MEASUREMENTS OF RADIAL FLUX DISTRIBUTIONS.

Fig. V 1 : REACTIVITY EXCESS AT NOMINAL LEVEL AS A FUNCTION OF THE CRITICAL LEVEL.

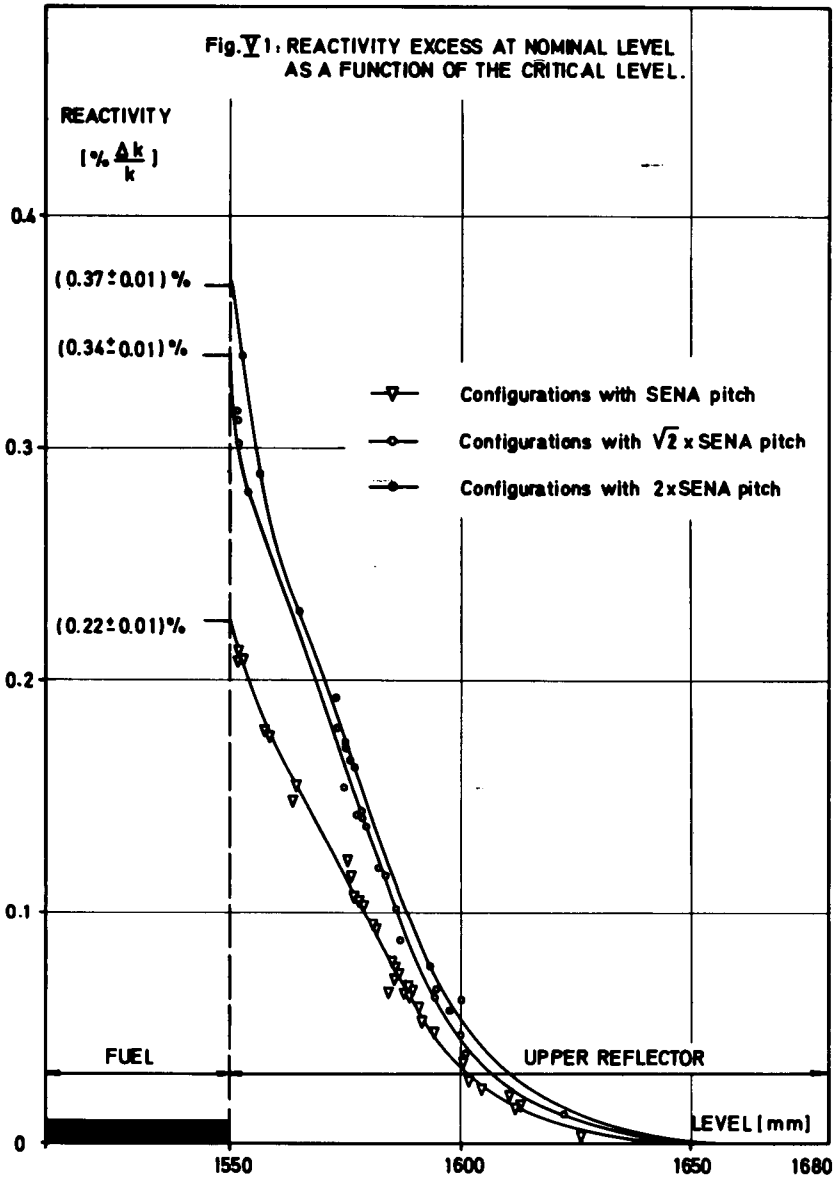

Fig. V 2 : SUBCRITICALITY DETERMINATION BY SUBCRITICAL COUNTINGS (CONFIGURATION 4)

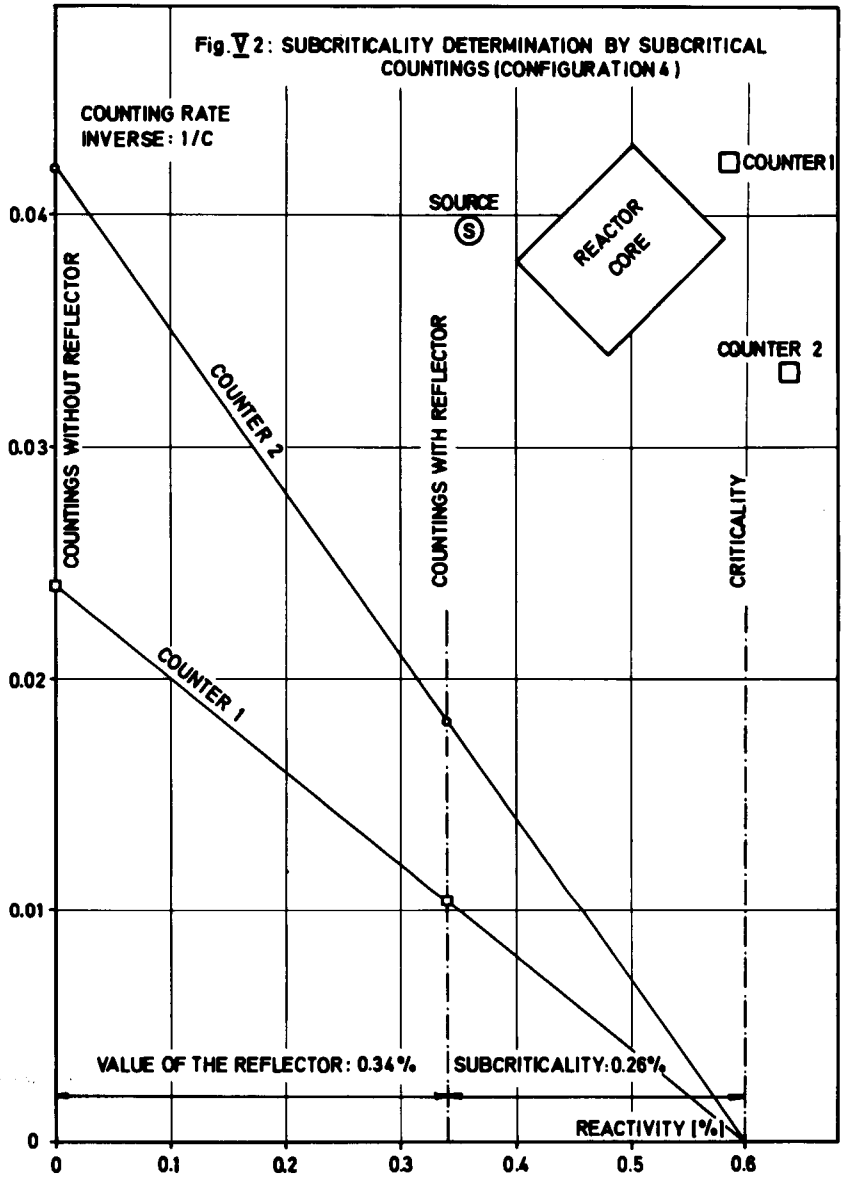

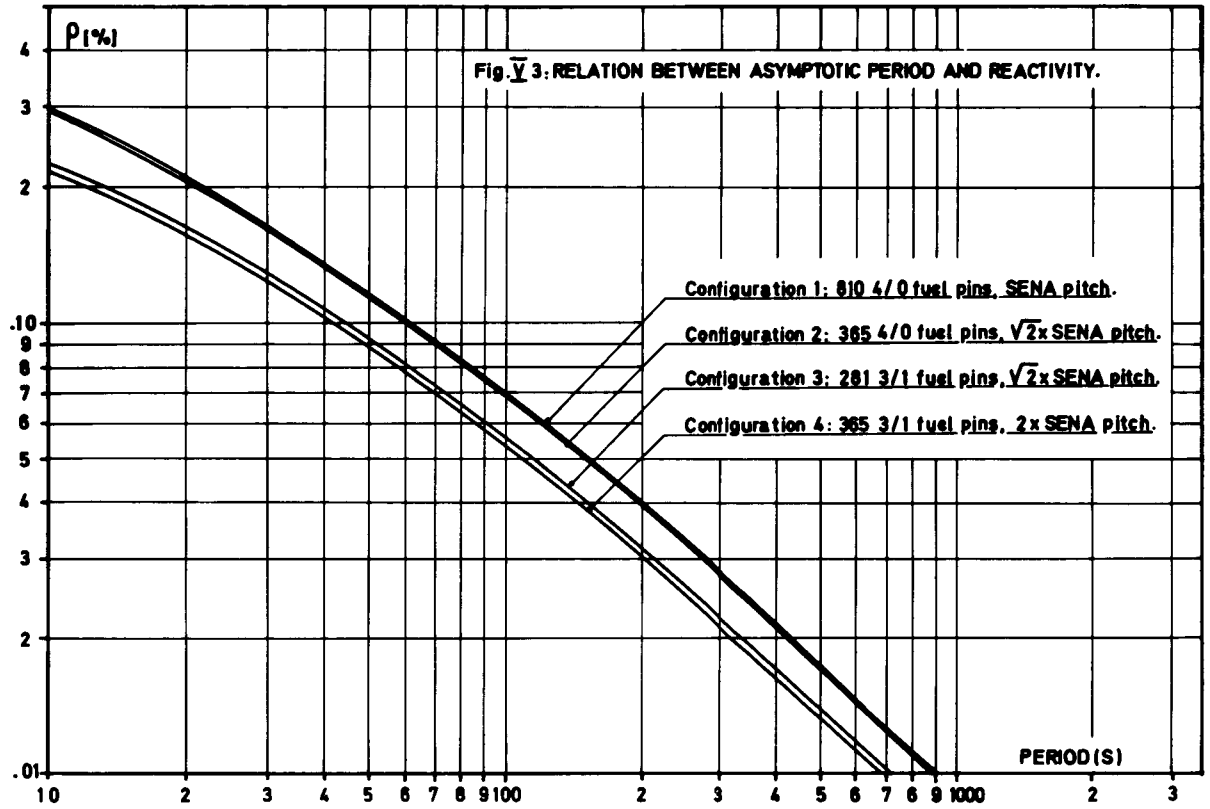

Fig. V 4: AXIAL POWER DISTRIBUTION BY FISSION CHAMBER

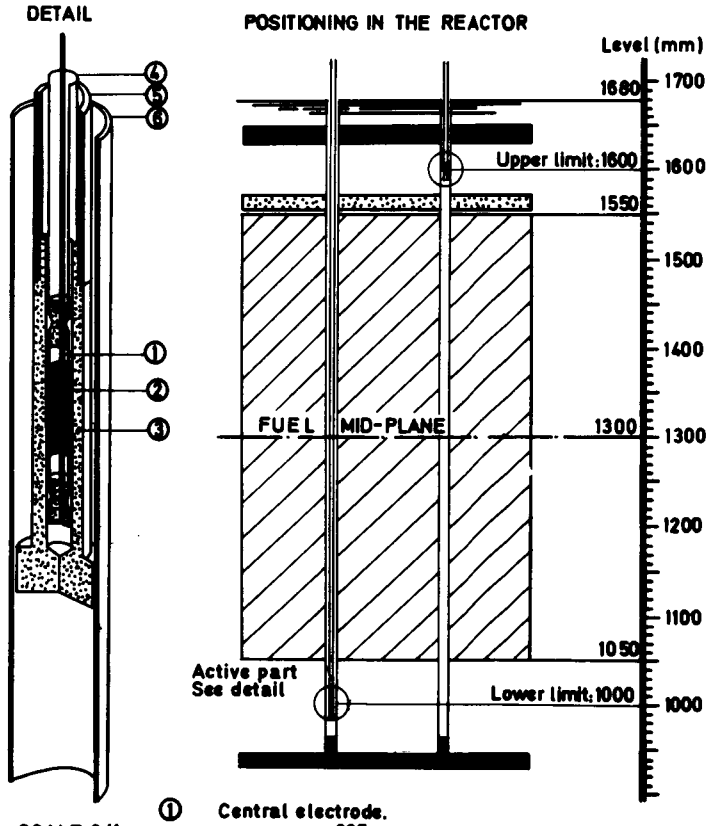

Fig.V 5: AXIAL POWER DISTRIBUTION BY ϑ-SCANNING.

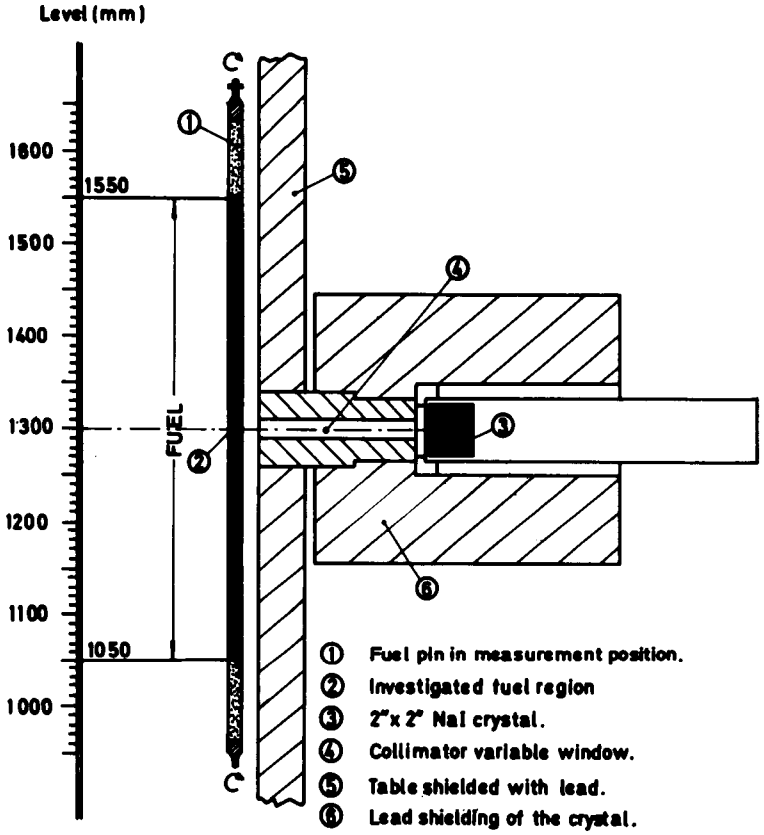

Fig.V 6: INFLUENCE OF THE HETEROGENEITY OF THE VIBROCOMPACTED PLUTONIUM FUEL ON THE ϑ-SCANNING MEASUREMENTS.

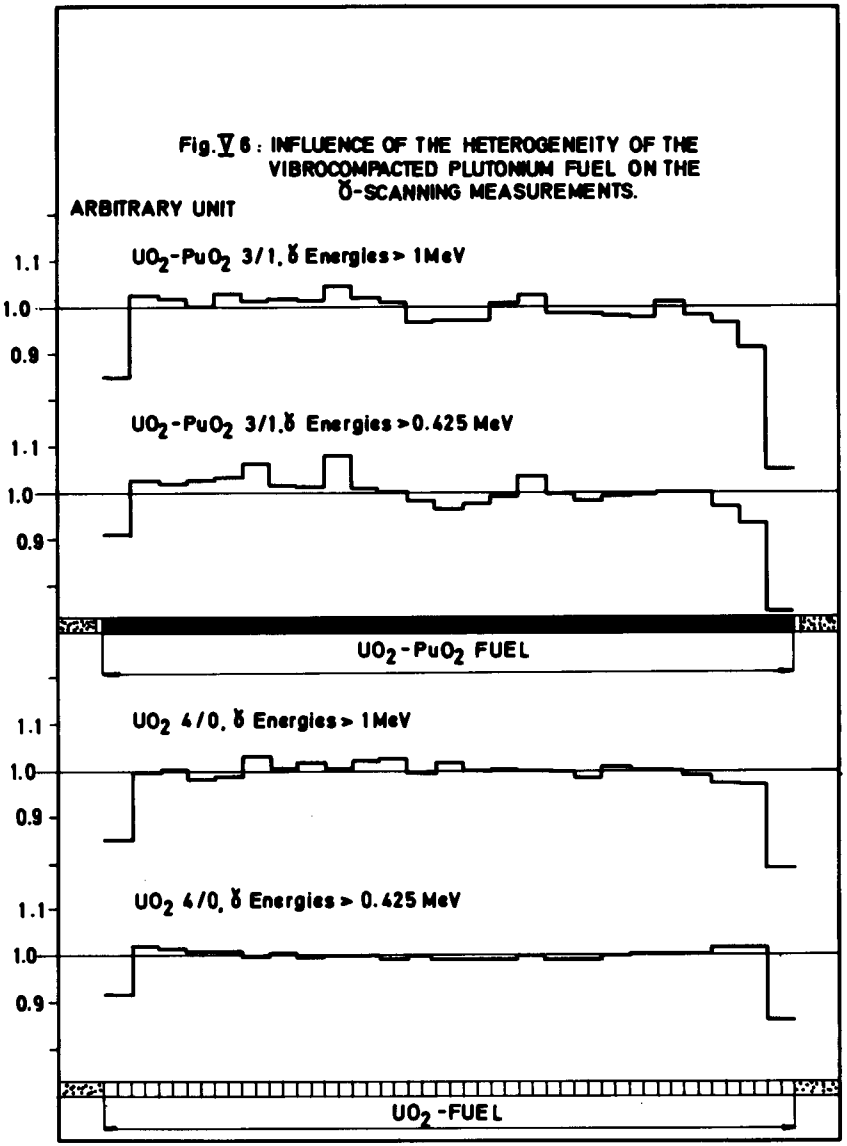

CONFIG. N°	FISSION CHAMB. [10^{-6} cm^{-2}]	γ-SCANNING [10^{-6} cm^{-2}]
1	$2577^{\pm 10}$	$2579^{\pm 10}$
2	$2579^{\pm 12}$	$2607^{\pm 20}$
3	$2598^{\pm 15}$	$2589^{\pm 36}$
4	$2602^{\pm 14}$	$2623^{\pm 33}$
5	$2623^{\pm 13}$	$2576^{\pm 47}$
7	$2451^{\pm 22}$	$2444^{\pm 28}$

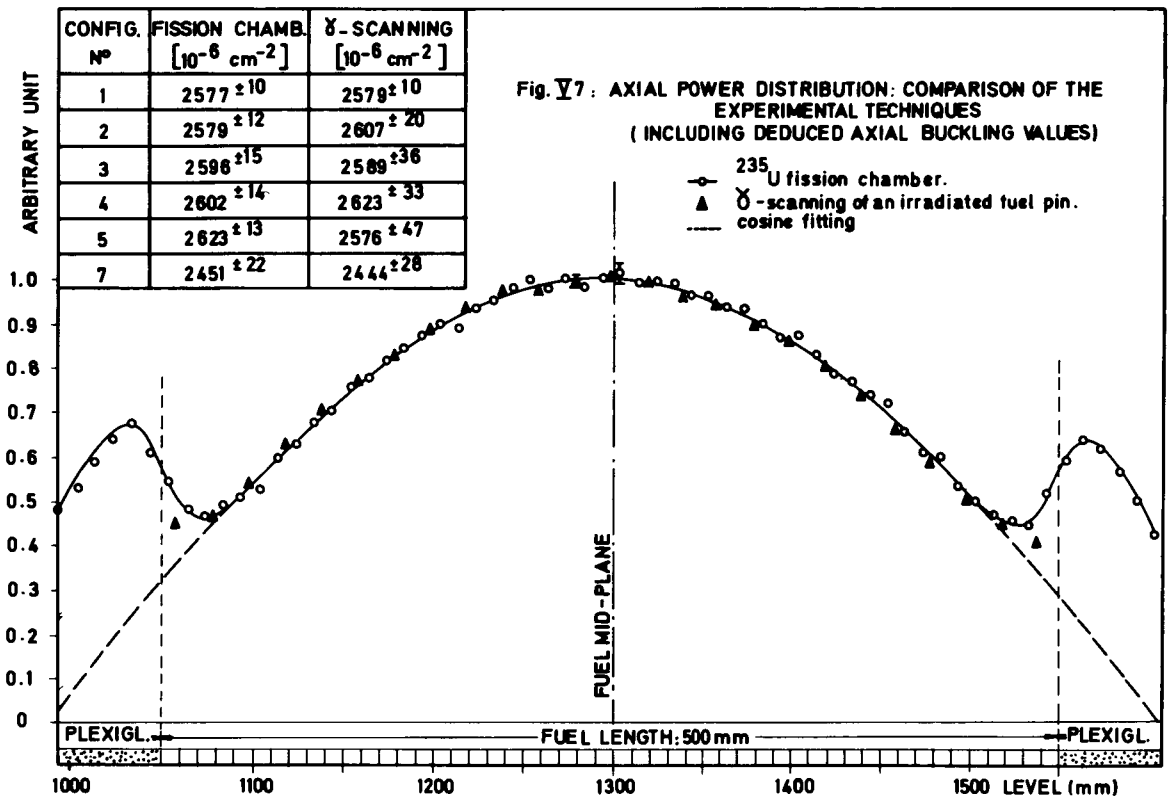

Fig. V 7 : AXIAL POWER DISTRIBUTION: COMPARISON OF THE EXPERIMENTAL TECHNIQUES (INCLUDING DEDUCED AXIAL BUCKLING VALUES)

^{235}U fission chamber.
γ-scanning of an irradiated fuel pin.
cosine fitting

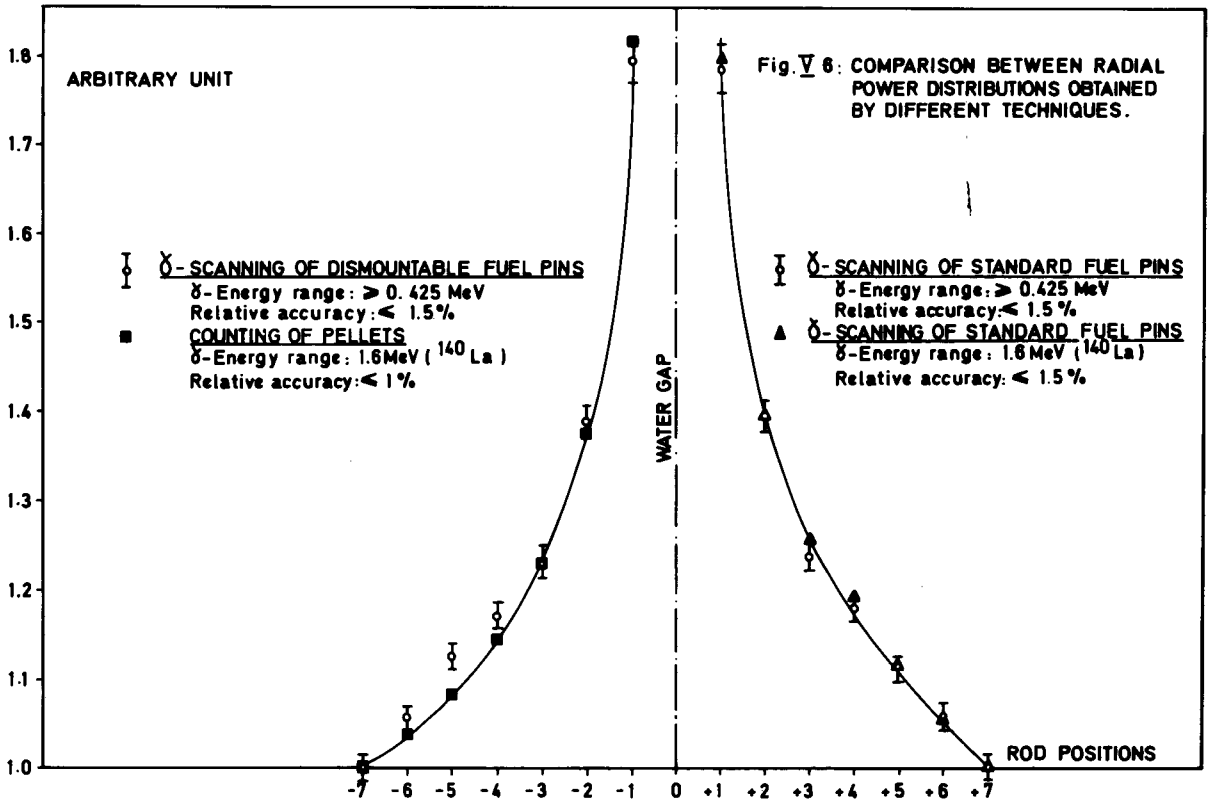

Fig. V 6: COMPARISON BETWEEN RADIAL POWER DISTRIBUTIONS OBTAINED BY DIFFERENT TECHNIQUES.

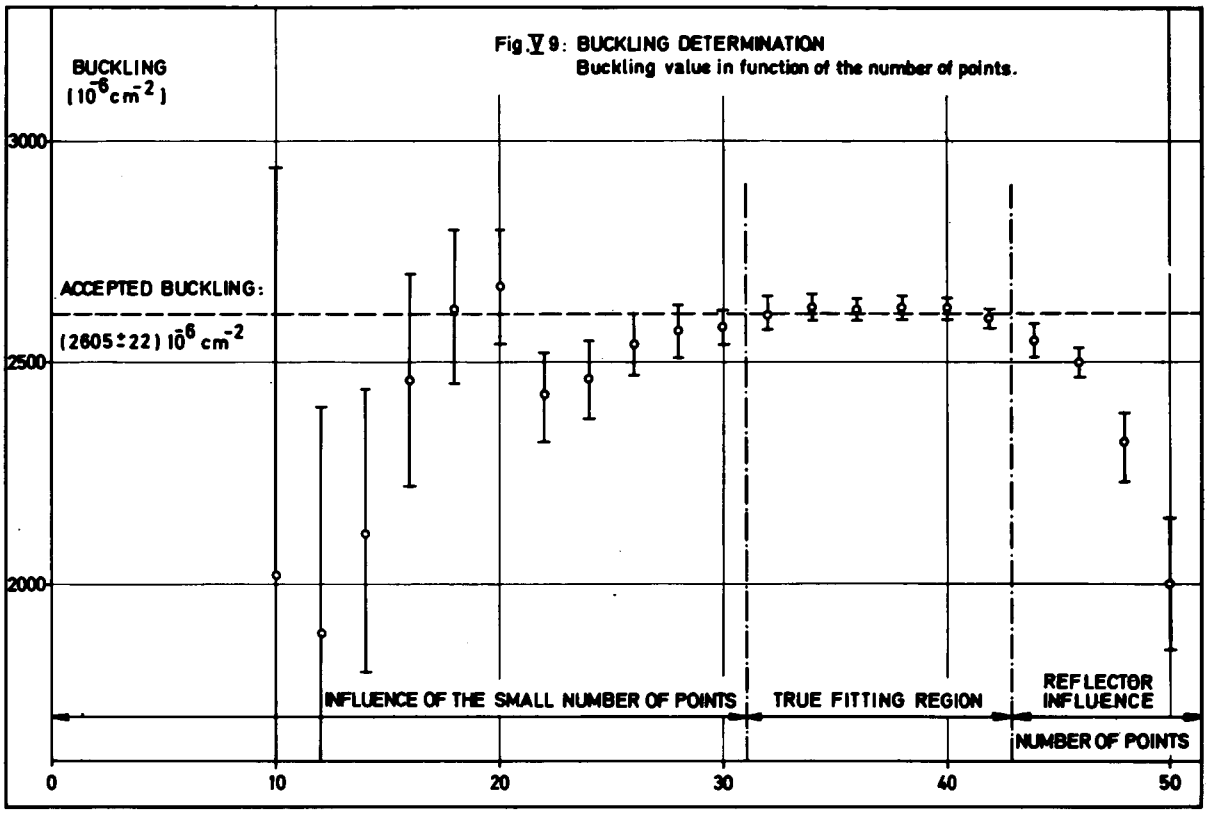

Fig. V 9: BUCKLING DETERMINATION
Buckling value in function of the number of points.

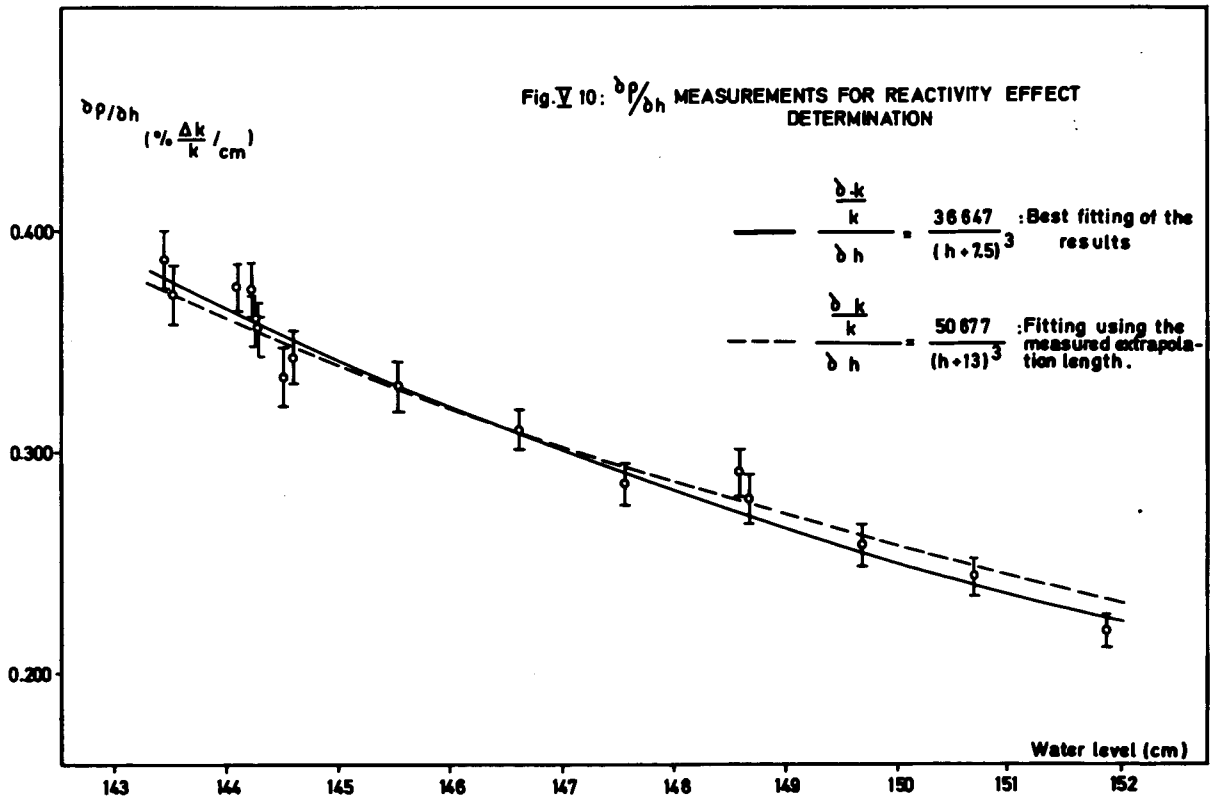

Fig. V 10: $\delta\rho/\delta h$ MEASUREMENTS FOR REACTIVITY EFFECT DETERMINATION

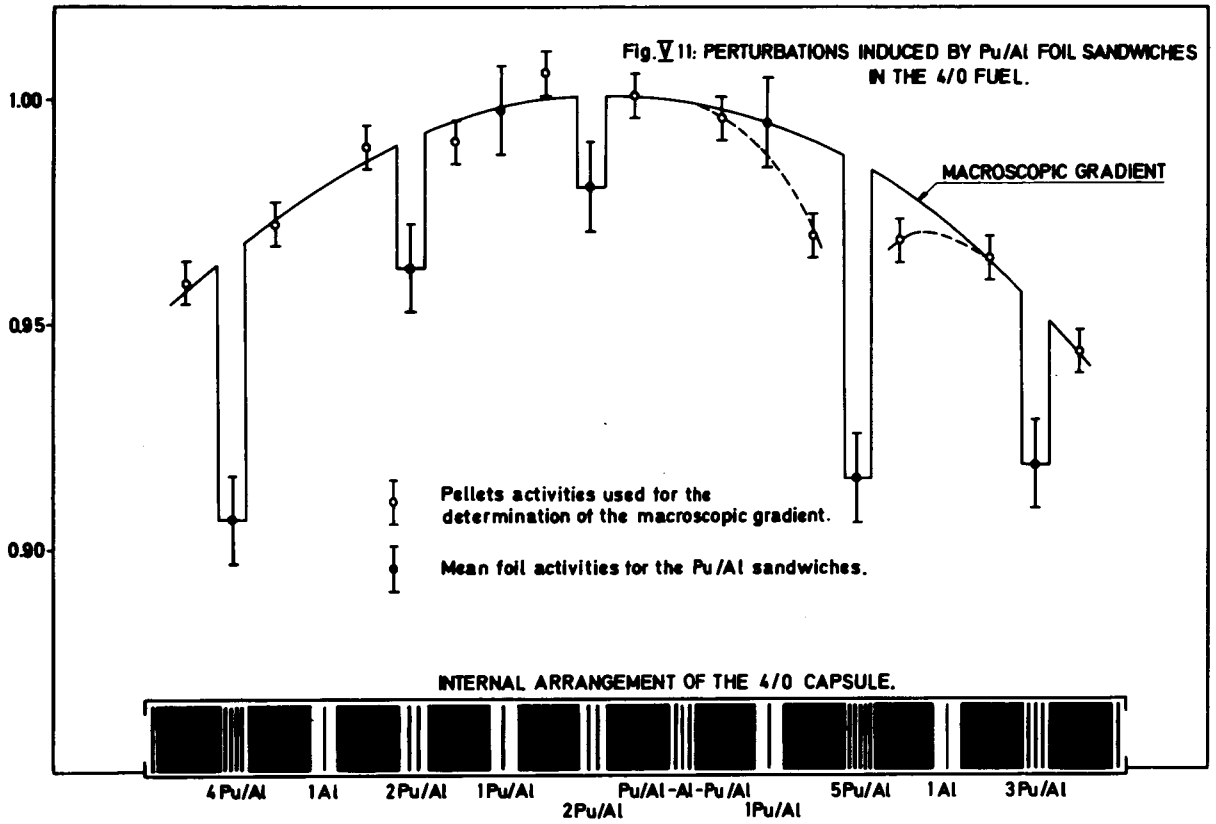

Fig.V 11: PERTURBATIONS INDUCED BY Pu/Al FOIL SANDWICHES IN THE 4/0 FUEL.

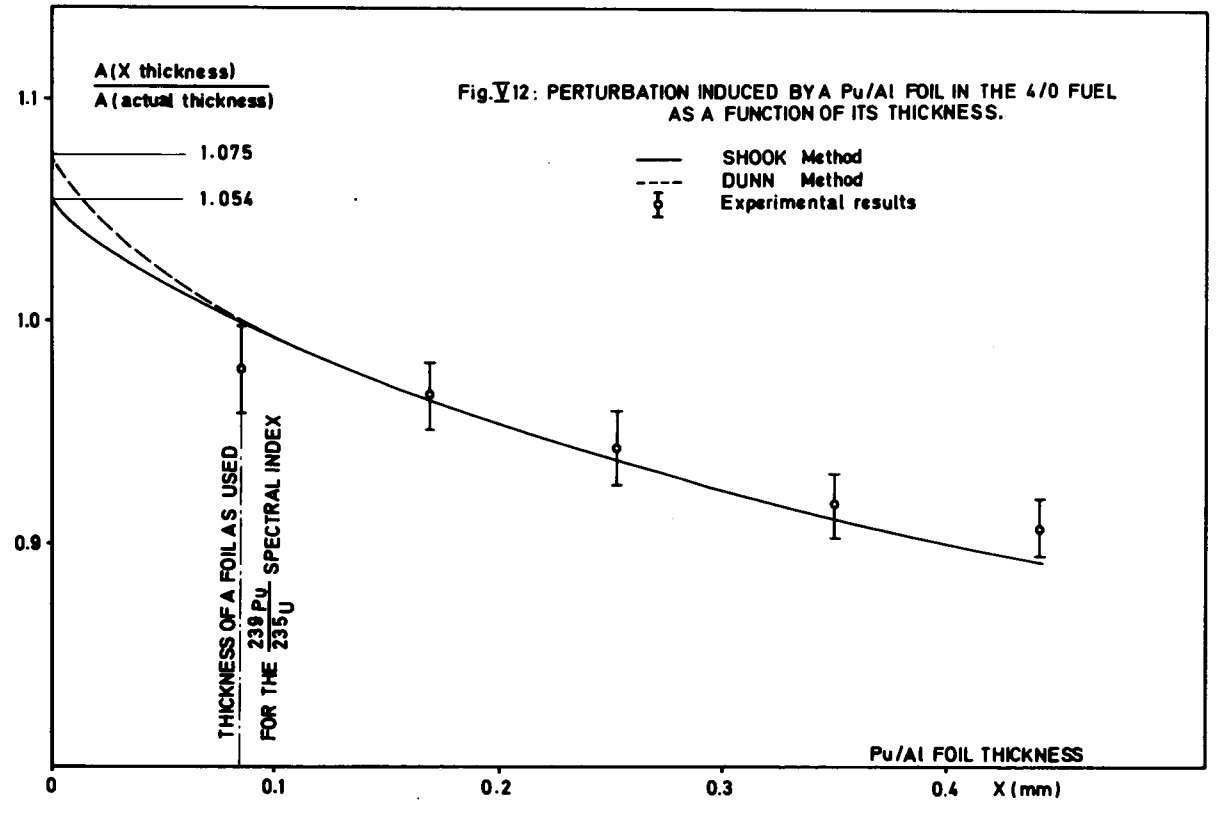

Fig.V 12: PERTURBATION INDUCED BY A Pu/Al FOIL IN THE 4/0 FUEL AS A FUNCTION OF ITS THICKNESS.

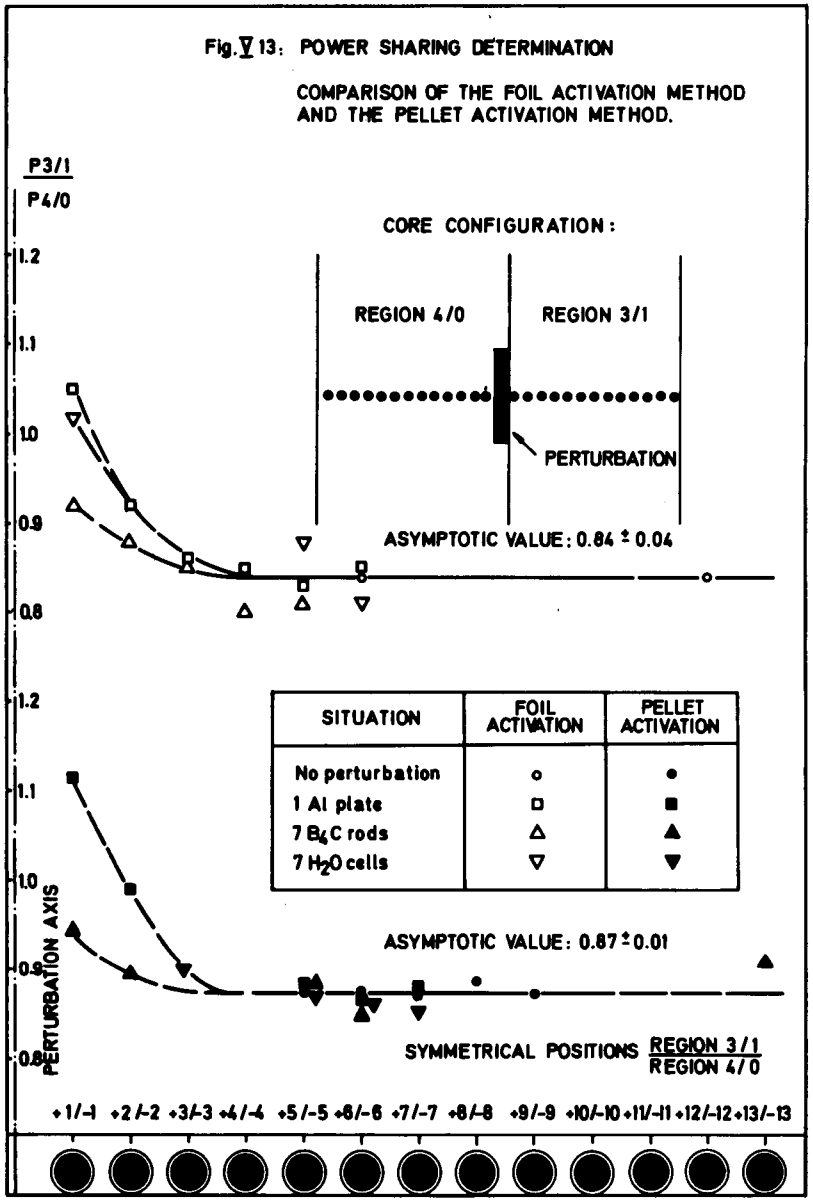

PANTHER CODE CHAIN

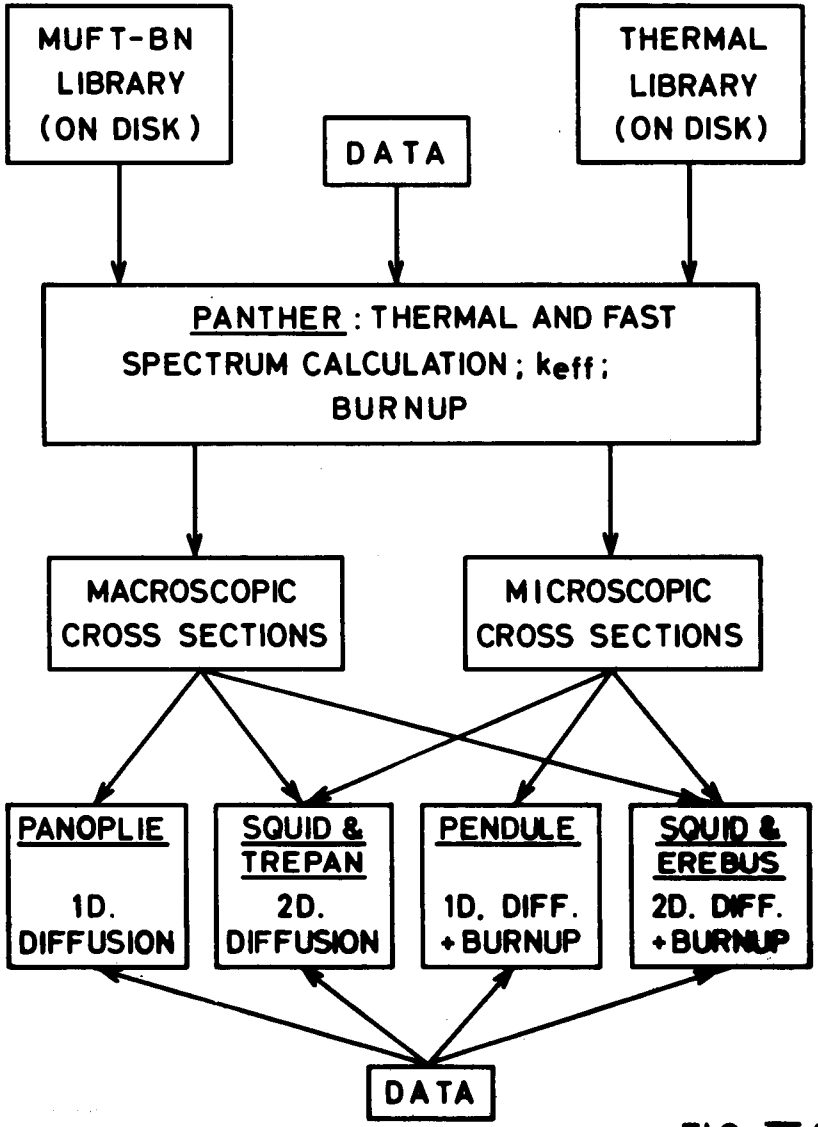

FIG. VI 1

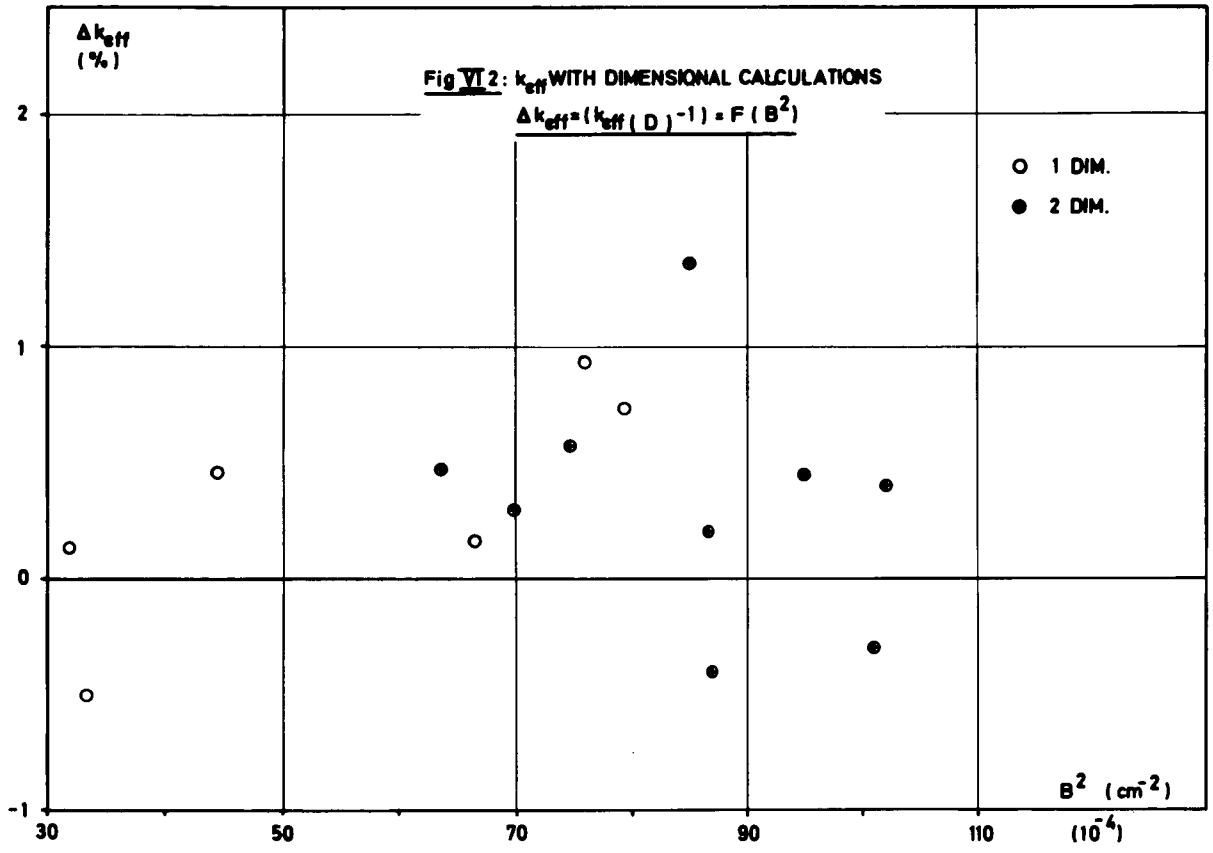

Fig VI 2 : k_{eff} WITH DIMENSIONAL CALCULATIONS

$\Delta k_{eff} = (k_{eff}(D)^{-1}) = F(B^2)$

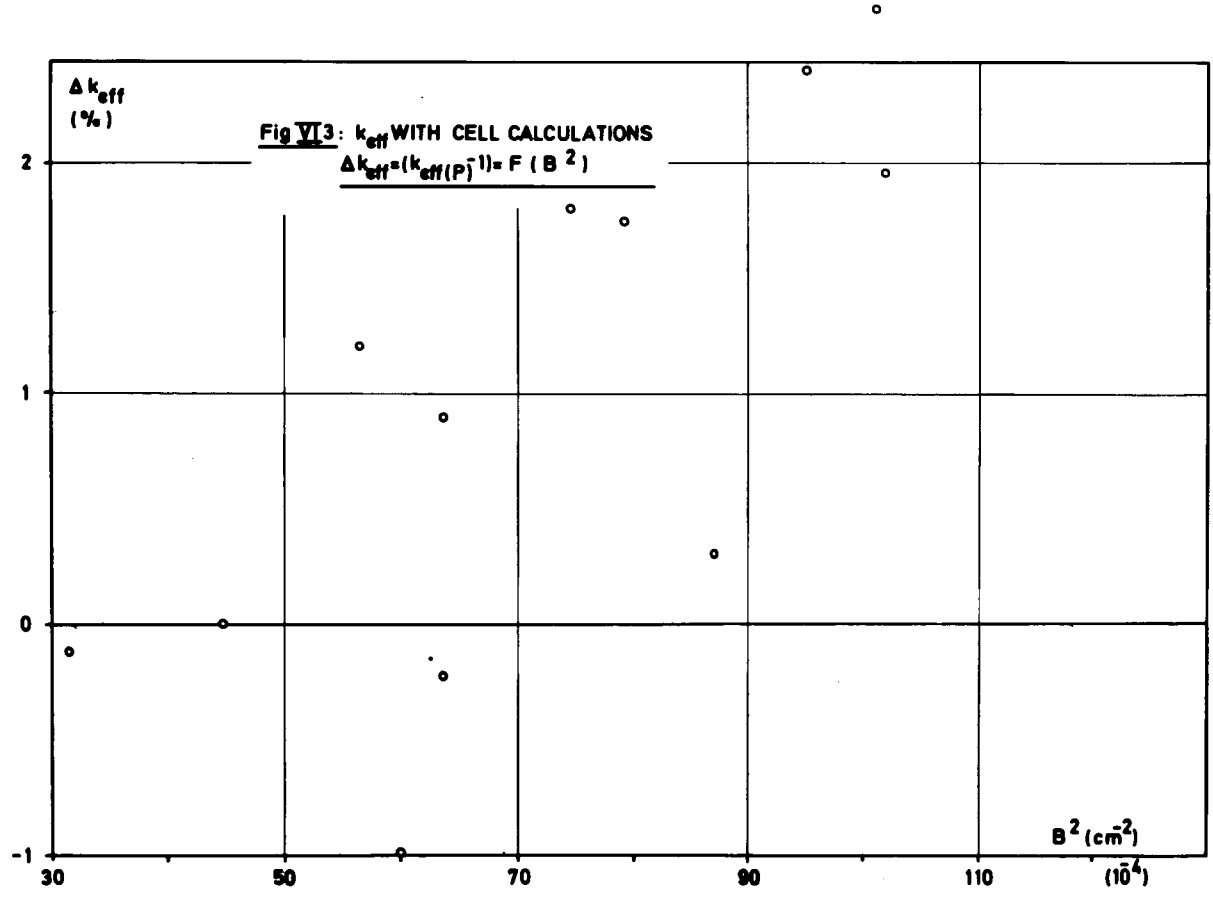

Fig VI 3 : k_{eff} WITH CELL CALCULATIONS

$\Delta k_{eff} = (k_{eff(P)}^{-1}) = F(B^2)$

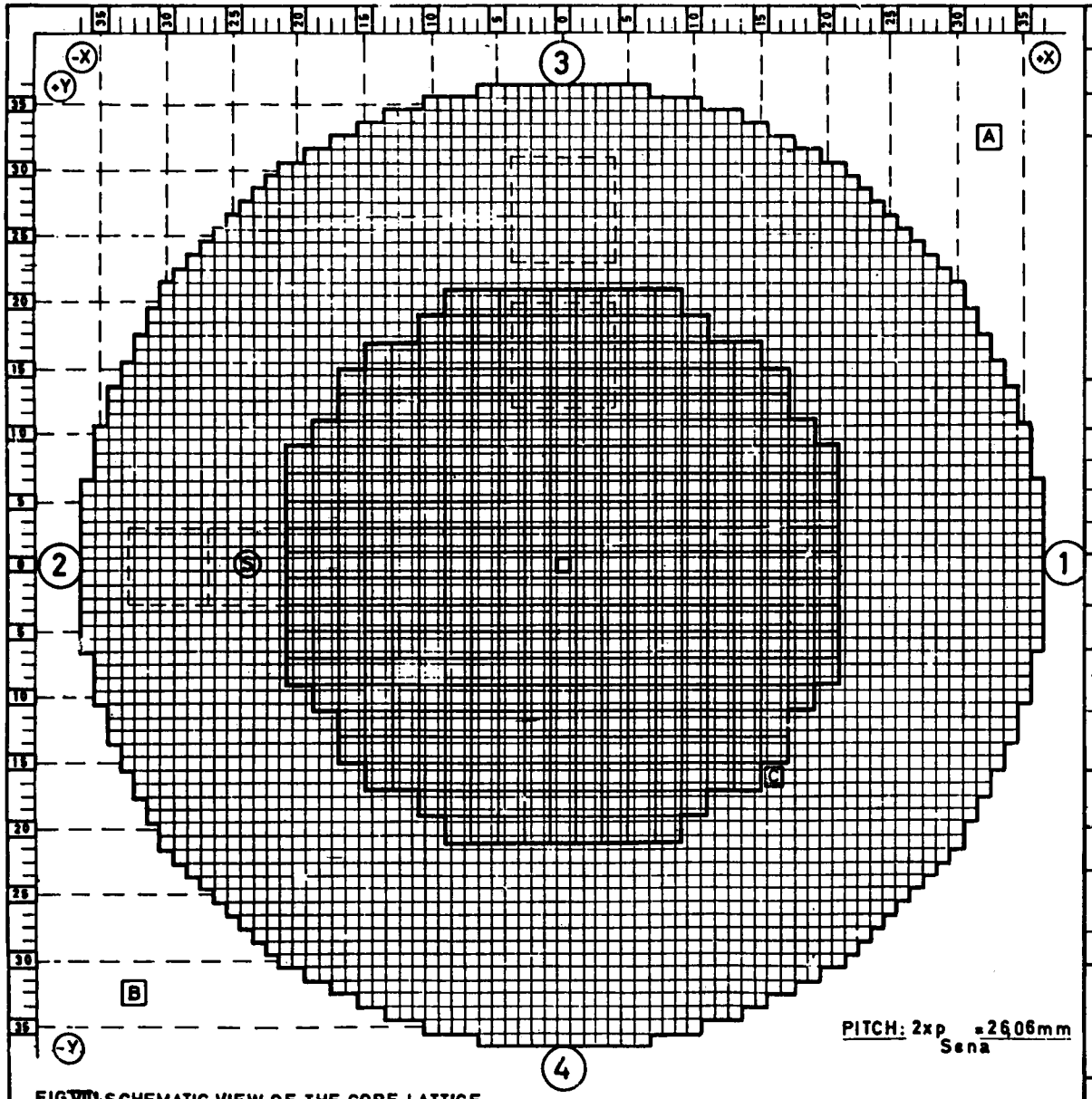

FIG VII: SCHEMATIC VIEW OF THE CORE LATTICE

C.E.N-S.C.K	VENUS CRITICAL EXPERIMENT

EXPERIMENT : Critical Mass Determination

DATE : 05.10.67

CONFIGURATION N° 5

DENSITY RODS : No

BORON CONCENTRATION (p.p.m) : No

START-UP SOURCE (S)

NEUTRON GENERATOR (N) No

ABSORBING ROD ■ R OR M No

FUEL REGIONS

DESIGNAT.	%U5/%Pu	COLOUR OR SYMBOL	NUMBER OF FUEL PINS	EQ. RADIUS OR X . Y	INVESTIGATED CELL
	3/1 VIPAK		290		
	3/1 SWG		75		
	(0,27mm)				
	TOTAL		365	28,09cm	

MEASUREMENT DETECTORS

DESIGNAT.	DIAMET.	SYMBOL	N°	LOCATION	LEVEL	CHANNEL
PROPORTIONAL BF_3 COUNTER	1/4"	C	3^B	+16 /-16	mid.pl	C
FISSION CHAMBER						

CONTROL DETECTORS

DESIGNAT.	DIAMET.	SYMBOL	N°	LOCATION	LEVEL	CHANNEL
PROPORTIONAL COUNTER	1"	A	A	32	mid.pl	A
	1"	B	B	14	mid.pl	B
ION CHAMBER						

VERIFIED BY:

APPROVED BY:

REMARKS : THE 3/1 SWG 0.27 FUEL PINS ARE LOADED AT THE BOUNDARY OF THE CORE.

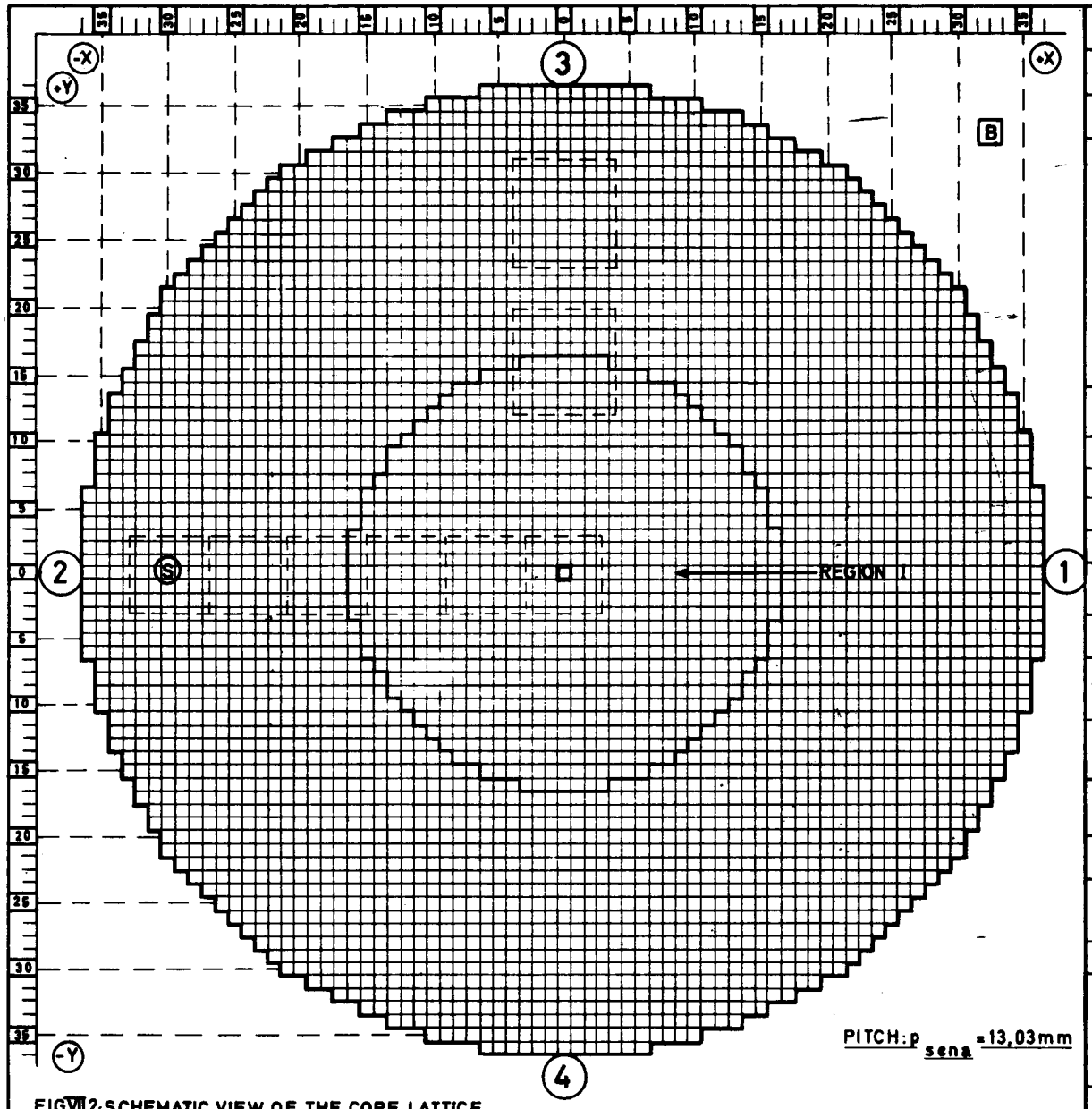

FIG VI 2: SCHEMATIC VIEW OF THE CORE LATTICE

C.E.N-S.C.K	VENUS CRITICAL EXPERIMENT

EXPERIMENT : CRITICAL MASS DETERMINATION

DATE : 10.12.69.

CONFIGURATION N° 8bis

DENSITY RODS : No

BORON CONCENTRATION (p.p.m) : No

START-UP SOURCE (S)

NEUTRON GENERATOR (N) No

ABSORBING ROD ■ R OR M No

FUEL REGIONS

DESIGNAT.	%U5/%Pu	COLOUR OR SYMBOL	NUMBER OF FUEL PINS	EQ. RADIUS OR X . Y	INVESTIGATED CELL
I	4/0	WHITE	833	21.22cm	

MEASUREMENT DETECTORS

DESIGNAT.	DIAMET.	SYMBOL	N°	LOCATION	LEVEL	CHANNEL
PROPORTIONAL BF_3 COUNTER						
FISSION CHAMBER						

CONTROL DETECTORS

DESIGNAT.	DIAMET.	SYMBOL	N°	LOCATION	LEVEL	CHANNEL
PROPORTIONAL COUNTER	1"	A	A	OUT	ON THE WALL	A
	1"	B	B	32	Mid-pl.	B
ION CHAMBER						

VERIFIED BY:

APPROVED BY:

REMARKS :

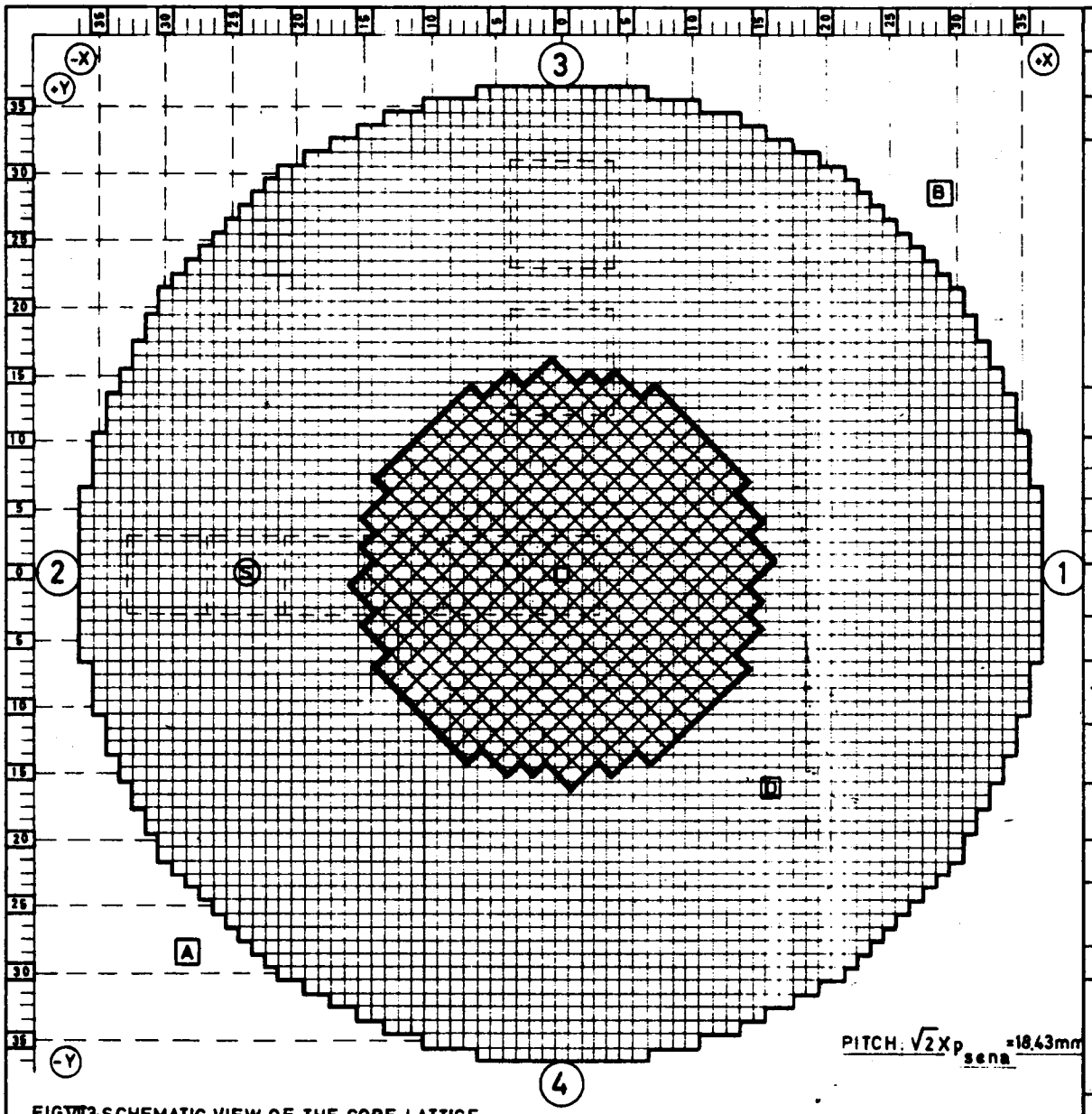

FIG VII.3: SCHEMATIC VIEW OF THE CORE LATTICE

C.E.N-S.C.K | **VENUS CRITICAL EXPERIMENT**

EXPERIMENT : Critical Mass Determination

DATE : 12.06.67

CONFIGURATION N° 1

DENSITY RODS : No

BORON CONCENTRATION (p.p.m) : No

START-UP SOURCE (S)

NEUTRON GENERATOR (N) No

ABSORBING ROD ■ R OR M No

FUEL REGIONS

DESIGNAT.	%U5/%Pu	COLOUR OR SYMBOL	NUMBER OF FUEL PINS	EQ. RADIUS OR X . Y	INVES - TIGATED CELL
-	4/0	-	353	195.36	-

MEASUREMENT DETECTORS

DESIGNAT	DIAMET	SYMBOL	N°	LOCATION	LEVEL	CHANNEL
PROPORTIONAL BF_3 COUNTER	1/4"	D	3^B	+16/-16	mid.pl.	C
FISSION CHAMBER						

CONTROL DETECTORS

DESIGNAT	DIAMET	SYMBOL	N°	LOCATION	LEVEL	CHANNEL
PROPORTIONAL COUNTER	1"	A	A	14	mid.pl.	A
	1"	B	B	32		B
ION CHAMBER						

Keff measured by a positive period equals: 1.000 8.

VERIFIED BY: [signature] APPROVED BY: [signature]

REMARKS :

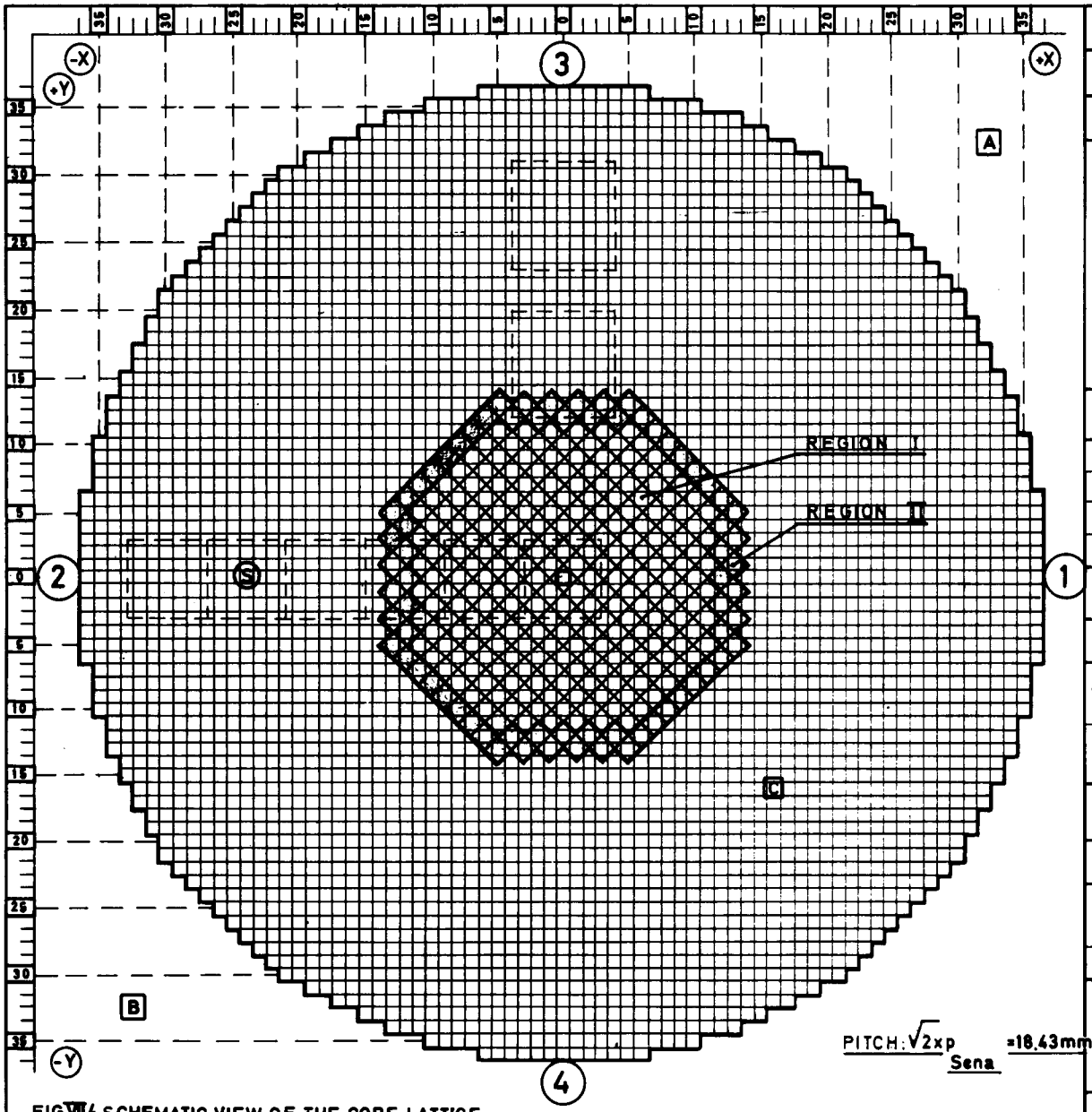

FIG VI.4: SCHEMATIC VIEW OF THE CORE LATTICE

C.E.N-S.C.K	VENUS CRITICAL EXPERIMENT

EXPERIMENT : Critical Mass Determination.

DATE : 19.09.67

CONFIGURATION N° 3/1 bis

DENSITY RODS : No

BORON CONCENTRATION (p.p.m) : No

START-UP SOURCE (S) _____

NEUTRON GENERATOR (N) No

ABSORBING ROD ■ R OR M No

FUEL REGIONS

DESIGNAT.	%U5/%Pu	COLOUR OR SYMBOL	NUMBER OF FUEL PINS	EQ. RADIUS OR X . Y	INVESTIGATED CELL
I	3/1 VIPAK	WHITE	229	-	-
II	3/1 SWG	GREY	72		
	0,27				
TOTAL			301	18.04 cm.	

MEASUREMENT DETECTORS

DESIGNAT.	DIAMET.	SYMBOL	N°	LOCATION	LEVEL	CHANNEL
PROPORTIONAL BF_3 COUNTER	1/4"	C	3B	+16/-16	mid.pl.	C
FISSION CHAMBER						

CONTROL DETECTORS

DESIGNAT.	DIAMET.	SYMBOL	N°	LOCATION	LEVEL	CHANNEL
PROPORTIONAL COUNTER	1"	A	A	32	mid.pl.	A
	1"	B	B	-14	mid.pl.	B
ION CHAMBER						

VERIFIED BY: [signature] APPROVED BY: [signature]

REMARKS :

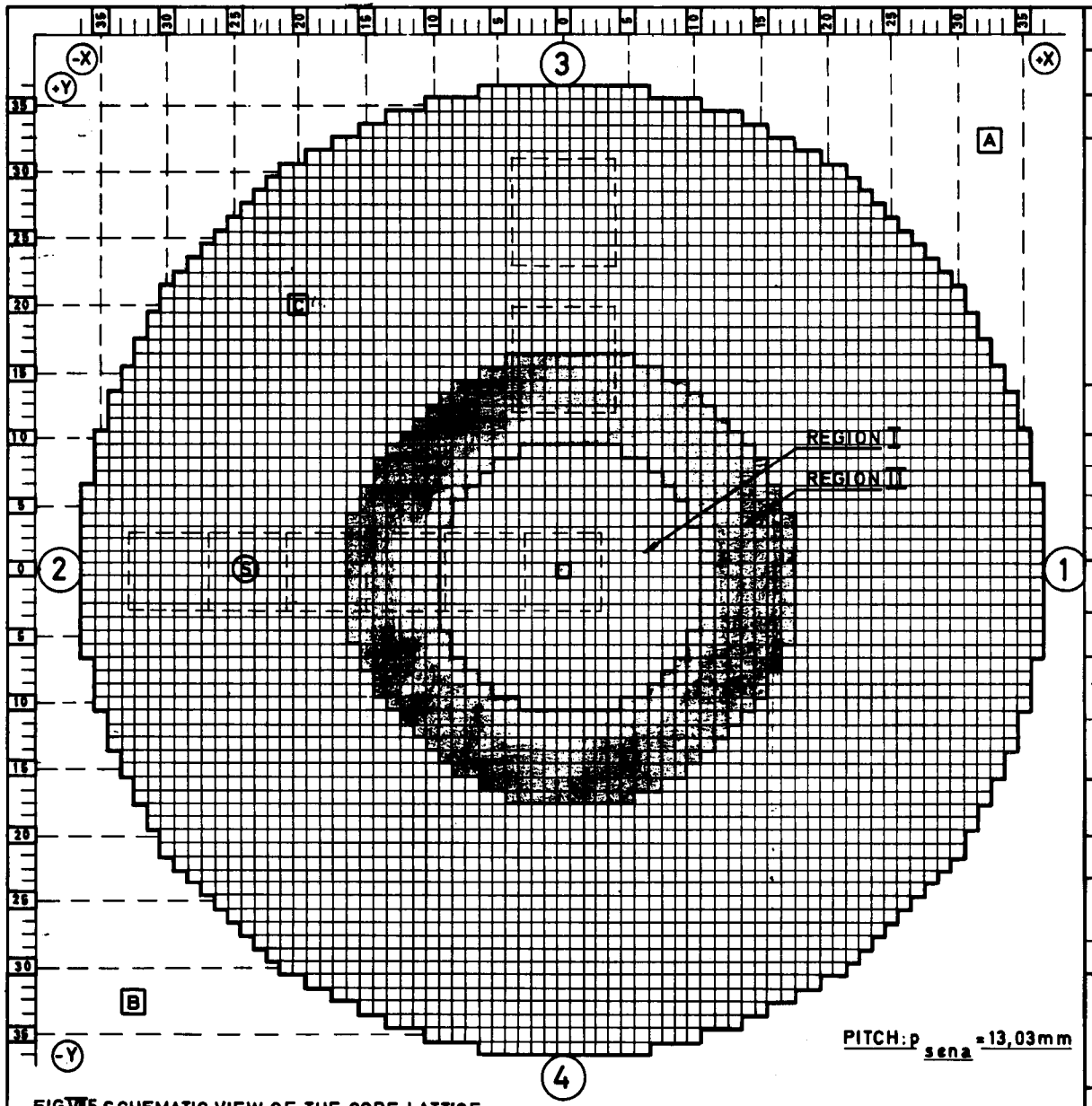

FIG. 15: SCHEMATIC VIEW OF THE CORE LATTICE

REMARKS :

C.E.N-S.C.K | **VENUS CRITICAL EXPERIMENT**

EXPERIMENT : Critical Mass and Radial Buckling Measur.

DATE : 14.12.67

CONFIGURATION N° 7/1

DENSITY RODS : No

BORON CONCENTRATION (p.p.m) : No

START-UP SOURCE (S)

NEUTRON GENERATOR (N) No

ABSORBING ROD ■ R OR M No

FUEL REGIONS

DESIGNAT.	%U5/%Pu	COLOUR OR SYMBOL	NUMBER OF FUEL PINS	EQ. RADIUS OR X . Y	INVESTIGATED CELL
I	3/1 VIPAK	WHITE	260	13.39cm	
	3/1 SWG 0.27	WHITE	72		
II	4/0	GREY	580	22.20cm	
TOTAL			912		

MEASUREMENT DETECTORS

DESIGNAT.	DIAMET.	SYMBOL	N°	LOCATION	LEVEL	CHANNEL
PROPORTIONAL BF_3 COUNTER	1/4"	C	3^B	-20/+20	mid-pl.	C
FISSION CHAMBER						

CONTROL DETECTORS

DESIGNAT.	DIAMET.	SYMBOL	N°	LOCATION	LEVEL	CHANNEL
PROPORTIONAL COUNTER	1"	A	A	32	mid-pl.	A
	1"	B	B	14	mid-pl.	B
ION CHAMBER						

VERIFIED BY: APPROVED BY:

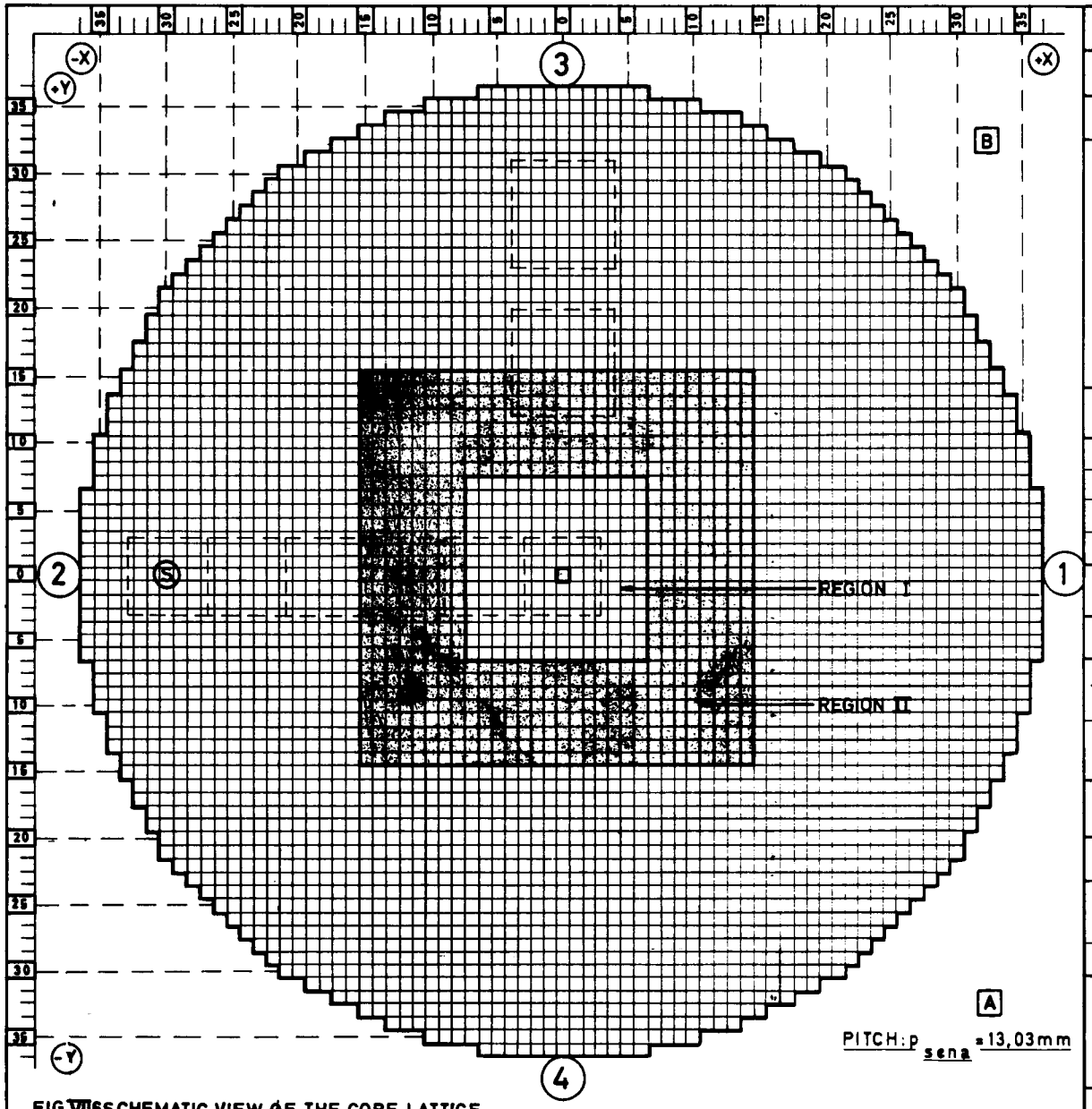

FIG. VII.6 SCHEMATIC VIEW OF THE CORE LATTICE

C.E.N-S.C.K	VENUS CRITICAL EXPERIMENT

EXPERIMENT : CRITICAL MASS DETERMINATION.

DATE : 05.12.66.

CONFIGURATION N° 7/2

DENSITY RODS : No

BORON CONCENTRATION (p.p.m) : No

START-UP SOURCE (S)

NEUTRON GENERATOR (N) No

ABSORBING ROD ■ R OR M No

FUEL REGIONS

DESIGNAT.	%U5/%Pu	COLOUR OR SYMBOL	NUMBER OF FUEL PINS	EQ. RADIUS OR X . Y	INVESTIGATED CELL
I	3/1 VIPAK	WHITE	196	18.24x18.24	
II	4/0	GREY	704	39.09x39.09	
TOTAL			900		

MEASUREMENT DETECTORS

DESIGNAT.	DIAMET.	SYMBOL	N°	LOCATION	LEVEL	CHANNEL
PROPORTIONAL BF_3 COUNTER						
FISSION CHAMBER						

CONTROL DETECTORS

DESIGNAT.	DIAMET.	SYMBOL	N°	LOCATION	LEVEL	CHANNEL
PROPORTIONAL COUNTER	1"	A	A	5	mid.pl.	A
	1"	B	B	32	mid.pl.	B
ION CHAMBER						

VERIFIED BY:

APPROVED BY:

REMARKS :

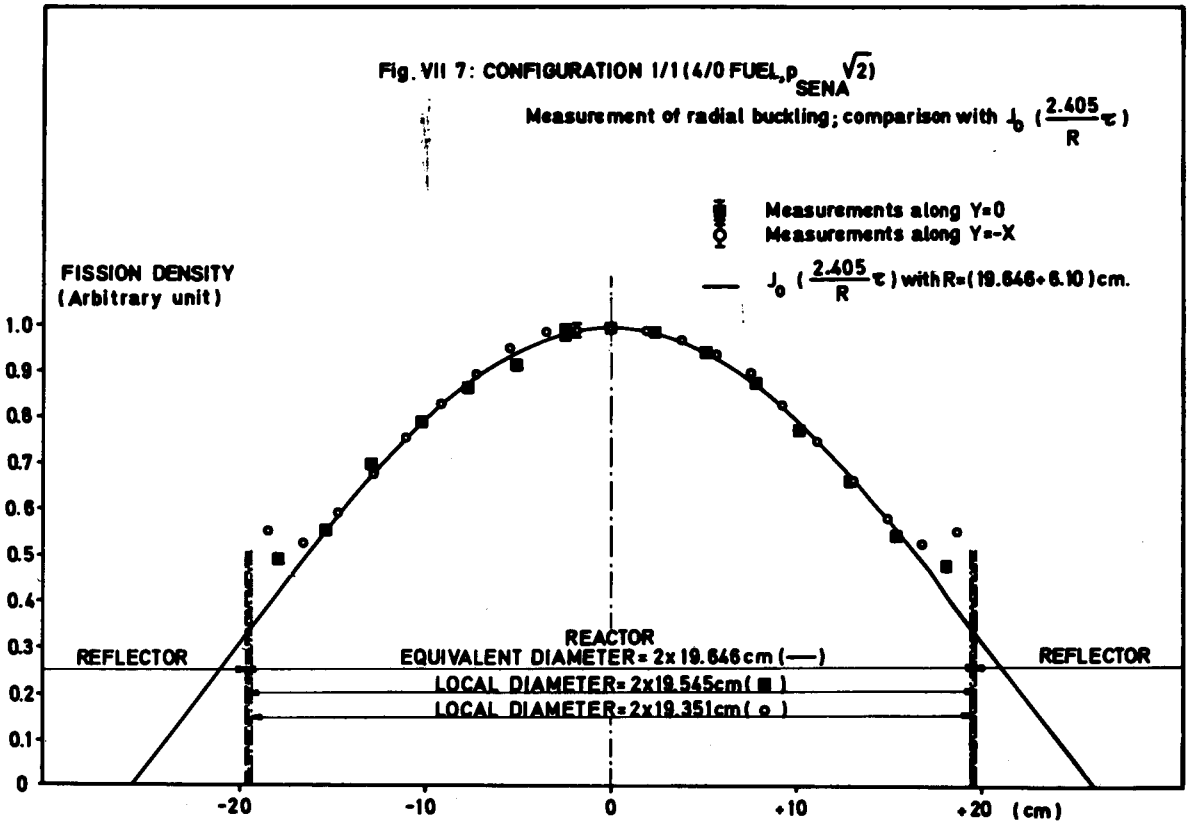
Fig. VII 7: CONFIGURATION 1/1 (4/0 FUEL, $p_{SENA}\sqrt{2}$)
Measurement of radial buckling; comparison with $J_0\left(\frac{2.405}{R}\tau\right)$
Measurements along Y=0
Measurements along Y=-X
$J_0\left(\frac{2.405}{R}\tau\right)$ with R=(19.646±6.10)cm.
FISSION DENSITY
(Arbitrary unit)
1.0
0.9
0.8
0.7
0.6
0.5
0.4
0.3
0.2
0.1
0
REFLECTOR
REACTOR
EQUIVALENT DIAMETER=2x19.646cm (—)
LOCAL DIAMETER=2x19.545cm (■)
LOCAL DIAMETER=2x19.351cm (○)
REFLECTOR
-20
-10
0
+10
+20 (cm)

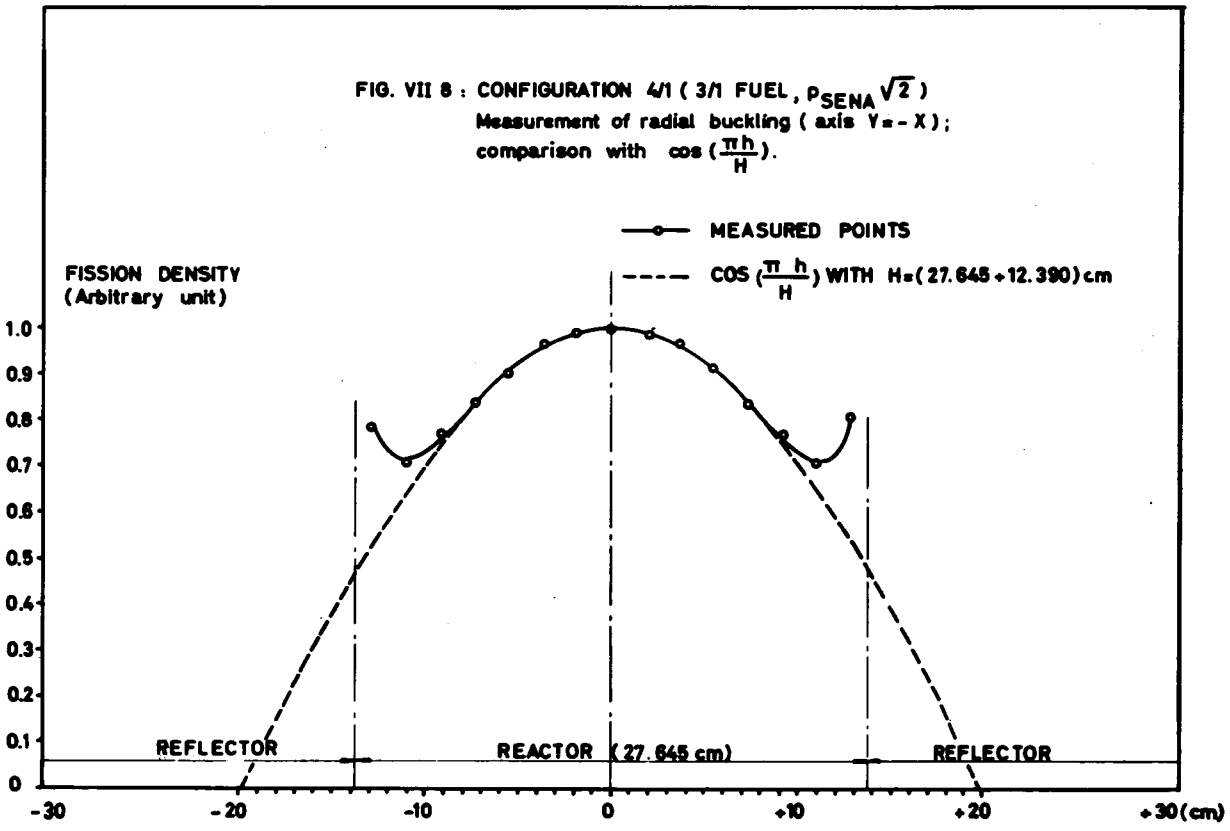
FIG. VII 8 : CONFIGURATION 4/1 (3/1 FUEL , $p_{SENA}\sqrt{2}$)
Measurement of radial buckling (axis Y=-X);
comparison with $\cos\left(\frac{\pi h}{H}\right)$.
MEASURED POINTS
$\cos\left(\frac{\pi h}{H}\right)$ WITH H=(27.645±12.390)cm
FISSION DENSITY
(Arbitrary unit)
1.0
0.9
0.8
0.7
0.6
0.5
0.4
0.3
0.2
0.1
0
REFLECTOR
REACTOR (27.645 cm)
REFLECTOR
-30
-20
-10
0
+10
+20
+30(cm)

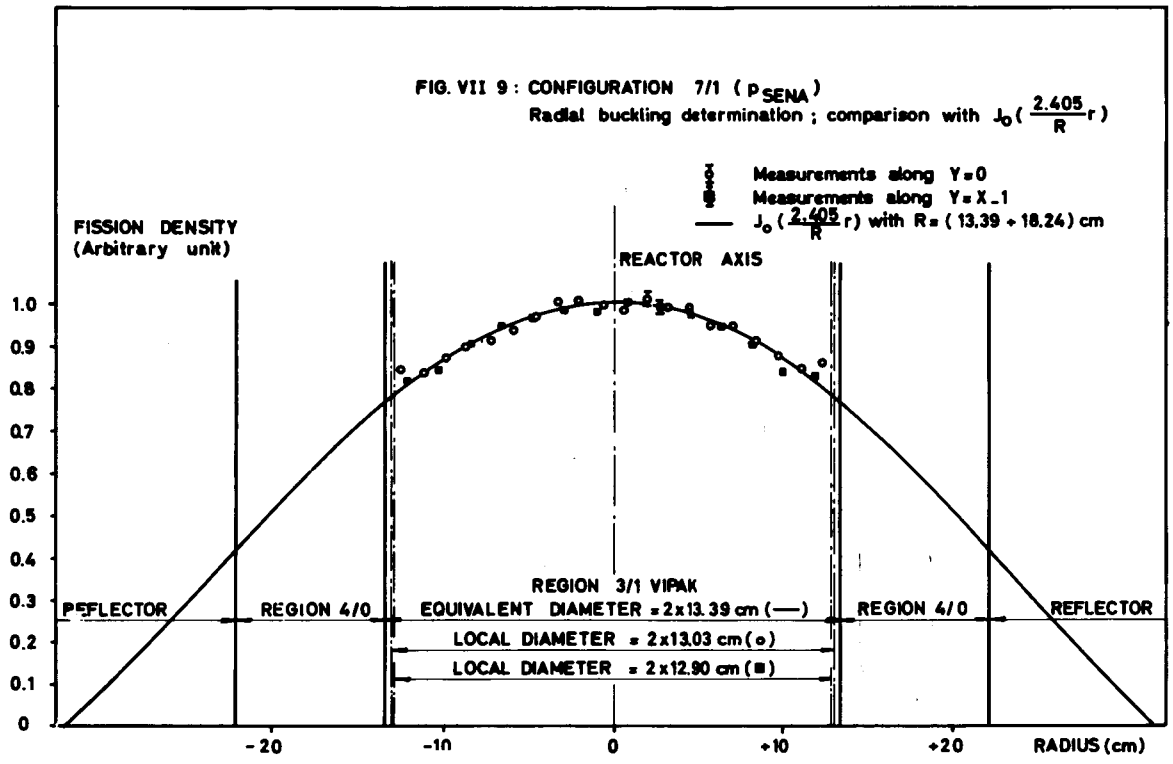
FIG. VII 9 : CONFIGURATION 7/1 (ρ_{SENA})
Radial buckling determination ; comparison with $J_0(\frac{2.405}{R}r)$
Measurements along Y=0
Measurements along Y=X_1
$J_0(\frac{2.405}{R}r)$ with R= (13.39 ÷ 18.24) cm
FISSION DENSITY
(Arbitrary unit)
REACTOR AXIS
1.0
0.9
0.8
0.7
0.6
0.5
0.4
0.3
0.2
0.1
0
REFLECTOR
REGION 4/0
REGION 3/1 VIPAK
EQUIVALENT DIAMETER = 2x13.39 cm (—)
LOCAL DIAMETER = 2x13.03 cm (o)
LOCAL DIAMETER = 2x12.90 cm (■)
REGION 4/0
REFLECTOR
-20
-10
0
+10
+20
RADIUS (cm)

Fig. VII.10 : REACTIVITY EXCESS AT NOMINAL LEVEL AS A FUNCTION OF THE CRITICAL LEVEL.

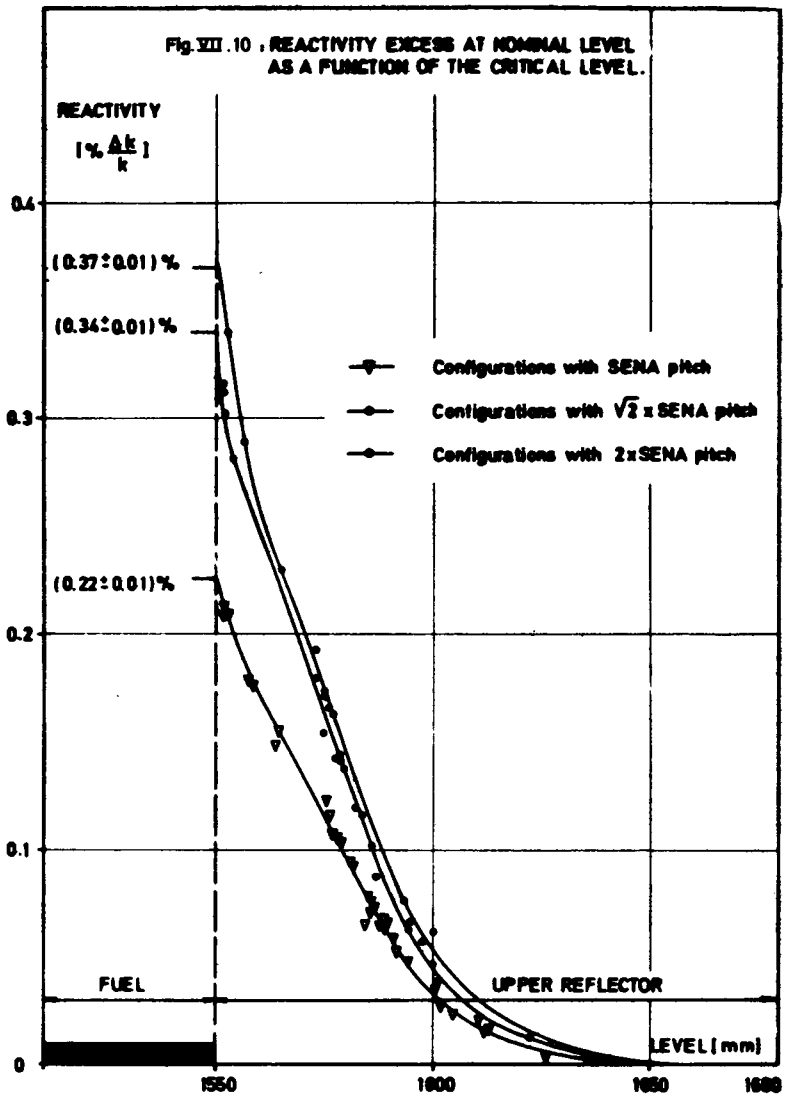

FIG. VII 11: CONFIGURATION 8/0
Radial fission density distribution
along the X - axis (with cosine fitting)

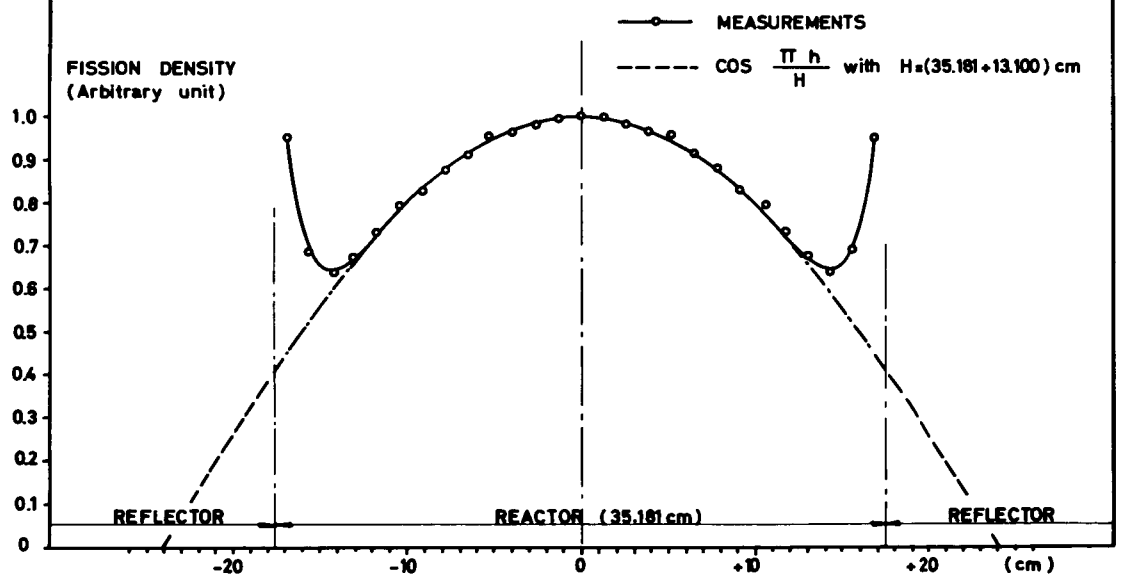

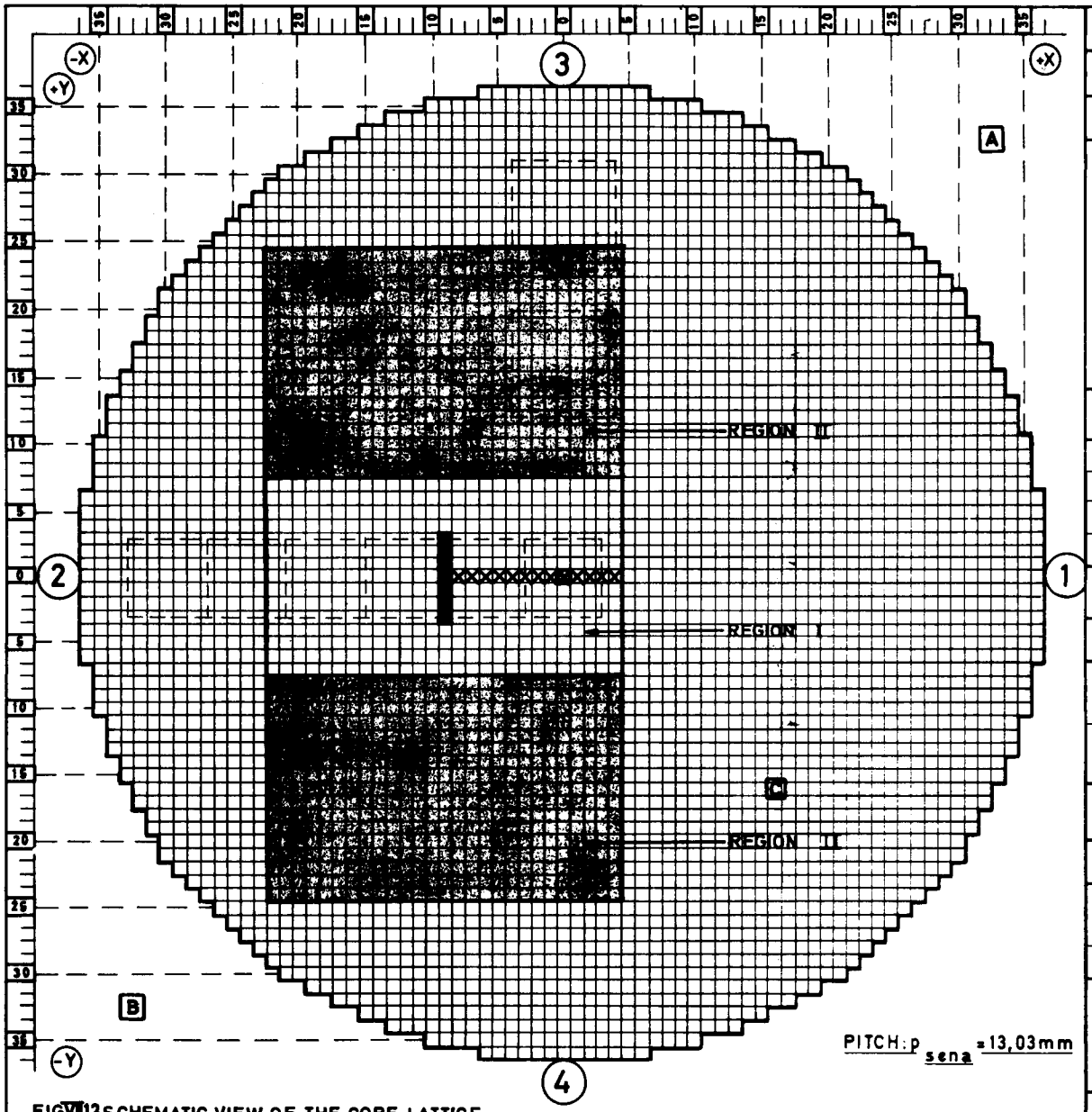

FIG. 2 SCHEMATIC VIEW OF THE CORE LATTICE

REMARKS : The black cells indicate the location of the perturbations.

C.E.N-S.C.K	VENUS CRITICAL EXPERIMENT

EXPERIMENT : PERTURBATIONS EXPERIMENTS

DATE : 20.05.68

CONFIGURATION N° 10

DENSITY RODS : No

BORON CONCENTRATION (p.p.m) : No

START-UP SOURCE (S)

NEUTRON GENERATOR (N) No

ABSORBING ROD ■ R OR M No

FUEL REGIONS

DESIGNAT.	%US/%Pu	COLOUR OR SYMBOL	NUMBER OF FUEL PINS	EQ. RADIUS OR X Y	INVESTIGATED CELL
I	3/1 VIPAK	WHITE	405	35.18 x 19.54	⊠
II	4/0	GREY	2 x 459	35.18 x 22.15	
TOTAL			1323	35.18 x 63.85	

MEASUREMENT DETECTORS

DESIGNAT.	DIAMET.	SYMBOL	N°	LOCATION	LEVEL	CHANNEL
PROPORTIONAL BF_3 COUNTER	1"	A	A	32	mid-pl	A
	1"	B	B	14	mid-pl	B
FISSION CHAMBER						

CONTROL DETECTORS

DESIGNAT.	DIAMET.	SYMBOL	N°	LOCATION	LEVEL	CHANNEL
PROPORTIONAL COUNTER	1/4"	C	3 B	+16/-16	mid-pl	C
ION CHAMBER						

VERIFIED BY: J.A. Stoop

APPROVED BY:

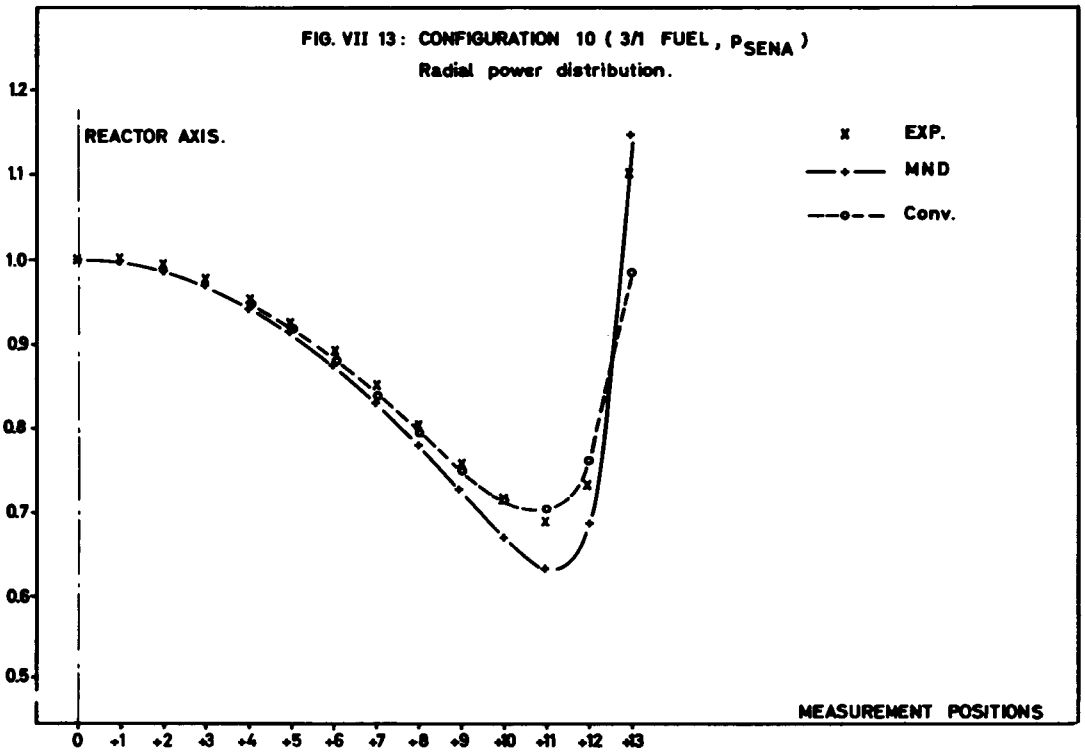
FIG. VII 13 : CONFIGURATION 10 (3/1 FUEL , P SENA)
Radial power distribution.
REACTOR AXIS.
x EXP.
MND
Conv.
1.2
1.1
1.0
0.9
0.8
0.7
0.6
0.5
MEASUREMENT POSITIONS
0 +1 +2 +3 +4 +5 +6 +7 +8 +9 +10 +11 +12 +13

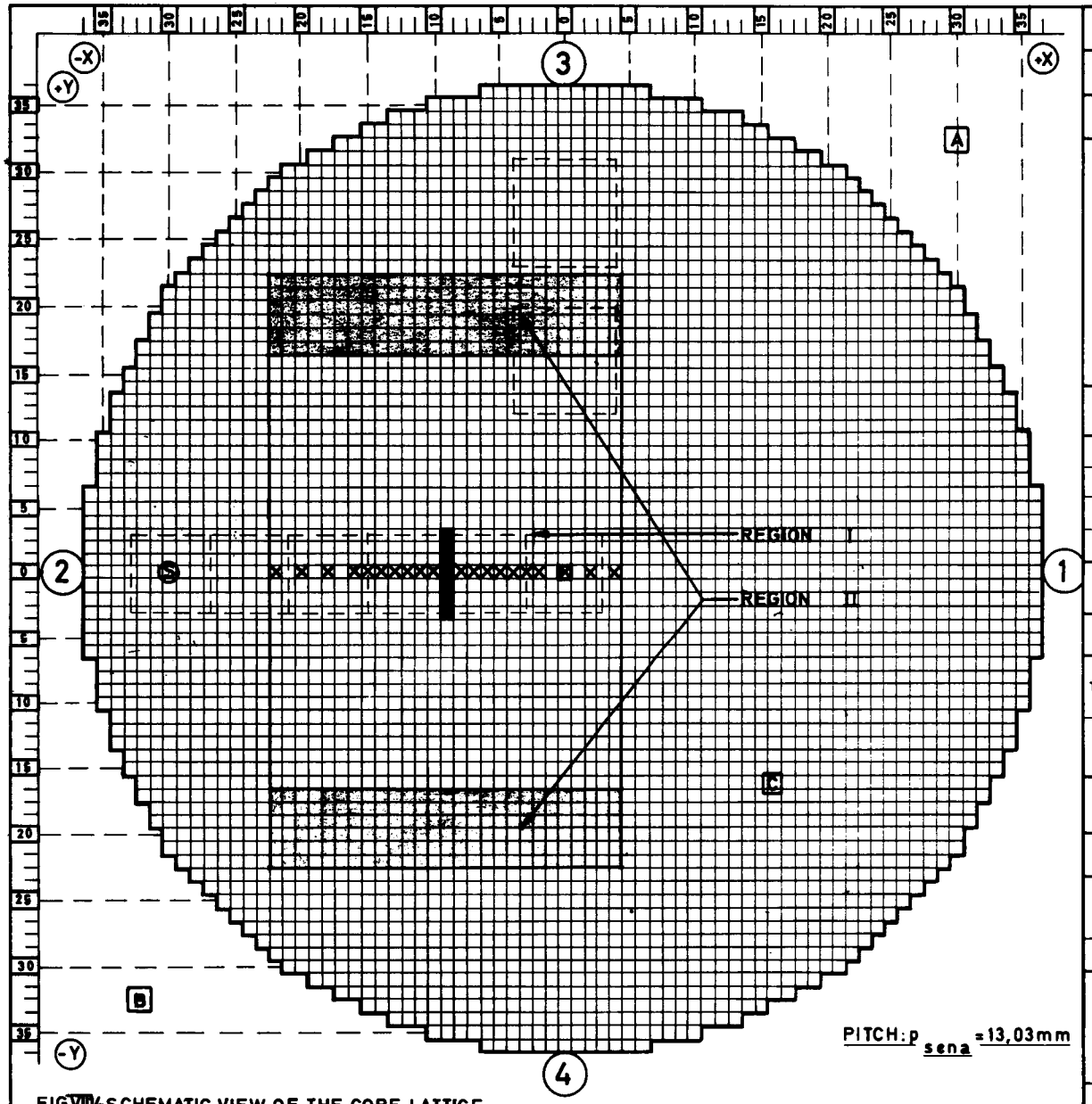

FIG. VII.4 SCHEMATIC VIEW OF THE CORE LATTICE

C.E.N-S.C.K	VENUS CRITICAL EXPERIMENT

EXPERIMENT : PERTURBATIONS EXPERIMENTS

DATE : 29.02.68

CONFIGURATION N° 8/4

DENSITY RODS : No

BORON CONCENTRATION (p.p.m): No

START-UP SOURCE (S)

NEUTRON GENERATOR (N) No

ABSORBING ROD ■ R OR M No

FUEL REGIONS

DESIGNAT	%U5/%Pu	COLOUR OR SYMBOL	NUMBER OF FUEL PINS	EQ. RADIUS OR X . Y	INVES - TIGATED CELL
I	4/0	WHITE	891	35.91 x 43.00 cm	☒
II	3/1	GREY	324	-	
TOTAL			1215	35.91 x 58.63 cm	

MEASUREMENT DETECTORS

DESIGNAT	DIAMET	SYMBOL	N°	LOCATION	LEVEL	CHANNEL
PROPORTIONAL BF_3 COUNTER	1/4	C	3^B	-16/+16	mid.pl	C
FISSION CHAMBER						

CONTROL DETECTORS

DESIGNAT	DIAMET	SYMBOL	N°	LOCATION	LEVEL	CHANNEL
PROPORTIONAL COUNTER	1"	A	A	32	mid.pl	A
	1"	B	B	14	mid.pl	B
ION CHAMBER						

VERIFIED BY:

APPROVED BY:

REMARKS : The black cells indicate the position of the perturbation.

Fig. VII 15: CONFIGURATION 8 (4/0 FUEL): INFLUENCE OF LOCAL PERTURBATIONS ON THE FISSION DENSITY DISTRIBUTION

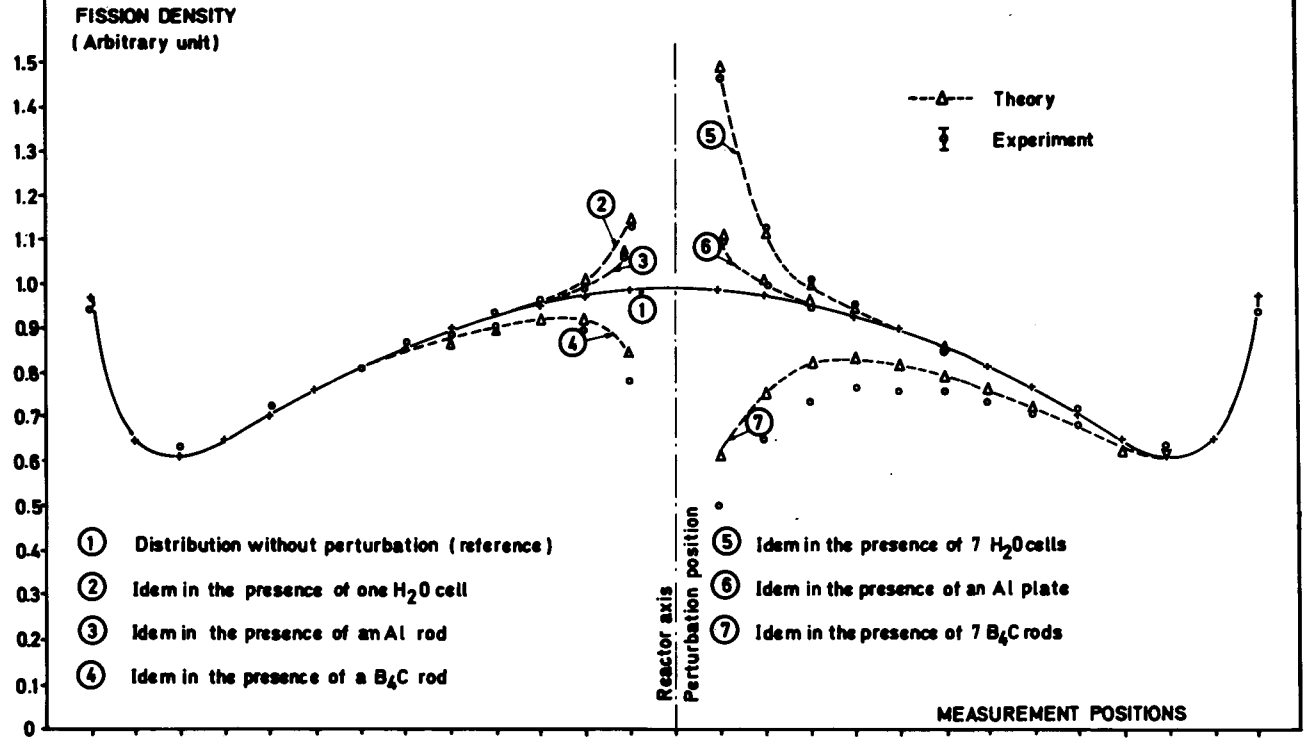

Fig. VII 16: CONFIGURATION 10 (3/1 FUEL): INFLUENCE OF LOCAL PERTURBATIONS ON THE FISSION DENSITY DISTRIBUTION

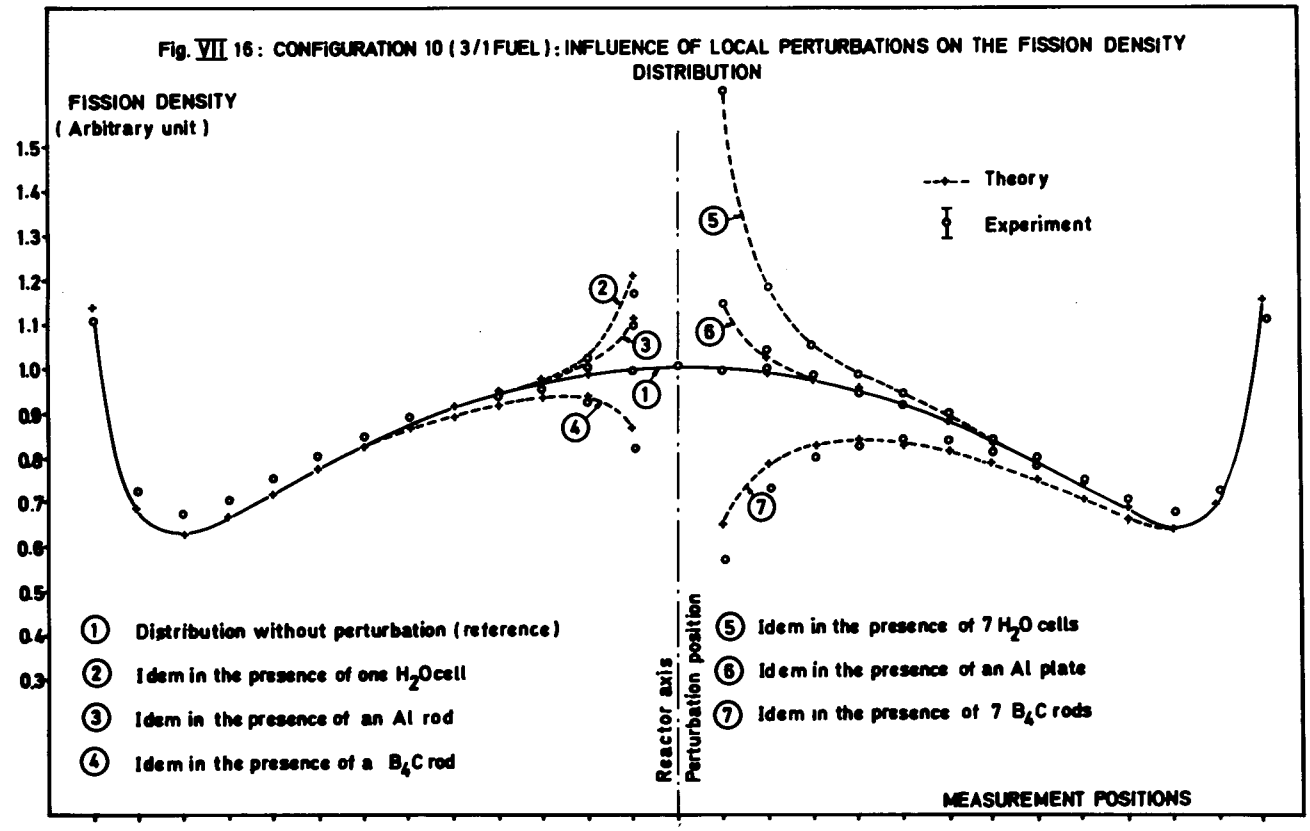

CONFIGURATION 8/5 _ 4/0 FUEL WITH WATER CROSS

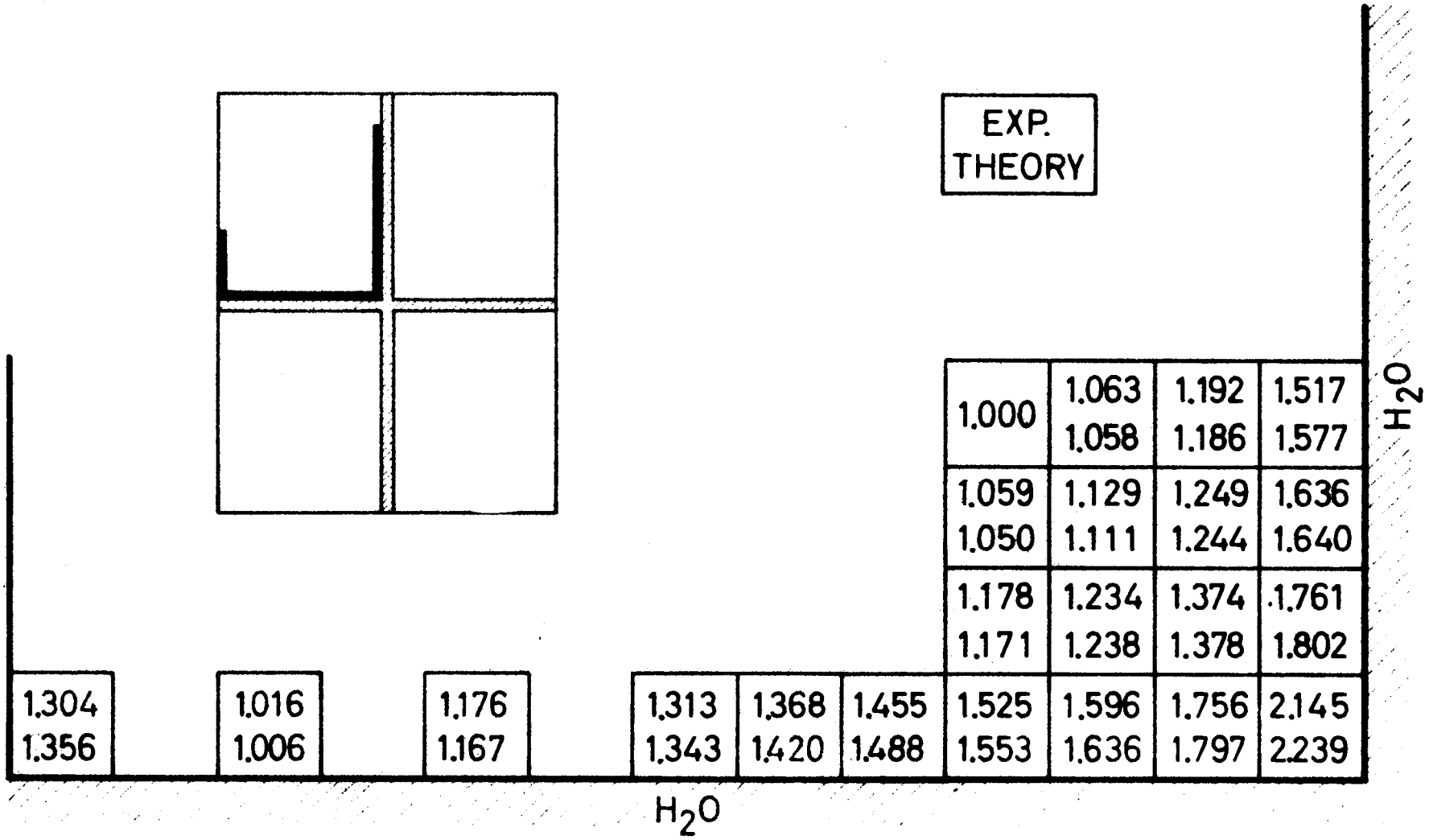

FIG. VII 17

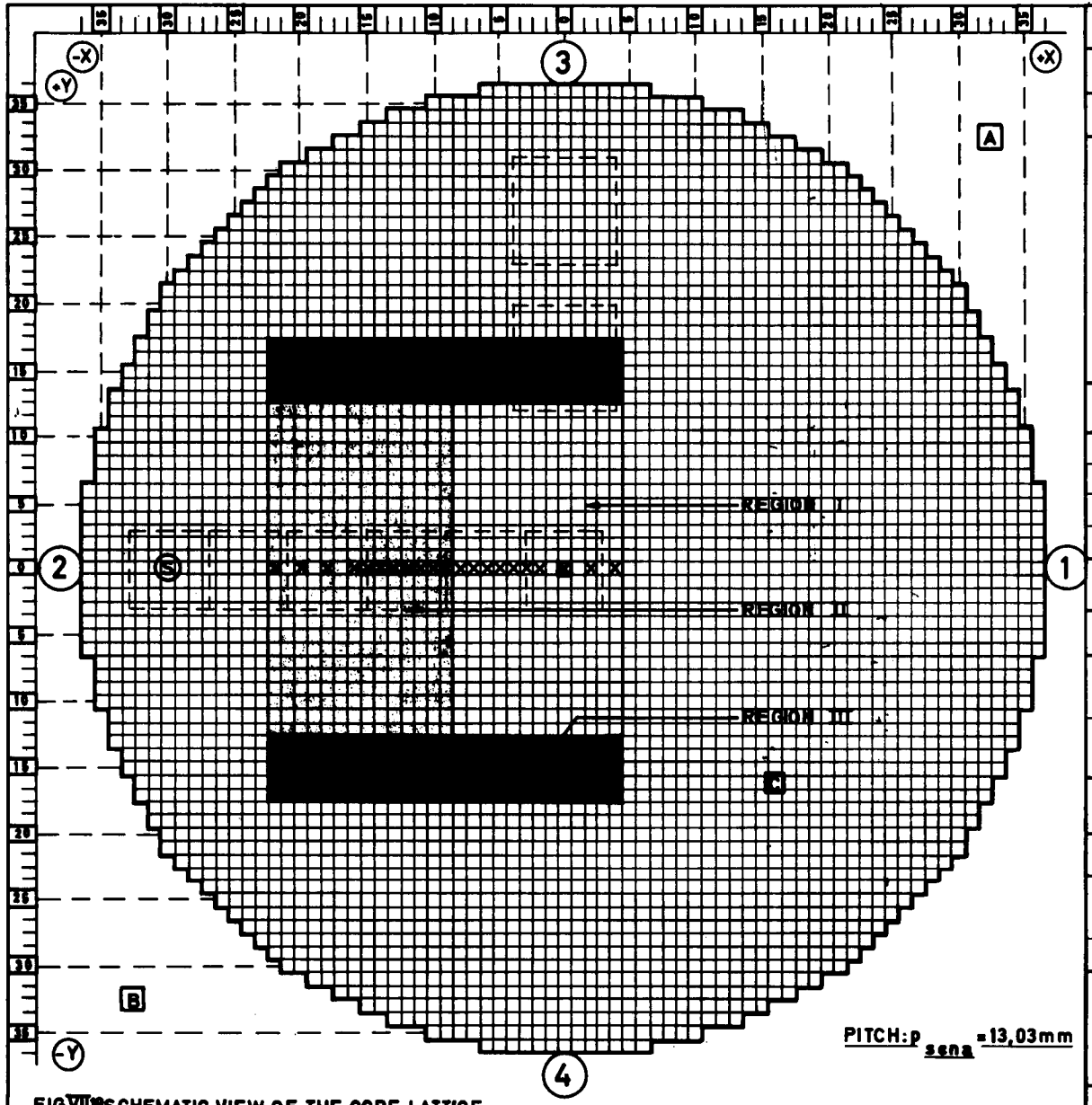

FIG VII.8 SCHEMATIC VIEW OF THE CORE LATTICE

C.E.N-S.C.K	VENUS CRITICAL EXPERIMENT

EXPERIMENT : POWER SHARING MEASUREMENTS

DATE : 28.03.68

CONFIGURATION N° 9

DENSITY RODS : No

BORON CONCENTRATION (p.p.m) : No

START-UP SOURCE (S) _____

NEUTRON GENERATOR (N) No

ABSORBING ROD ■ R OR M No

FUEL REGIONS

DESIGNAT.	%U5/%Pu	COLOUR OR SYMBOL	NUMBER OF FUEL PINS	EQ. RADIUS OR X . Y	INVESTIGATED CELL
I	3/1VIPAK	WHITE	325	16.94 x 32.57	⊠
II	4/0 (1)	LIGHT GREY	350	18.24 x 32.57	⊠
III	4/0 (2)	DARK GREY	2 x 135	35.18 x 6.51	
TOTAL			945	35.18 x 45.60	

MEASUREMENT DETECTORS

DESIGNAT.	DIAMET.	SYMBOL	N°	LOCATION	LEVEL	CHANNEL
PROPORTIONAL BF_3 COUNTER	1"	A	A	32	mid-pl.	A
	1"	B	B	14	mid-pl.	B
FISSION CHAMBER						

CONTROL DETECTORS

DESIGNAT.	DIAMET.	SYMBOL	N°	LOCATION	LEVEL	CHANNEL
PROPORTIONAL COUNTER	1/4"	C	3 B	+16/-16	mid-pl.	C
ION CHAMBER						

VERIFIED BY: _____ APPROVED BY: _____

REMARKS : (1) First furniture
(2) Second furniture

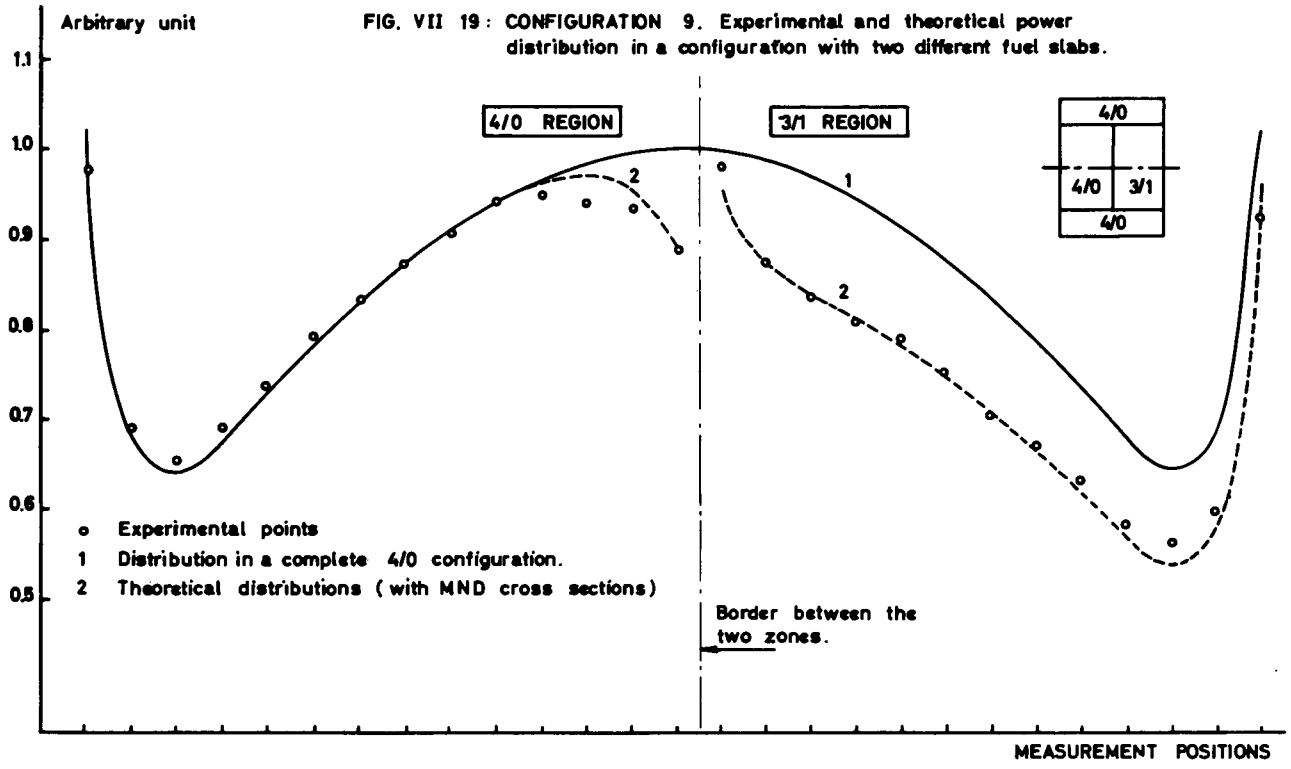

FIG. VII 19 : CONFIGURATION 9. Experimental and theoretical power distribution in a configuration with two different fuel slabs.

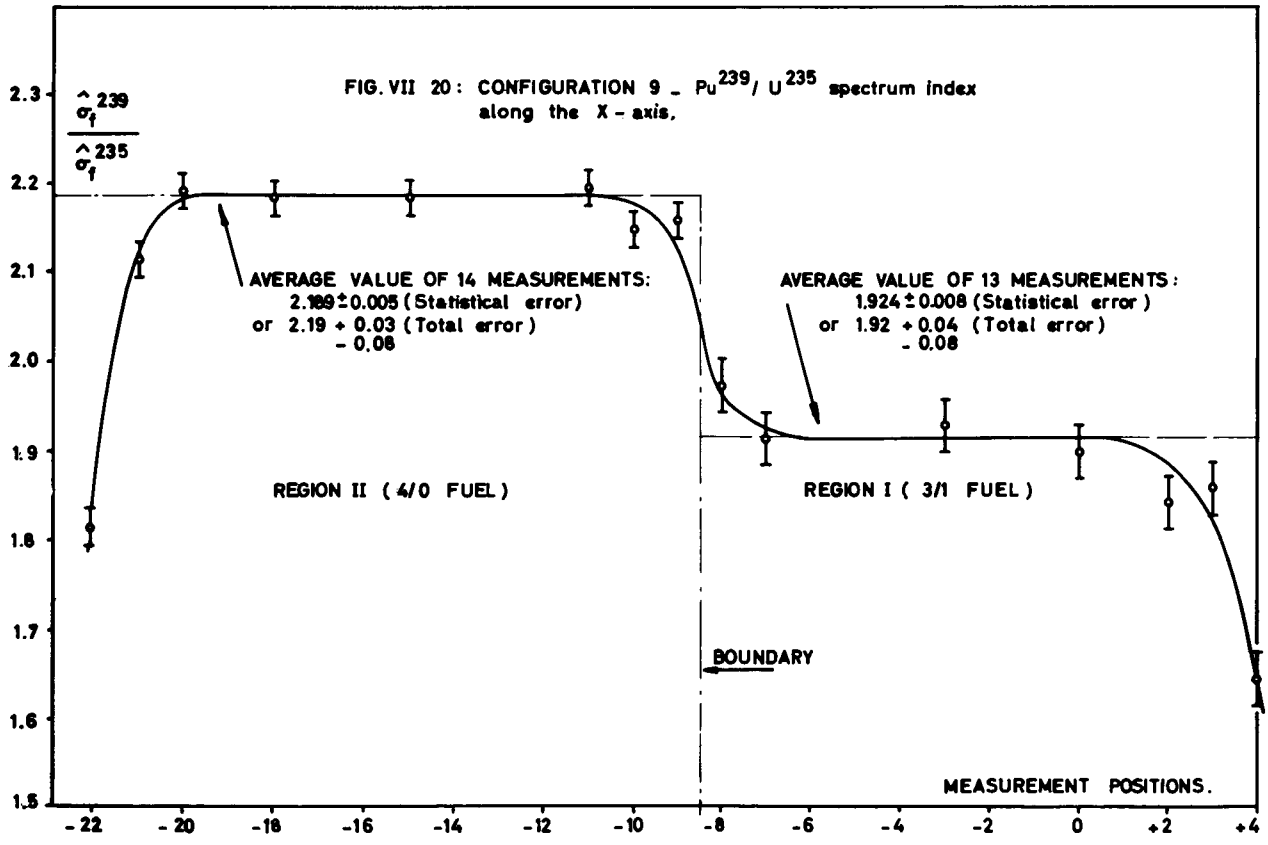

FIG. VII 20 : CONFIGURATION 9 _ Pu^{239}/U^{235} spectrum index along the X - axis.

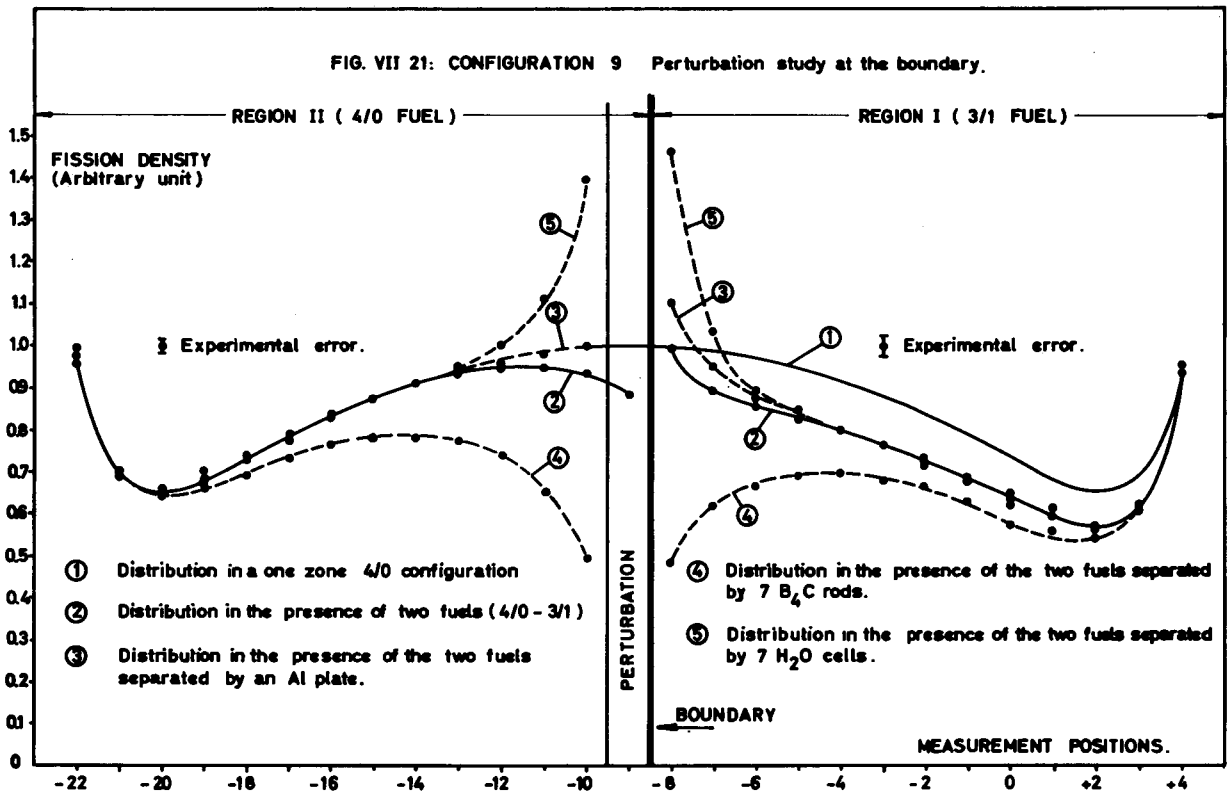

FIG. VII 21: CONFIGURATION 9 Perturbation study at the boundary.

Fig. VII 23: FISSION DENSITY DEPRESSION INSIDE FUEL RODS

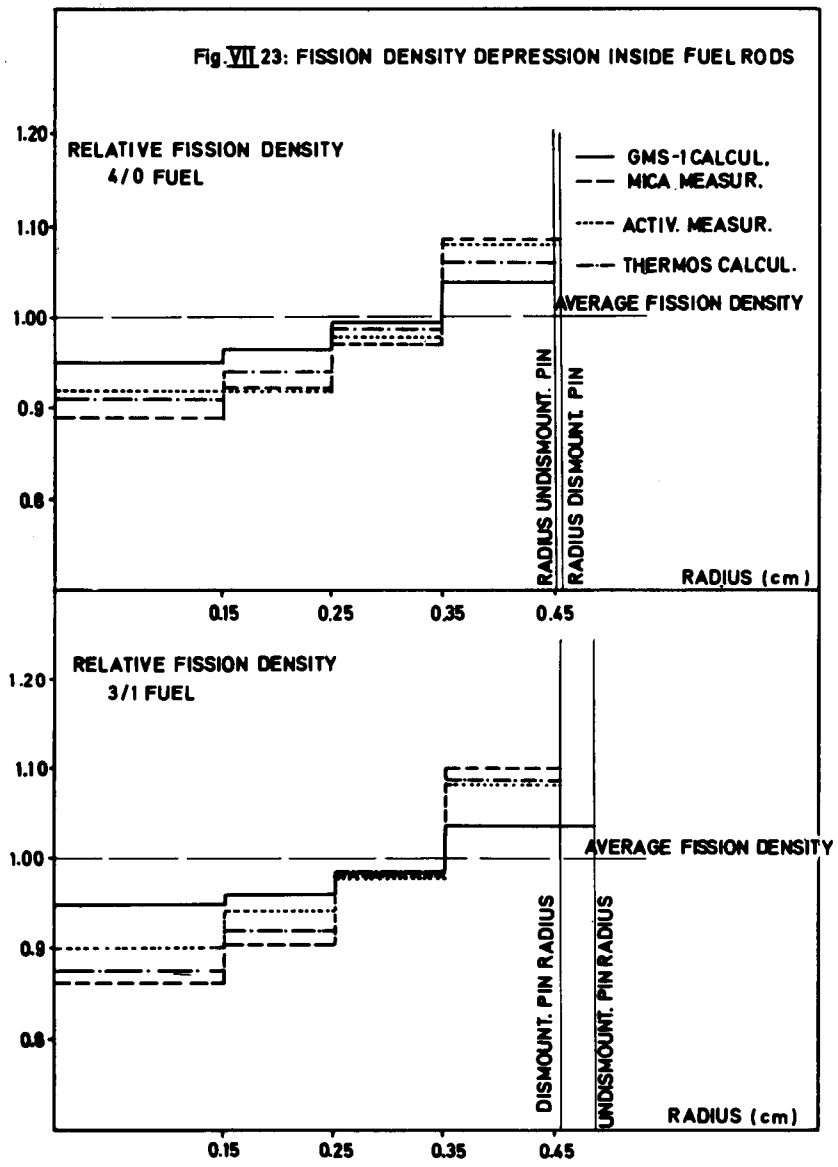

Fig. VII 22: CONFIGURATION 9: INFLUENCE OF PERTURBATIONS ON THE $^{239}Pu/^{235}U$ SPECTRUM INDEX.

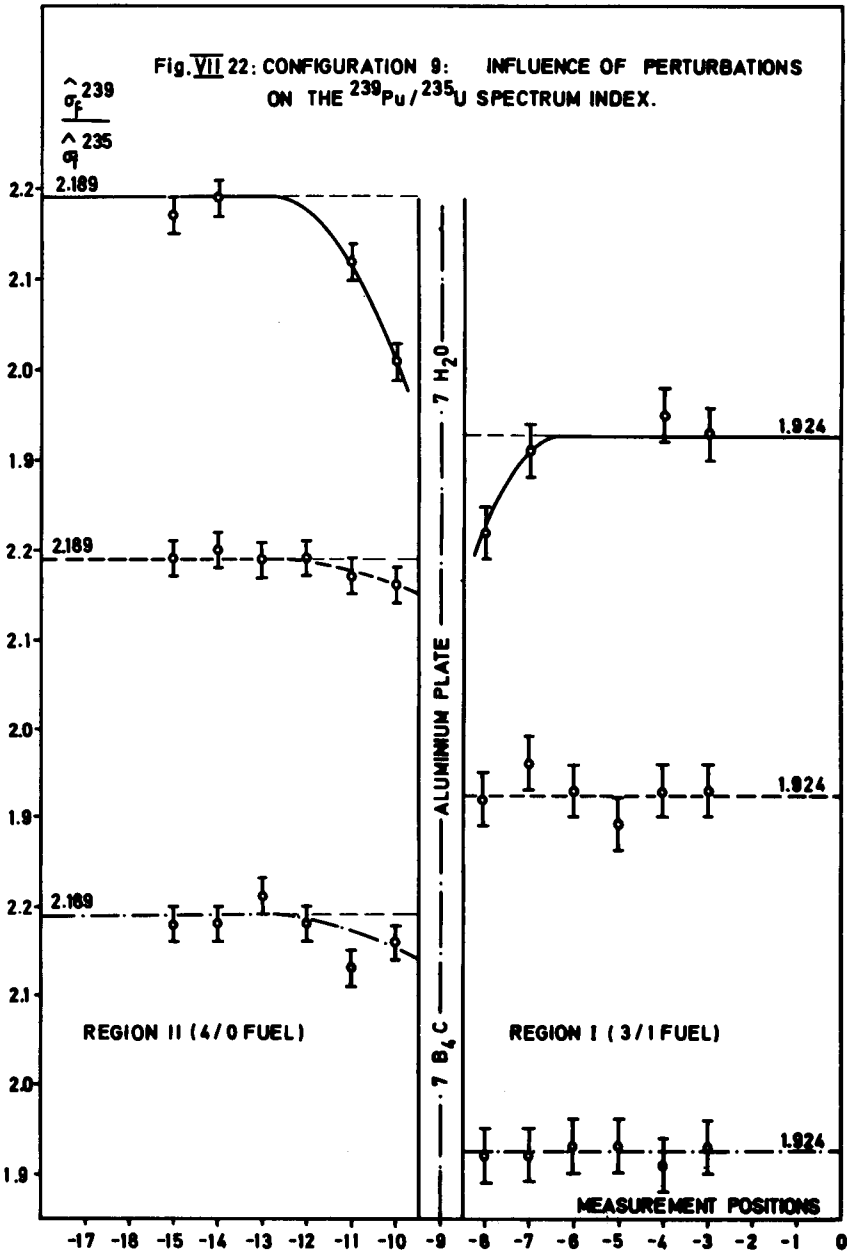

To disseminate knowledge is to disseminate prosperity — I mean general prosperity and not individual riches — and with prosperity disappears the greater part of the evil which is our heritage from darker times.

Alfred Nobel

SALES OFFICES

All reports published by the Commission of the European Communities are on sale at the offices listed below, at the prices given on the back of the front cover. When ordering, specify clearly the EUR number and the title of the report which are shown on the front cover.

OFFICE FOR OFFICIAL PUBLICATIONS OF THE EUROPEAN COMMUNITIES
P.O. Box 1003 - Luxembourg 1
(Compte chèque postal N° 191-90)

BELGIQUE — BELGIË
MONITEUR BELGE
Rue de Louvain, 40-42 - B-1000 Bruxelles
BELGISCH STAATSBLAD
Leuvenseweg 40-42 - B-1000 Brussel

DEUTSCHLAND
VERLAG BUNDESANZEIGER
Postfach 108 006 - D-5 Köln 1

FRANCE
SERVICE DE VENTE EN FRANCE
DES PUBLICATIONS DES
COMMUNAUTÉS EUROPÉENNES
rue Desaix, 26 - F-75 Paris 15e

ITALIA
LIBRERIA DELLO STATO
Piazza G. Verdi, 10 - I-00198 Roma

LUXEMBOURG
OFFICE DES
PUBLICATIONS OFFICIELLES DES
COMMUNAUTÉS EUROPÉENNES
Case Postale 1003 - Luxembourg 1

NEDERLAND
STAATSDRUKKERIJ-
en UITGEVERIJBEDRIJF
Christoffel Plantijnstraat - Den Haag

UNITED KINGDOM
H. M. STATIONERY OFFICE
P.O. Box 569 - London S.E.1

Commission of the European Communities
D.G. XIII - C.I.D.
29, rue Aldringen
Luxembourg